Me UDC 539.37:676.028.24

ACTA
POLYTECHNICA
SCANDINAVICA

MECHANICAL ENGINEERING SERIES No. 146

Contact Mechanical Model for Winding Nip

MARKO JORKAMA

Valmet Corporation
Winders
Wärtsilänkatu 100
04400 Järvenpää, Finland

Dissertation for the degree of Doctor of Science in Technology to be presented with due permission of the Department of Engineering Physics and Mathematics for public examination and debate in Auditorium E at Helsinki University of Technology (Espoo, Finland) on the 12th of January, 2001, at 12 o'clock noon.

ESPOO 2001

Jorkama, M., **Contact Mechanical Model for Winding Nip.** Acta Polytechnica Scandinavica, Mechanical Engineering Series No. 146, Espoo 2001, 96 pp. Published by the Finnish Academies of Technology. ISBN 951-666-559-4. ISSN 0001-687X. UDC 539.37:676.028.24

Keywords: Elastic contact, winding, paper, nip-induced tension, orthotropic, elastic half-space, elastic cylinder, elastic thin sheet

ABSTRACT

A winding simulation model predicting the internal stress state of a wound roll would provide an indispensable tool for the optimal selection of the winding parameters and, above all, a fast way to design new winding concepts – such as winding drum covers and winding geometry. Hence, the nip-induced stresses and nip-induced tension are of the outmost interest to the manufacturer of the winding apparatus. In this thesis, a rigorous contact mechanical model for the winding nip is presented. Under the assumptions of the linear elastic web and paper roll material and compliant winding drum, the indentation, stick and slip equations are derived. The wound-on-condition, a mathematical statement for the initially free sheet becoming finally a part of the roll, is presented. A variant of the Panagiotopoulos Process is introduced as a solution procedure and numerical results are presented. An invariant condition is derived and, hence, the number of independent winding parameters is reduced from three to two. In the numerical part of the thesis, the basic mechanism of the nip-induced tension is presented and the following items are studied: the influence of the winding force, the layer-to-layer friction coefficient, the wound roll and winding drum radius, drum cover compliancy and the elastic constants of paper on the nip-induced tension. The calculated results obtained are shown to comply well with the experiments and literature.

PREFACE

This doctoral thesis has been prepared at the Winding Technology Group of Valmet Winders, Järvenpää, Finland. When I completed my licentiate thesis on two-drum winder vibrations in 1996, I conceived that I would pursue the very same subject towards my doctoral thesis. However, after discussions with the Valmet Winders RTD and Engineering people I was convinced that winding and especially nip phenomena are much more substantial from the operational point of view in winding and reeling. As a dedicated "dynamicist" I had to start almost from scratch to learn topics on elasticity and contact mechanics. Thus, it was maybe due to my inexperience in the subject that I spent four inane months trying to overcome a numerical problem related to the iteration of the solution of the rolling contact problem. Finally, when that problem was solved (thanks to Raimo von Hertzen) the rest of the work required to put this thesis intact was more or less straightforward.

Many have helped me during the writing of this thesis. At Valmet the immediate availability of scientifically oriented persons like Matti Tervonen, Reijo Pietikäinen, Matti Innala and Erkki Leinonen has been invaluable for quick responses to occasional questions raised during the study. I am indebted to Prof. James K. Good and the other staff for their hospitality and assistance during the six months I spent at the Web Handling Reseach Center of Oklahoma State University. Finally, I would like to thank Dr. Raimo von Hertzen from the Helsinki University of Technology for countless discussions and guidance in the writing process of this thesis.

In closing, I would like to thank my family members Katri, Miro, Andre and Sara for tolerating me working long hours at work and at home during the last few years. Even though I sometimes thought that they involve me too much in daily routines, the truth is that I could never have completed this work without them.

Järvenpää, January 2001
Marko Jorkama

CONTENTS

Preface 3

Nomenclature 6

1 Introduction 11

1.1 Wound-on-tension 13

1.2 Elastic rolling contact 16

2 Elastic Solutions of the contacting bodies 22

2.1 Linear, elastic, orthotropic half-space 24

2.2 Linear, elastic, orthotropic cylinder 29

2.3 Linear, elastic, orthotropic thin strip 35

3 Winding contact problem 40

3.1 Contact equations 40

3.2 Wound-on-condition 45

3.3 Hertz half-width equation for linear and orthotropic half-space 46

3.4 Discretized contact equations 48

3.5 Extended model accounting for the wound roll wrap 56

3.6 Modified Panagiotopoulos Process 63

4 Numerical results 65

4.1 Independent winding parameters 65

4.2 Basic mechanism of nip-induced tension 67

4.3 Influence of the winding force 69

4.4 Influence of the layer-to-layer friction coefficient 71

4.5 Influence of the wound roll and winding drum radius 72

4.6 Winding drum cover design aspects 74

4.7 Influence of the elastic constants of paper 77

4.8 Computational aspects 80

4.9 Evaluation of the Wound-On-Condition 83

5 Experimental comparison 88

6 Conclusions 92

References 94

NOMENCLATURE

A, B, C	coefficients in the integral presentation of the displacements in the elastic half-space theory
$A,\ B,\ B_{lm}^{\pm}$	influence coefficients of $v_l^+ - v_l^-$
$C_{lm}^{\pm},\ D_{lm}^{\pm},\ D$	influence coefficients of $\varepsilon_l^{\pm}$
A_{rr}	radial direction elastic constant in the elastic cylinder theory
$A_{r\theta}$	radial-tangential direction cross elastic constant in the elastic cylinder theory
$A_{\theta\theta}$	tangential direction elastic constant in the elastic cylinder theory
A_{xx}	tangential direction elastic constant in the elastic half-space theory
A_{xy}	tangential-normal direction cross elastic constant in the elastic half-space theory
A_{yy}	normal direction elastic constant in the elastic half-space theory
$A_{lm,i}, B_{lm,i}$	influence coefficients of $v_{l,i}$
$C_{lm,i}, D_{lm,i}$	influence coefficients of $\varepsilon_{l,i}$
$\mathcal{D}_{lm}^{\pm}$	influence coefficients of $\varepsilon_l^{\pm}$
a	semi-contact width
a_{nm}	constant coefficient of the mth characteristic solution in the expansion of the Fourier coefficients u_n^s and v_n^c
b_{nm}	constant coefficient of the mth characteristic solution in the expansion of the Fourier coefficients u_n^c and v_n^s
c_{11}	tangential direction elastic compliance in the elastic thin sheet theory
c_{12}	normal-tangential direction cross elastic compliance in the elastic thin sheet theory
c_{22}	normal direction elastic compliance in the elastic thin sheet theory
c_{66}	shear elastic compliance in the elastic thin sheet theory
c_0	0^{th} coefficient in the Fourier series presentation of $p(.)$
c_n	nth coefficient of $\cos n\theta$ in the Fourier series presentation of $p(.)$
d_n	nth coefficient of $\sin n\theta$ in the Fourier series presentation of $p(.)$
G	shear modulus in the elastic half-space theory
$G_{r\theta}$	shear modulus in the elastic cylinder theory
e_0	0^{th} coefficient in the Fourier series presentation of $q(.)$
e_n	nth coefficient of $\cos n\theta$ in the Fourier series presentation of $q(.)$
F	winding force = Q^-

F_r	radial direction body force
F_θ	tangential direction body force
f_n	nth coefficient of sin$n\theta$ in the Fourier series presentation of $q(.)$
h	half of the web thickness
i	imaginary unit $\sqrt{-1}$
M	number of the evenly spaced grid points in the contact
M_1	wound roll torque
M_2	winding drum torque
NIT	nip-induced tension
P	radial compressive load between the paper roll and winding drum
$p(.)$	distributed normal traction (pressure) in the contact or general normal traction in the elastic half-space or cylinder problems
p_m	contact pressure at x_m
Q^+	total tangential traction in the contact between the wound roll and the sheet
Q^-	total tangential traction in the contact between the winding drum and the sheet
Q_w^+	total tangential traction in the contact between the topmost paper layer and wound roll behind the nip
$q(.)$	distributed tangential traction in the elastic half-space or cylinder problems
$q^+(.)$	distributed tangential traction in the wound roll-sheet contact
$q^-(.)$	distributed tangential traction in the winding drum-sheet contact
$q_m^+,\ q_m^-$	tractions of the top (+) and bottom (-) of the sheet at x_m
R	wound roll radius
R_0	radius of the rigid core in the elastic cylinder theory
R_1	wound roll radius
R_2	winding drum radius
r	radial coordinate in the polar coordinates
s	lengthwise coordinate of the web
s_d	dual slip ratio
s_{r1}	leading edge roll slip ratio
s_{r2}	trailing edge roll slip ratio
$T(s)$	web tension at s
T_{in}	web tension of the first paper layer prior to the nip
T_{out}	web tension of the first paper layer just after the nip

u_0	0^{th} coefficient function in the Fourier series presentation of u_r
u_n^c	nth coefficient of cos$n\theta$ in the Fourier series presentation of u_r
u_n^s	nth coefficient of sin$n\theta$ in the Fourier series presentation of u_r
$u_r,\ u_\theta$	radial and tangential displacements of the elastic cylinder
$u_{r1},\ u_{r2}$	radial displacements of the roll and drum
$u_{\theta1},\ u_{\theta2}$	tangential displacements of the roll and drum
$u_1,\ u_2$	tangential displacements of the roll and drum
$u_{l,1},\ u_{l,2}$	tangential displacements of the roll and drum at x_l
$\bar{u}_r,\ \bar{u}_\theta$	radial and tangential surface displacements of the elastic cylinder
$U_x,\ U_y$	Fourier transforms of $u_x,\ u_y$, respectively
$u_x,\ u_y$	x- and y-direction displacements in the elastic half-space or thin sheet theory
$\bar{u}_x,\ \bar{u}_y$	x- and y-direction surface displacements in the elastic half-space or thin sheet theory
$V_{\theta1}$	absolute tangential surface speed of the paper roll
$V_{\theta2}$	absolute tangential surface speed of the winding drum
V^+	absolute tangential speed of the top surface of the sheet
V^-	absolute tangential speed of the bottom surface of the sheet
v_0	0^{th} coefficient function in Fourier series presentation of u_θ
v_n^c	nth coefficient of cos$n\theta$ in the Fourier series presentation of u_θ
v_n^s	nth coefficient of sin$n\theta$ in the Fourier series presentation of u_θ
$v_1,\ v_2$	radial (normal) displacements of the roll and drum
$v_{l,1},\ v_{l,2}$	radial displacements of the roll and drum at x_l
$v^+,\ v^-$	normal displacements of the top (+) and bottom (-) of the sheet
$v_l^+,\ v_l^-$	normal displacements of the top (+) and bottom (-) of the sheet at x_l
WOT	wound-on-tension
x_m	mth nip discretization point
Δx	nip discretization step
$\alpha_{0m,1},\ \alpha_{0m,2}$	0^{th} coefficient in the Fourier series presentation of $\psi_m(x)$
$\alpha_{nm,1},\ \alpha_{nm,2}$	nth coefficient of cos$n\theta$ in the Fourier series presentation of $\psi_m(x)$
$\beta_{nm,1},\ \beta_{nm,2}$	nth coefficient of sin$n\theta$ in the Fourier series presentation of $\psi_m(x)$
$\varepsilon_1,\ \varepsilon_2,\ \varepsilon_3$	principal strains
ε_z	axial strain in the cylindrical coordinates

ε^+, ε^-	tangential strains at the top (+) and bottom (-) of the sheet
ε_l^+, ε_l^-	tangential strains at the top (+) and bottom (-) of the sheet at x_l
$\varepsilon_{\theta 1}$, $\varepsilon_{\theta 2}$	tangential surface strain of the paper roll and winding drum
ε_1, ε_2	tangential surface strain of the paper roll and winding drum
$\varepsilon_{l,1}$, $\varepsilon_{l,2}$	tangential surface strain of the paper roll and winding drum at x_l
γ_0	characteristic sequence of the 0^{th} Fourier coefficient of u_r
$\gamma_{n,1}$, $\gamma_{n,2}$	1^{st} and 2^{nd} characteristic sequences of the nth Fourier coefficients of u_r
γ_{nt}	shear angle between the tangential and normal directions
δ	mutual approach of the paper roll and the winding drum centers
δ^+, δ^-	mutual approach of the sheet and wound roll and sheet and winding drum centers, respectively
δ_x^+, δ_{x1}	x-component of the rigid translation of the sheet and upper cylinder, respectively
δ_y^+, δ_{y1}	y-component of the rigid translation of the sheet and upper cylinder, respectively
η_{nm}	ratio of the characteristic solutions $\varphi_{nm}(.)$ and $\phi_{nm}(.)$
θ	polar angle in the polar coordinates
κ	elasticity parameter in the elastic half-space theory
λ_i	characteristic roots of the elastic half-space or cylinder problems
λ_{nm}	mth root of the nth Fourier coefficient function characteristic equation in the elastic cylinder problem
μ	elasticity parameter in the elastic half-space theory
μ_k	kinetic coefficient of friction between the paper layers
μ^+	layer-to-layer friction coefficient
μ^-	winding drum-sheet friction coefficient
ξ^+	creep ratio of the paper roll-sheet contact
ξ^-	creep ratio of the winding drum-sheet contact
ρ	density of the paper roll
ρ_0	reference density prior to the deformation
ρ^+	radius of curvature of the wound roll
σ_r	radial stress of the cylinder
σ_x	tangential stress in the elastic half-space or thin sheet theory
σ_y	normal stress in the elastic half-space or thin sheet theory
σ_θ	tangential stress of the cylinder

τ_{xy}	shear stress in the elastic half-space theory
$\upsilon^+,\ \upsilon^-$	relative speed differences at the top (+) and bottom (-) of the sheet
$\phi_{nm}(.)$	mth characteristic solution of the base functions spanning the nth Fourier coefficient of u_r
$\varphi_{nm}(.)$	mth characteristic solution of the base functions spanning the nth Fourier coefficient of u_θ
χ_0	characteristic sequence of the 0^{th} Fourier coefficient of u_θ
$\chi_{n,1}, \chi_{n,2}$	1^{st} and 2^{nd} characteristic sequences of the nth Fourier coefficients of u_θ
$\psi_m(.)$	piecewise linear base function at x_m
ω	independent variable in the Fourier transform $F(\omega)$ of the function $f(x)$
ϑ_m	mth coefficient of ψ_m in the expression of $u_{r1}'' - 2u_{r1}/R_1^2$
Δ	tangential distance between the center of the contact and the line initially connecting the centers of the paper roll and winding drum
Δ^+, Δ^-	tangential shift of the upper and lower contact centers, respectively
$\Gamma_{nm}^{\pm}, \hat{\Gamma}_n$	coefficients of $q_m^{\pm}$ and T_{in} in the expression of $c_{n,1}$
$\Lambda_{nm}^{\pm}, \hat{\Lambda}_n$	coefficients of $q_m^{\pm}$ and T_{in} in the expression of $d_{n,1}$

1 INTRODUCTION

The paper sheet is wound and unwound several times during the paper manufacturing process. The winding or reeling should be done in a manner that minimizes the amount of reject. Hence, the winders and reelers should strain the paper as little as possible during the winding process and produce rolls or reels that are not susceptible to defects during transportation or any other further processing. Due to the tendency of increasing the reel diameters and roll widths, these demands are not always easy to fulfill. In addition, development in the paper making process and paper grades can be unfavorable to winding and wound roll quality.

Accordingly, the tendency among the winder and reeler suppliers during the last decade has been to reduce the stress on the paper during winding and to improve the cross-machine direction uniformity of the reel or rolls [38]. This has been achieved by reducing the nip-induced stresses on the wound rolls with soft winding drum covers and belt-supports, and partial elimination of the non-uniform nip loads due to reel or roll deflection. However, presently there is no solid contact mechanical theory of the winding nip and, hence, it is not possible to reliably evaluate the strain on the paper or wound roll in the vicinity of the nip. Also, the mechanism of the nip-induced tension (NIT), due to the (micro) slip of the incoming paper layer, is not fully understood. This impedes the optimization of the winding device based on the predicted stress distribution of the winding nip and wound roll. Accordingly, currently the design of the winding equipment is based on empirical knowledge, trial and error tests and more or less incoherent engineering science. Of course winding with the nip has been studied experimentally and theoretically for many years, but surprisingly rigorous contact mechanical theory has not yet been developed. The goal of this thesis is to partially fill this gap. The scope of this thesis on this complex matter will by no means be comprehensive, rather foundational. With this beginning, several simplifications will be made, and the problem is focused to include mainly the contact mechanics of the winding nip. Hence, the main outcome of the model should be regarded phenomenological and methodological with only limited applicability to yield quantitatively accurate results. However, it is hoped that the model will be able to capture some essential features of the winding nip behavior – like the mechanism for nip-induced tension. As the initial phase on a larger project on winding mechanics, this thesis will serve as a basis for a stepwise refinement process leading towards a winding nip theory of required accuracy.

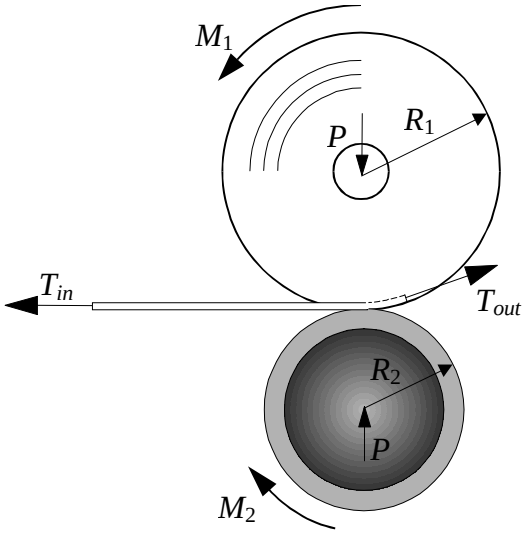

Figure 1. Winding configuration.

The winding configuration to be studied in this work is shown in Figure 1. The wound roll is depicted as the upper circle and the winding drum as the lower circle. The paper web is fed into the winding nip, formed by the wound roll and winding drum, from the left and it enters the roll after the nip. The wound roll and winding drum are pressed against each other with uniform line load P [N/m] and driven by torques M_1 and M_2 [Nm/m], respectively. The tension of the web, prior to entering the nip, is T_{in} [N/m]. The problem statement is to find the surface stresses of the sheet, wound roll and winding drum in the nip and the web tension T_{out} just after the nip. The last mentioned quantity is important when extending the current center wound winding models [1,19] to also include winding with a nip.

In the past few years, winding with a nip has been studied intensively at the Web Handling Research Center (WHRC) of Oklahoma State University. They have recently reached good agreement between their theoretical model and the experimental data on center ($M_2 = 0$) and surface winding ($M_1 = 0$) [15]. This model, developed by Dr. Good, consists of a simplified contact mechanical model of the winding nip with several non-rigorous assumptions based predominantly on intuition. In this thesis, the goal is to develop a simple but rigorous contact mechanical model of the winding nip, which is based on the first principles. Since winding with the nip has not been previously modeled as a 2-dimensional contact mechanical problem, the degree of difficulty is kept to a minimum by:

a) Applying a linear, orthotropic and elastic material model for the wound roll and intervening sheet
b) Neglecting the wrap of the sheet around the winding drum before it enters the nip
c) Neglecting the air entrapment into the nip and the wound roll

Finally, it is hoped that the numerical results calculated with the model will enhance the development and offer improved insight to the more intuitive theories.

1.1 Wound-on-tension

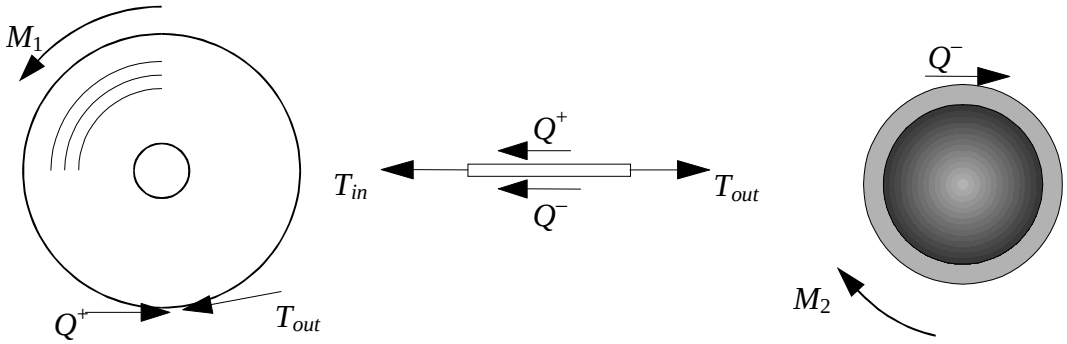

Figure 2. Tangential total contact loads and torques of the system.

With respect to extending winding models to include winding with a nip, the most important output is the web tension of the incoming paper web after the nip T_{out}. Closely related term, Wound-On-Tension or acronym WOT, is defined as the web tension of the topmost paper layer further behind the nip when the nip induced deformations have become negligible. Due to the rolling contact in the winding nip, a normal and tangential traction arises between wound roll-web and winding drum-web contacts. Let us consider the torque balance of the wound roll and winding drum and horizontal force balance of the paper web in the nip (Figure 2). If the radius of the wound roll is R_1 and the radius of the winding drum is R_2, the static balance equations are (the contact width is assumed to be negligible with respect to the radius of the contacting bodies and, hence, all the loads are approximately horizontal.)

$$\begin{aligned} M_1 &= T_{out} R_1 - Q^+ R_1 \,, \\ T_{out} &= Q^+ + Q^- + T_{in} \,, \\ M_2 &= -Q^- R_2 \,, \end{aligned} \tag{1}$$

where Q^+ and Q^- are the total tangential loads [N/m] between the wound roll and the web and winding drum and the web, respectively. Elimination of Q^+ and Q^- from Eqs. (1) yields the global balance of the winding configuration of Figure 1:

$$\frac{M_1}{R_1}+\frac{M_2}{R_2}=T_{in} \tag{2}$$

Hence, only two of the three external longitudinal control parameters M_1, M_2 and T_{in} are independent.

For reasons which come apparent later, the most convenient choice of the three independent *winding parameters* is the compressive load P, incoming web tension T_{in} and the *Winding Force* F, which is defined by

$$F=Q^{-}=-\frac{M_2}{R_2}\ . \tag{3}$$

In terms of these winding parameters, the wound-on tension from (1) becomes

$$T_{out}=Q^{+}+F+T_{in}\ . \tag{4}$$

It should be noted that in this expression only Q^{+} is a function of P.

The two last terms in Eq. (4) are controllable winding parameters, but Q^{+} is unknown and, hence, T_{out} cannot be solved without any additional assumptions on the kinematical or kinetic conditions within the nip. This is the basic dilemma of the winding models, which include a nip.

For center and surface winding equation (4) reads

$$\begin{aligned} T_{out}&=T_{in}+Q^{+}\ ,\ (F=0),\\ T_{out}&=Q^{+}\ ,\ (F=-T_{in}), \end{aligned} \tag{5}$$

Hence, in the case of pure surface winding the incoming tension T_{in} does not directly affect the Wound-On-Tension. It is also seen from Eqs. (4) and (5) that the difference $T_{out}-Q^{+}$ can readily be solved from the static equilibrium equations, but to determine T_{out} the total or net tangential load Q^{+} has to be known. Hence, in order to completely solve the wound-on tension it is obvious that the contact stress distributions have to be determined.

D. J. Pfeiffer [41] was perhaps the first who proposed that NIT was due to interlayer slippage inside the nip zone. Traditional and applied J-line measurement [32,17] studies show that it is indeed the slippage of the incoming paper layer which evidently contributes the most on NIT. If it is assumed that NIT is due to slippage between the incoming paper sheet and the wound roll, then at least for very light nip loads P, one could approximate the total tangential load to be

$$Q^+ = \mu_k P \text{ , light nip load,} \qquad (6)$$

where μ_k is the kinetic coefficient of friction between paper layers. When this equation is substituted to Eq. (5), a result equivalent to the earliest WOT-theories proposed by Dr. Good [14] is obtained. Experiments done by Dr. Good and his crew confirm that these results are accurate as long as the product $\mu_k P$ is sufficiently small. The graphs of the WOT measurements done on WHRC's WIT-WOT winder as a function of the nip load are shown in Figure 3. The tests were run for newsprint with μ_k = 0.19. The bold straight lines correspond to the theory as follows (from the bottom to the top): Surface winding, Center winding with T_{in} = 175 N/m, Center winding with T_{in} = 263 N/m and Center winding with T_{in} = 350 N/m. We see that for nip loads below 1 kN/m relatively good agreement is obtained, while for higher nip loads the theory gives values too high for WOT.

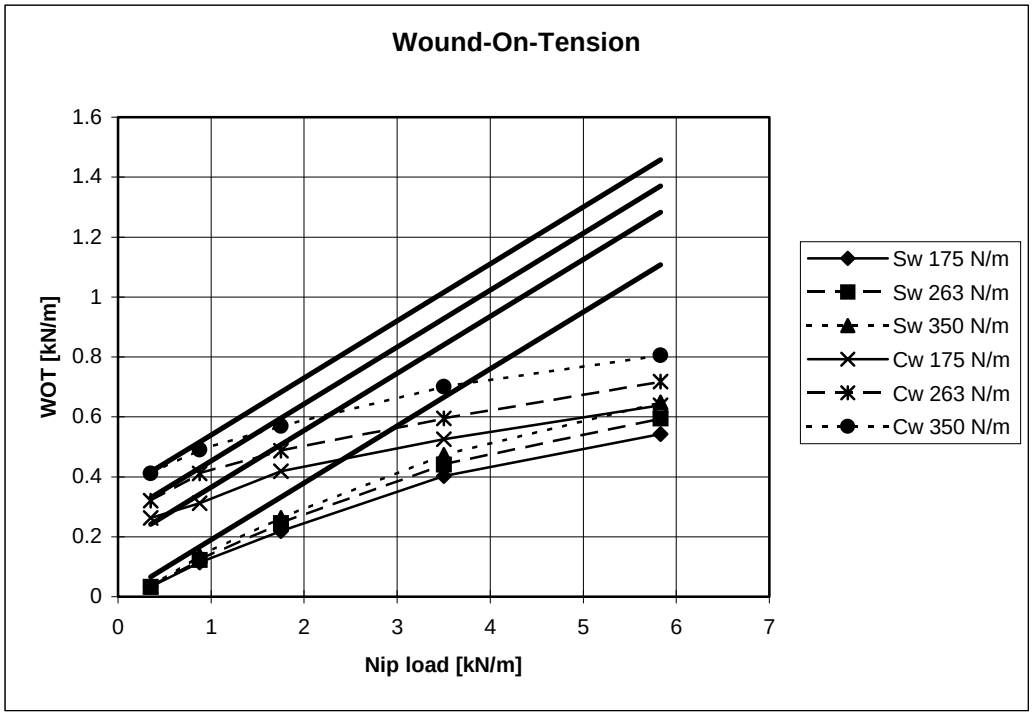

Figure 3. The measured WOT values for Center wound (Cw) and Surface wound (Sw) rolls for T_{in}=175, 263 and 350 N/m.

As seen from Eq. (4) the Nip-Induced Tension is due to the total tangential surface load Q^+ and winding force F. The winding force is directly controllable via the winding drum torque but Q^+ is an unknown function of the winding parameters P, F and T_{in} (actually, as will be shown in Chapter 4, Q^+ depends only on P and F). Hence, the global picture of the nip mechanism can be condensed to the determination of Q^+ as a function of the winding parameters. On the other hand, although F is a given load, the distribution of the corresponding tangential traction between the

wound roll and winding drum will be determined by the contact mechanical considerations. When Eq. (4) is applied within the contact then T_{out} is to be replaced by the web tension within the contact, $T(x)$. Then another interpretation of the NIT mechanism is that nip-induced tension is developed in areas where the tangential tractions of the top and bottom of the sheet do not cancel each out.

1.2 Elastic rolling contact

The elastic deformation on the rolling contact between the wound roll and winding drum induces local speed differences (local slip) in the contact. This phenomenon is easily understood by considering the tangential traction in the free rolling contact between rigid and deformable cylinders. In the steady state conditions, the peripheral speed of the rigid cylinder must be constant across the periphery, whereas the apparently non-uniform tangential strain on the deformable cylinder in the contact causes non-uniformity in the local speed. Hence, if the cylinders are not sliding, then some points of the contact must slip and some stick. A similar kind of argument also applies to the case of rolling contact between deformable cylinders. If, owing to elastic deformation under normal load, the tangential strain in the cylinder is tensile, the surface of the cylinder is stretched where it is in sticking contact. The cylinder then behaves as though it had an enlarged circumference and, in one revolution, moves forward a distance greater than its undeformed perimeter by a fraction known as the creep ratio. In the other cylinder, the strain is then compressive and the effect is reversed. If there is net tangential traction transmitted through the contact, then the situation gets more complicated and the tangential strain can be tensile in some parts of the contact and compressive on other parts.

In the areas of adhesion, the basic contact mechanical equations are naturally kinematical and geometrical relations between the deformed and undeformed states of the contacting bodies. In the slip areas, a definite relationship between the local pressure and shear stress is usually assumed. Linear dependence, described by Amonton's friction law, is most commonly used mainly due its simplicity.

In the normal direction of the contact surface, a relationship describing the mutual approach of the contacting bodies relative to the undeformed original state is written. This relation is called the *indentation equation*. This equation can be illustrated by considering two linear springs in series, loaded by a force F at the ends (Figure 4). Initially the springs are undeformed and in the deformed state the mutual approach of the ends is $\delta = \delta_1 + \delta_2$ and the compression of the upper and lower springs is x_1 and x_2, respectively. The indentation equation is now

$$x_1 + x_2 = \delta \tag{7}$$

and the relation between the loads and displacements

$$F = k_1 x_1 \ , \ F = k_2 x_2 \ , \tag{8}$$

where k_1 and k_2 are the spring constants of the upper and lower springs, respectively. In the distributed contact problems the right hand side of the indentation equation (7) is a function of the tangential coordinate of the contact curve and the load displacement relationship is replaced by the elastic solution describing relationship between the local displacements and stresses at the contact surface. The net loads are usually known in the distributed contact problems but the distributions of the induced contact stresses are unknown. Indentation equation (7) expressed in terms of the surface tractions (with aid of the analogous relationship to (8)) then yields a functional relation for the stresses as a function of the tangential contact coordinate.

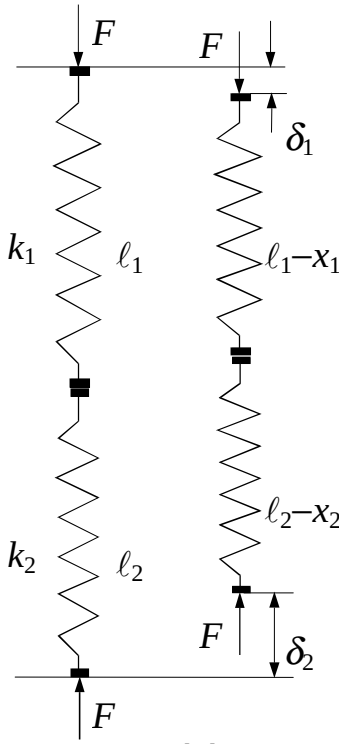

Figure 4. Loaded system of two springs

In the rolling contact problems, the stick condition is expressed by the equality of the local surface speeds of the contacting bodies. Utilizing the conservation of mass in the steady flow, the stick condition can be written in terms of the tangential strains. With the aid of the elastic solutions of the contacting bodies, this equation is written in terms of the contact stresses, so that a second functional relation for stresses as a function of the tangential coordinate is obtained. However, this relation applies only in the stick regions, which are not known in advance. Hence, an iteration scheme is usually applied for the determination of the location of the stick and slip areas.

One of the flaws in many winding nip studies [53,26] is that the contact is considered static instead of rolling. In static contact, the stick condition is expressed in terms of the tangential displacements and, hence, will result in significantly different equations and location of the stick and slip regions. As an example, consider the static and rolling contacts of two similar isotropic cylinders. The solutions were first presented by Cattaneo 1936 [7] (static) and Carter 1926 [6] (rolling). The diameter of the cylinders in this example is 0.5 m, the friction coefficient 0.5, Young's modulus $2.06 \cdot 10^{11}$ N/m^2 and Poisson's ratio 0.3 (steel). In both cases the other cylinder is driven by a torque of 21000 Nm/m and a compressive line load of 89000 N/m. The tangential tractions

resulting from the both cases are shown in Figure 5 as a function of the nip widthwise coordinate *x*. The dashed curve corresponds to the static contact, the solid line to the rolling contact. The material flow in the rolling contact is from left to right. Significant differences in the location of the slip areas and functional form of the curves is seen. The static tangential traction is symmetric with slip areas located at the leading and trailing edges. The mid area between the two maxima is in a state of stick. In the rolling contact there is a wide stick range starting from the leading edge and ending in the maximum of the tangential traction. In this example, the tangential tractions coincide in the short area along the trailing edge. As this simple example shows, the tangential tractions and hence, the stress state in the static and rolling contact are strikingly different.

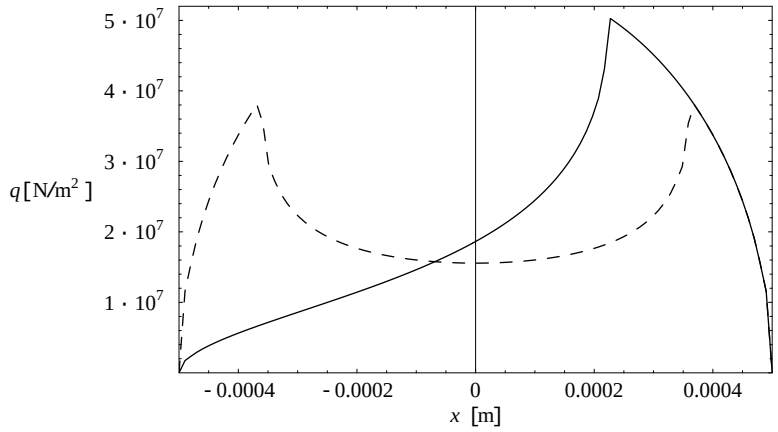

Figure 5. Tangential tractions in the rolling (solid line) and static (dashed line) contact of two similar cylinders.

In general, the normal and tangential tractions in the rolling contact are interacting [24]. However, the influence of tangential tractions upon the normal pressure and the contact area is generally small. The reverse is not true because the normal traction considerably affects the relative size and location of the stick zones. Hence, the normal pressure given by Hertz theory [20] for the frictionless contact does not differ significantly from the results obtained from the more general rolling contact theory (unless the winding drum cover is very thin). Hertz theory is based on three simplifying assumptions:

- The contact area is in general elliptical. In the case of contact of two cylinders with parallel axes, one of the semi-axes is infinite.
- Each contacting body can be regarded as an elastic half-space loaded over a small elliptical region on its plane surface
- The surfaces are assumed frictionless so that only normal pressure is transmitted.

Under these assumptions, an analytic expression can be derived for the contact pressure between contacting isotropic bodies. In Chapter 3, a generalization of the Hertz result for orthotropic contacting bodies will be derived. This result proves to be useful in the general winding contact problem because it gives an estimate of the contact width as a function of the compressive line load. Hence, it will be possible to eliminate or enhance the iteration of the contact area of the general solution procedure.

Despite the vast amount of literature that exists on the rolling contact of two parallel cylinders, a rigorous theory applicable to the winding nip is still lacking. Roughly speaking, the articles of interest fall into two non-overlapping categories:

a) two-dimensional rolling contact problem of calendering or two parallel cylinders
b) winding nip studies and models without proper contact mechanical treatment

In the following the most important publications from the both categories are briefly presented.

Bentall & Johnson [3,4] have studied the rolling contact of two cylinders with and without an elastic strip going through the nip. They restricted their treatment to isotropic materials, identical cylinders and essentially free rolling conditions. In addition, a half-space approximation for the cylinders was used and, hence, the theory is not suitable for a drum with a thin elastic cover. Tervonen [49] has extended the treatment to linear, viscoelastic cylinders and tractive rolling. His model includes covered cylinders and a sheet in the nip but is also restricted to isotropic materials. Soong & Li [45,46] have considered the rolling contact of two cylinders with linear, elastic and isotropic layers bonded to a hard core and driving an elastic thin sheet with extensional stiffness. The rolling contact articles referred above provide the closest analysis of the present problem. The only missing feature is that the paper web does not enter one of the cylinders.

J. D. Pfeiffer [41] reported in 1968 on extensive winding simulation tests done by rolling a drum on a flat horizontal bed with several paper layers clamped rigidly from the other end. This simulates the surface winding of an infinite radius wound roll. He observed that the sheets nearest the nip would displace in the direction of the moving nip while sheets further off the nip would travel in the opposite direction. He concluded that somewhere under the contact interface there must be an instant center of rotation. The tension increase was explained to be due to the velocity gradient between a point in the high-pressure area and another point in the direction of the outgoing nip having zero velocity. A corollary is that WOT is due to the interlayer slippage.

Jalkanen presented in 1968 [23] a theoretical model for calculating the Nip-Induced Tension in his M. Sc. thesis. His derivation was based on the assumption that the speed of the incoming sheet is equal to the speed of the winding drum from the leading edge to the center of the contact

and equal to the speed of the wound roll thereafter. He arrived at the following expression for nip-induced tension:

$$\mathrm{NIT} = E_t t \frac{\delta}{R} \ , \tag{9}$$

where E_t is the tangential modulus of the sheet, t the thickness of the sheet, δ the indentation depth in the middle of the nip and R the radius of the wound roll. Despite Pfeiffer's and Jalkanen's credit as forerunners in this field, their trains of thoughts were mainly kinematical and thus they could not give a comprehensive or general explanation for the NIT mechanism.

In 1993, J. K. Good and Z. Wu wrote an article entitled "The Mechanism of Nip-Induced Tension in Wound Rolls" [16] where they proposed a new explanation for the nip-induced tension. Their theory was based on similar phenomena as seen when rolling dough with a rolling pin: dough is extruding away from the nip under the rolling pin. The nip-induced tension was concluded to be caused by Poisson's effect, i.e., elongation of the sheet due to the compressive radial stress. Although Good & Wu seem to be the first to account for the stress state of the sheet, the shortcomings of their model include fairly strong initial assumptions on the internal nip mechanics and the lack of proper force equilibrium considerations.

Perhaps the first paper, where an attempt to apply the well-developed machinery of contact mechanics to the winding problem was made, is due to E. G. Welp and B. Guldenburg in 1997 [54]. The force equilibrium equations were correctly formed but their model did not properly describe the conditions of the sheet entering the wound roll after the nip, which is a distinctive feature of winding compared to calendering. Their model was also restricted to an isotropic material model of the paper web, which is actually known to be strongly anisotropic. Although their approach was a contact mechanical one, the solution methods used were not correct, since the stick and slip behavior was assumed and the iterative schemes for calculating the contact tractions were not carried out in full. The main deficiency in all previously mentioned studies is the lack of proper *Wound-On-Condition* (WOC) for the web wound onto the roll. WOC would provide an additional equation to the contact formulation describing mathematically the fact that the paper sheet fed into the winding nip will later become part of the wound roll.

Typically, the most elaborate part of the solution process of the rolling contact problem is the derivation of the elastic solutions of the contacting bodies, even if linear constitutive equations are used. An analytic, elastic solution for the isotropic half-space was originally derived by Flamant [11] and is concisely summarized by Johnson [24]. The Fourier series solution for the isotropic

covered cylinder is presented in the paper of Soong & Li [45,46]. Chapter 2 will be devoted to the derivation of the solutions for the two-dimensional traction boundary value problems of the orthotropic and elastic half-space, cylinder and thin sheet. The cylinder (or half-space) geometry is used for the wound roll, although it resembles rather the Archimedean spiral wrapped around the core. Actually, in addition to the contact pressure and tangential traction of the sheet, web tension on the first paper layer is loading the wound roll. In a solid cylinder model, this last mentioned load cannot properly be introduced. In this work, this defect is compensated for by the Wound-On-Condition.

It is well know that the relation between pressure and strain is nonlinear in the compression tests of paper stacks and thus the elastic moduli become state dependent [39]. Paper stacks display hysteresis when loaded and unloaded repeatedly [40]. Accounting for the nonlinear material behavior and hysteresis is beyond the scope of this work. As the goal here is to obtain a phenomenological description of the winding nip behavior, suitable "average" constant elastic moduli will be used.

2 ELASTIC SOLUTIONS OF THE CONTACTING BODIES

Procedures for determining the elastic solutions of the bodies in contact are needed in the solution process of the contact problem. This is because some of the basic contact equations are written in terms of the kinematical quantities within the contact and some in terms of the tractions. For a numerical solution of contact problems, it is often more convenient to work in terms of unknown tractions rather than displacements. Hence, the elastic solutions presented in this chapter provide the surface displacements in terms of the prescribed boundary tractions.

Non-conforming elastic bodies in contact whose deformation is sufficiently small for the linear small strain theory of elasticity to be applicable, inevitably make contact over an area whose dimensions are small compared with the radii of curvature (radius of the wound roll and winding drum) of the undeformed surfaces. The contact stresses are highly concentrated close to the contact region and decrease rapidly in intensity with distance from the point of contact, so that the region of practical interest lies close to the contact interface. Thus, provided the dimensions of the bodies themselves are large compared with the dimensions of the contact area the stresses in the region are not critically dependent upon the shape of the bodies at a distance from the contact area, nor upon the precise way in which they are supported (Saint Venant's principle). The stresses may be approximated accurately by considering the body as a semi-infinite elastic solid bounded by a plane surface, i.e., an elastic half-space.

The elastic solution for the loaded anisotropic half-space was first outlined by Lekhnitskii [27]. Lekhnitskii’s results were compiled for the orthotropic half-space in the papers of Tomlin *et al.* [51] and Mantič *et al.* [31]. Distinct methods, namely the so-called Stroh formalism, were utilized in the papers of Ting [50] and Nakamura *et al.* [33] to obtain the fundamental solution of anisotropic elasticity. Function theoretic methods for second order elliptic systems have been applied by Gilbert *et al.* [13] and Hua *et al.* [22] to present the general solution for the boundary value problems of orthotropic half-space and unit disks. In this thesis, the derivation of the solution for the elastic, orthotropic half-space follows the outline of Bjarnehed [5], although he formulated the problem in terms of the stress function, whereas here the elastic equations are written for the displacements. The solution generalizes the corresponding result for the elastic, isotropic half-space presented by Johnson [24]. As described above the half-space solution can be utilized for the wound roll when the radius of the roll and the thickness of the paper wound around the core are large compared to the width of the contact. Similarly, the half-space solution can be applied to the winding drum of uniform shell thickness.

When the assumptions for utilizing the half-space solution are not valid, the elastic solution for the orthotropic cylinder must be used. This is the case when the winding drum is covered with a layer of some soft material or the thickness of the paper wound around the core is small. In this work, the core of the cylinder is assumed to be rigid and, hence, a situation when only a few layers of paper has been wound would not yield satisfactory results if the core is compliant. When the number of wound paper layers is increased, the solution becomes acceptable according to Saint Venant's principle.

The elastic solution for the isotropic cylinder with a rigid core can be found in the references [18,45,46] but for the orthotropic material, the corresponding treatment seems to be lacking. However, the Fourier series solution presented for the isotropic cylinder can easily be extended for the orthotropic case as well. The disadvantage of the cylinder solution is that several thousands of Fourier series terms must by added to obtain a solution of reasonable accuracy. Hence, the half-space solution, being computationally more cost effective, will be utilized whenever suitable.

The exact elastic solution of the paper sheet is more difficult to obtain because of the finite dimensions of the sheet. In the half-space solution the boundary conditions on only one surface have to be imposed, whereas for a strip solution the boundary conditions on all four bounding surfaces must be accounted for.

An analytical solution for the sheet can be obtained by using the method of homogeneous solutions and biorthogonality properties of the 2D elasticity problem formulated in terms of the stress function and generalized biharmonic equation [28], by using the method of separation of variables leading to a general series representation [42,21], or by using a sixth degree polynomial for the stress function accounting for linearly changing boundary loads [21]. These solutions would be valid for any sheet thickness. However, due to the complexity of these methods, an alternative approximate solution, utilizing the thinness of the sheet, is considered here. An approximate solution of an arbitrary degree of accuracy can be obtained by a series expansion for the stress function in terms of polynomials in the transverse coordinate. This technique has been proposed by Donnell [8,9] for isotropic beams in plane bending, Duva and Simmonds [10] for orthotropic strips subjected to equal distributed transverse loads acting on the top and bottom surfaces and Tullini and Savoia [52] for orthotropic strips subjected to any given continuous distribution of both normal and shear loads. In this thesis a consistent, low order expansion, similar to what Tullini and Savoia presented, is developed by forcing the stresses to satisfy the boundary conditions and then integrating the displacements from the constitutive equations. The calculations are performed in the rectangular geometry, although the treatment could easily be extended to cylindrical coordinates.

2.1 Linear, elastic, orthotropic half-plane

Consider an elastic, orthotropic half-space loaded by a distributed pressure $p(x)$ and tangential traction $q(x)$ over the region from $x = -a$ to $x = a$ (Figure 6). It is required to find the components $\bar{u}_x$ and $\bar{u}_y$ of the elastic surface displacements. It is assumed that a state of plane strain ($\varepsilon_z = 0$) is produced by the loading. This is justified because the thickness of the solid is large compared with the width of the loaded region. The linear constitutive equations of the orthotropic half-plane can be written as

$$\sigma_x = A_{xx}\frac{\partial u_x}{\partial x} + A_{xy}\frac{\partial u_y}{\partial y},$$
$$\sigma_y = A_{xy}\frac{\partial u_x}{\partial x} + A_{yy}\frac{\partial u_y}{\partial y}, \qquad (10)$$
$$\tau_{xy} = G\left(\frac{\partial u_x}{\partial y} + \frac{\partial u_y}{\partial x}\right),$$

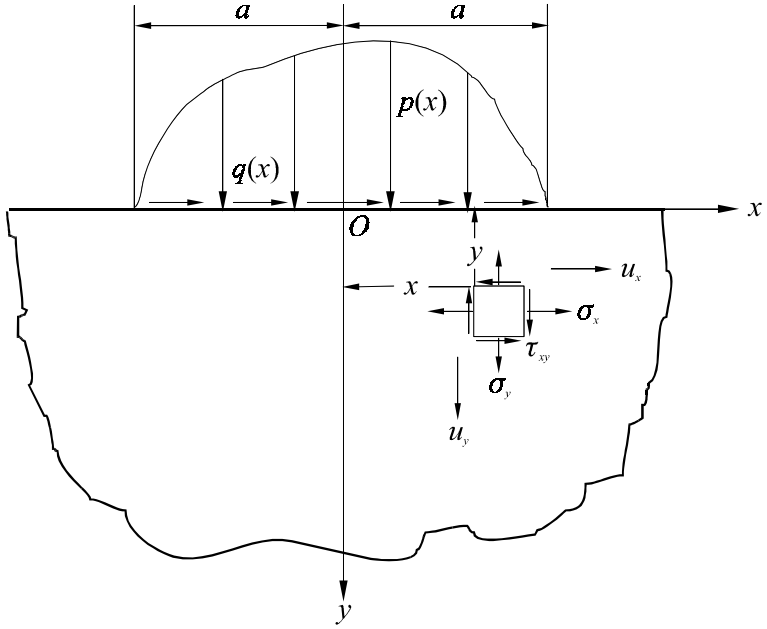

Figure 6. The orthotropic half-space loaded by tractions $p(x)$ and $q(x)$.

where the coefficients A_{xx}, A_{xy}, A_{yy} and G are the *orthotropic elastic constants* of the half-space. Incompressible materials will be excluded from the following treatment and, hence, it is assumed that $A_{xx}A_{yy} - A_{xy}^2 \neq 0$. Substituting Eqs. (10) into the equations of equilibrium with the absence of the body forces:

$$\frac{\partial \sigma_x}{\partial x} + \frac{\partial \tau_{xy}}{\partial y} = 0,$$
$$\frac{\partial \sigma_y}{\partial y} + \frac{\partial \tau_{xy}}{\partial x} = 0, \qquad (11)$$

the generalized *Navier equations* of the orthotropic elastic solid are obtained:

$$A_{xx}\frac{\partial^2 u_x}{\partial x^2}+G\frac{\partial^2 u_x}{\partial y^2}+(A_{xy}+G)\frac{\partial^2 u_y}{\partial x\partial y}=0\ ,$$
$$A_{yy}\frac{\partial^2 u_y}{\partial y^2}+G\frac{\partial^2 u_y}{\partial x^2}+(A_{xy}+G)\frac{\partial^2 u_x}{\partial x\partial y}=0\ . \tag{12}$$

Taking the Fourier transform with respect to the x-coordinate, and assuming that $u\to 0$ and $v\to 0$, as $x\to\pm\infty$ we get

$$-\omega^2 A_{xx}U_x+GU_x''-i\omega(A_{xy}+G)U_y'=0\ ,$$
$$A_{yy}U_y''-\omega^2 GU_y-i\omega(A_{xy}+G)U_x'=0\ , \tag{13}$$

where $'=d/dy$ and the Fourier transforms of u_x and u_y are defined by

$$U_x(\omega,y)=\int_{-\infty}^{\infty}u_x(x,y)e^{i\omega x}dx\ ,U_y(\omega,y)=\int_{-\infty}^{\infty}u_y(x,y)e^{i\omega x}dx\ . \tag{14}$$

In order to solve Eqs. (13) exponential trial solutions are introduced

$$U_x=ae^{\lambda y},$$
$$U_y=be^{\lambda y}, \tag{15}$$

where a, b and λ are constants, independent of y. After substituting (15) to (13) the following linear system for the coefficients a and b is obtained:

$$\begin{bmatrix}\lambda^2 G-\omega^2 A_{xx} & -i\omega\lambda(A_{xy}+G)\\ -i\omega\lambda(A_{xy}+G) & \lambda^2 A_{yy}-\omega^2 G\end{bmatrix}\begin{bmatrix}a\\ b\end{bmatrix}=\begin{bmatrix}0\\ 0\end{bmatrix}\ . \tag{16}$$

To obtain non-vanishing solutions the determinant of the coefficient matrix in Eq. (16) must be zero:

$$GA_{yy}\lambda^4-\left[G^2+A_{xx}A_{yy}-(A_{xy}+G)^2\right]\omega^2\lambda^2+A_{xx}G\omega^4=0\ . \tag{17}$$

The roots of the characteristic equation (17) are

$$\lambda_1 = -\frac{|\omega|}{\sqrt{2GA_{yy}}}\sqrt{\mu+\sqrt{\mu^2-\kappa}}\ ,\ \lambda_2 = -\frac{|\omega|}{\sqrt{2GA_{yy}}}\sqrt{\mu-\sqrt{\mu^2-\kappa}}\ ,$$
$$\lambda_3 = \frac{|\omega|}{\sqrt{2GA_{yy}}}\sqrt{\mu+\sqrt{\mu^2-\kappa}}\ \ ,\ \lambda_4 = \frac{|\omega|}{\sqrt{2GA_{yy}}}\sqrt{\mu-\sqrt{\mu^2-\kappa}}\ , \tag{18}$$

where the real constants μ and κ are defined as

$$\mu = A_{xx}A_{yy} + G^2 - (A_{xy}+G)^2\ ,$$
$$\kappa = 4A_{xx}A_{yy}G^2\ . \tag{19}$$

S. G. Lekhnitskii [27] showed that for general linear anisotropic material the roots (18) cannot have a vanishing real part. This imposes the constraint $\mu > -\sqrt{\kappa}$ on the elastic constants. It can be shown that that leads to the limitation $A_{xy} < \sqrt{A_{xx}A_{yy}}$ for the admissible values of the elastic constants. Hence, the roots can be rewritten as

$$\lambda_1 = -\alpha-\beta\ ,\ \lambda_2 = -\alpha+\beta\ ,$$
$$\lambda_3 = \alpha+\beta\ ,\ \lambda_4 = \alpha-\beta\ , \tag{20}$$

where

$$\alpha = \frac{|\omega|}{2\sqrt{A_{yy}G}}\sqrt{\mu+\sqrt{\kappa}}\ ,\ \beta = \frac{|\omega|}{2\sqrt{A_{yy}G}}\sqrt{\mu-\sqrt{\kappa}} \tag{21}$$

When $\mu \neq \sqrt{\kappa}$ the general solution of Eqs. (13) is

$$U_x = \sum_{i=1}^{4} a_i e^{|\omega|\tilde{\lambda}_i y}\ ,$$
$$U_y = i\sum_{i=1}^{4} \mathrm{sgn}(\omega)\eta_i a_i e^{|\omega|\tilde{\lambda}_i y}\ , \tag{22}$$

where

$$\tilde{\lambda}_i = \frac{\lambda_i}{|\omega|}\ ,\ \eta_i = \frac{A_{xx}-\tilde{\lambda}_i^2 G}{\tilde{\lambda}_i(A_{xy}+G)} \tag{23}$$

The boundary conditions on the plane $y = 0$ are

$$\begin{aligned}\sigma_y(x,0) &= A_{xy}\frac{\partial u_x}{\partial x}(x,0) + A_{yy}\frac{\partial u_y}{\partial y}(x,0) = -p(x)\,,\\ \tau_{xy}(x,0) &= G\frac{\partial u_x}{\partial y}(x,0) + G\frac{\partial u_y}{\partial x}(x,0) = -q(x)\,.\end{aligned} \tag{24}$$

Taking the Fourier transform from the equations above yields

$$\begin{aligned}-i\omega A_{xy}U_x(\omega,0) + A_{yy}U_y'(\omega,0) &= -P(\omega,0)\,,\\ GU_x'(\omega,0) - i\omega G U_y(\omega,0) &= -Q(\omega,0)\,,\end{aligned} \tag{25}$$

where P and Q are the Fourier transforms of p and q, respectively. The second set of boundary conditions is obtained by requiring that U_x and U_y are bounded functions of y. Inspection of the roots (20) reveals that λ_3 and λ_4 always have positive real parts when $\mu > -\sqrt{\kappa}$ and, hence, coefficients a_3 and a_4 in the solutions (22) must vanish.

Substitution of (22) to the boundary conditions (25) yields the following system for a_1 and a_2:

$$\begin{bmatrix} A_{yy}\tilde{\lambda}_1\eta_1 - A_{xy} & A_{yy}\tilde{\lambda}_2\eta_2 - A_{xy} \\ G(\tilde{\lambda}_1 + \eta_1) & G(\tilde{\lambda}_2 + \eta_2)\end{bmatrix}\begin{bmatrix} a_1 \\ a_2\end{bmatrix} = \begin{bmatrix} -P/(i\omega) \\ -Q/|\omega|\end{bmatrix}. \tag{26}$$

The solution is

$$\begin{bmatrix} a_1 \\ a_2\end{bmatrix} = \frac{1}{\Delta}\begin{bmatrix} G(\tilde{\lambda}_2 + \eta_2) & -A_{yy}\tilde{\lambda}_2\eta_2 + A_{xy} \\ -G(\tilde{\lambda}_1 + \eta_1) & A_{yy}\tilde{\lambda}_1\eta_1 - A_{xy}\end{bmatrix}\begin{bmatrix} -P/(i\omega) \\ -Q/|\omega|\end{bmatrix}. \tag{27}$$

where

$$\Delta = (A_{yy}\tilde{\lambda}_1\eta_1 - A_{xy})G(\tilde{\lambda}_2 + \eta_2) - (A_{yy}\tilde{\lambda}_2\eta_2 - A_{xy})G(\tilde{\lambda}_1 + \eta_1)\,. \tag{28}$$

Utilizing the result above, the Fourier transform of the displacements (22), evaluated at $y = 0$, becomes

$$U_x(\omega,0) = AP(\omega)/(i\omega) + BQ(\omega)/|\omega| ,$$
$$U_y(\omega,0) = CP(\omega)/|\omega| - AQ(\omega)/(i\omega) , \tag{29}$$

where the coefficients *A, B* and *C* are

$$A = \frac{1}{\sqrt{A_{xx}A_{yy}} + A_{xy}} ,$$
$$B = \sqrt{\frac{A_{yy}}{G}}\,\frac{\sqrt{A_{xx}A_{yy} + 2G\sqrt{A_{xx}A_{yy}} - A_{xy}(A_{xy}+2G)}}{A_{xx}A_{yy} - A_{xy}^2} , \tag{30}$$
$$C = \sqrt{\frac{A_{xx}}{G}}\,\frac{\sqrt{A_{xx}A_{yy} + 2G\sqrt{A_{xx}A_{yy}} - A_{xy}(A_{xy}+2G)}}{A_{xx}A_{yy} - A_{xy}^2} .$$

The inverse Fourier transforms

$$\bar{u}_x(x) = u_x(x,0) = \frac{1}{2\pi}\int_{-\infty}^{\infty} U_x(\omega,0)e^{-i\omega x}d\omega \ , \ \bar{u}_y(x) = u_y(x,0) = \frac{1}{2\pi}\int_{-\infty}^{\infty} U_y(\omega,0)e^{-i\omega x}d\omega , \tag{31}$$

can be written as convolution integrals

$$\bar{u}_x(x) = -\frac{A}{2}\left\{\int_{-a}^{x} p(s)ds - \int_{x}^{a} p(s)ds\right\} - \frac{B}{\pi}\int_{-\infty}^{\infty} q(s)\ln|x-s|ds + C_1 ,$$
$$\bar{u}_y(x) = -\frac{C}{\pi}\int_{-\infty}^{\infty} p(s)\ln|x-s|ds + \frac{A}{2}\left\{\int_{-a}^{x} q(s)ds - \int_{x}^{a} q(s)ds\right\} + C_2 , \tag{32}$$

when the inverse transforms of functions $1/|\omega|$ and $1/(i\omega)$

$$\frac{1}{2\pi}\int_{-\infty}^{\infty}\frac{e^{-i\omega x}}{|\omega|}d\omega == -\frac{1}{\pi}\ln|x| + \text{constant} ,$$
$$\frac{1}{2\pi}\int_{-\infty}^{\infty}\frac{e^{-i\omega x}}{i\omega}d\omega = -1/2\,\text{sgn}\,x \tag{33}$$

are utilized. Although result (32) was derived for $\mu \neq \sqrt{\kappa}$, it can be proved to be valid for all admissible ($\mu > -\sqrt{\kappa}$) values of the elastic constants.

2.2 Linear, elastic, orthotropic cylinder

An elastic, orthotropic cylinder of radius R is loaded by the distributed pressure $p(\theta)$ and tangential traction $q(\theta)$ over the outer surface (Figure 7). It is required to find the components $\overline{u}_r$ and $\overline{u}_\theta$ of the elastic surface displacements. The state of plane strain ($\varepsilon_z = 0$) is assumed to be produced by the loading. However, this assumption is not essential to the following treatment and the results are applicable to the state of plane stress as well. In either case the linear constitutive equations of the orthotropic cylinder can be written as

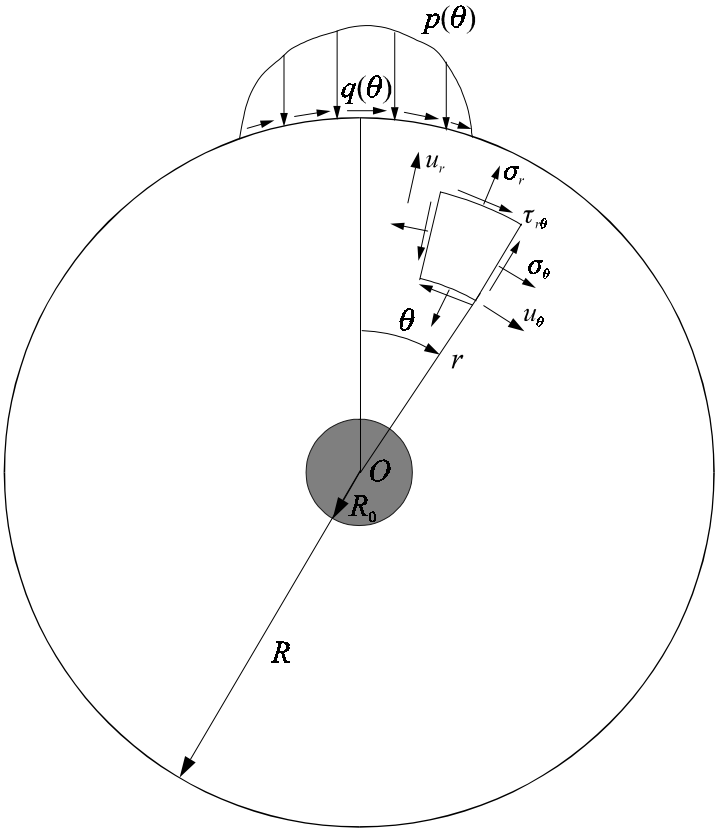

Figure 7. Orthotropic cylinder loaded by tractions $p(\theta)$ and $q(\theta)$.

$$\begin{aligned}
\sigma_r &= A_{rr}\frac{\partial u_r}{\partial r} + A_{r\theta}\left(\frac{u_r}{r} + \frac{1}{r}\frac{\partial u_\theta}{\partial \theta}\right),\\
\sigma_\theta &= A_{r\theta}\frac{\partial u_r}{\partial r} + A_{\theta\theta}\left(\frac{u_r}{r} + \frac{1}{r}\frac{\partial u_\theta}{\partial \theta}\right),\\
\tau_{r\theta} &= G_{r\theta}\left(\frac{1}{r}\frac{\partial u_r}{\partial \theta} + \frac{\partial u_\theta}{\partial r} - \frac{u_\theta}{r}\right),
\end{aligned} \tag{34}$$

where the coefficients A_{rr}, $A_{r\theta}$, $A_{\theta\theta}$ and $G_{r\theta}$ are the *orthotropic elastic constants* of the cylinder. The equations of equilibrium in the cylindrical coordinates (r, θ) are

$$\begin{aligned}
&\frac{\partial \sigma_r}{\partial r} + \frac{1}{r}\frac{\partial \tau_{r\theta}}{\partial \theta} + \frac{\sigma_r - \sigma_\theta}{r} + F_r = 0,\\
&\frac{\partial \tau_{r\theta}}{\partial r} + \frac{1}{r}\frac{\partial \sigma_\theta}{\partial \theta} + 2\frac{\tau_{r\theta}}{r} + F_\theta = 0,
\end{aligned} \tag{35}$$

where F_r and F_θ are the body force components in the radial and tangential directions, respectively. When the stress-displacement relations (34) are substituted into the equilibrium equations above, the following partial differential equation system for the displacements is obtained:

$$\begin{aligned} &A_{rr}\frac{\partial^2 u_r}{\partial r^2}+\frac{G_{r\theta'}}{r^2}\frac{\partial^2 u_r}{\partial \theta^2}+\frac{A_{r\theta}+G_{r\theta}}{r}\frac{\partial^2 u_\theta}{\partial r\partial\theta}+\frac{A_{rr}}{r}\frac{\partial u_r}{\partial r}-\frac{A_{\theta\theta}+G_{r\theta}}{r^2}\frac{\partial u_\theta}{\partial\theta}-\frac{A_{\theta\theta}}{r^2}u_r=F_r\ ,\\ &G_{r\theta}\frac{\partial^2 u_\theta}{\partial r^2}+\frac{A_{\theta\theta}}{r^2}\frac{\partial^2 u_\theta}{\partial \theta^2}+\frac{A_{r\theta}+G_{r\theta}}{r}\frac{\partial^2 u_r}{\partial r\partial\theta}+\frac{G_{r\theta}}{r}\frac{\partial u_\theta}{\partial r}+\frac{A_{\theta\theta}+G_{r\theta}}{r^2}\frac{\partial u_r}{\partial\theta}-\frac{G_{r\theta}}{r^2}u_\theta=F_\theta\ . \end{aligned} \tag{36}$$

Since the displacements must be 2π periodic with respect to θ, it is suitable to seek the solutions in the form of Fourier series, i.e.,

$$\begin{aligned} u_r(r,\theta)&=u_0(r)+\sum_{n=1}^{\infty}\left[u_n^s(r)\sin n\theta+u_n^c(r)\cos n\theta\right],\\ u_\theta(r,\theta)&=v_0(r)+\sum_{n=1}^{\infty}\left[v_n^s(r)\sin n\theta+v_n^c(r)\cos n\theta\right]. \end{aligned} \tag{37}$$

Utilizing the well known [44] orthogonality properties of the functions {1, sinθ, sin2θ, ..., cosθ, cos2θ,...} and assuming that the displacements are continuously twice differentiable with respect to θ, the following set of ordinary differential equations for the Fourier coefficient functions $u_0(r)$, $v_0(r)$, $u_n^s(r)$, $u_n^c(r)$, $v_n^s(r)$ and $v_n^c(r)$ is obtained after substitution of expansions (37) into (36) (with $F_r = F_\theta = 0$)

$$\begin{aligned} &A_{rr}u_0''+\frac{A_{rr}}{r}u_0'-\frac{A_{\theta\theta}}{r^2}u_0=0\ ,\\ &v_0''+\frac{1}{r}v_0'-v_0=0\ ,\\ &A_{rr}u_n''^s+\frac{A_{rr}}{r}u_n'^s-\frac{A_{\theta\theta}+n^2G_{r\theta}}{r^2}u_n^s-\frac{A_{r\theta}+G_{r\theta}}{r}nv_n'^c+\frac{A_{\theta\theta}+G_{r\theta}}{r^2}nv_n^c=0\ ,\\ &G_{r\theta}v_n''^c+\frac{G_{r\theta}}{r}v_n'^c-\frac{G_{r\theta}+n^2A_{\theta\theta}}{r^2}v_n^c+\frac{A_{r\theta}+G_{r\theta}}{r}nu_n'^s+\frac{A_{\theta\theta}+G_{r\theta}}{r^2}nu_n^s=0\ ,\\ &A_{rr}u_n''^c+\frac{A_{rr}}{r}u_n'^c-\frac{A_{\theta\theta}+n^2G_{r\theta}}{r^2}u_n^c+\frac{A_{r\theta}+G_{r\theta}}{r}nv_n'^s-\frac{A_{\theta\theta}+G_{r\theta}}{r^2}nv_n^s=0\ ,\\ &G_{r\theta}v_n''^s+\frac{G_{r\theta}}{r}v_n'^s-\frac{G_{r\theta}+n^2A_{\theta\theta}}{r^2}v_n^s-\frac{A_{r\theta}+G_{r\theta}}{r}nu_n'^c-\frac{A_{\theta\theta}+G_{r\theta}}{r^2}nu_n^c=0\ , \end{aligned} \tag{38}$$

where the prime denotes differentiation with respect to r. It should be noted that the third and fourth equations form a differential equation system solely for $u_n^s(r)$ and $v_n^c(r)$ and the fifth and sixth

solely for $u_n^c(r)$ and $v_n^s(r)$. In addition, it can be shown that if $u_n^s(r)=\phi(r)$ and $v_n^c(r)=\varphi(r)$ are solutions for the third and fourth equations then $u_n^c(r)=\phi(r)$ and $v_n^s(r)=-\varphi(r)$ will satisfy the fifth and sixth equations. Hence, it is sufficient to solve the first to fourth equations.

The first and second equations of (38) are easily solved since they are uncoupled. The result is

$$u_0(r)=\sum_{m=1}^{2} b_{0m}\phi_{0m}(r)\ ,\ v_0(r)=\sum_{m=1}^{2} a_{0m}\varphi_{0m}(r)\ , \tag{39}$$

where the coefficients b_{0m} and a_{0m} are determined from the boundary conditions and

$$\begin{aligned}&\phi_{0m}(r)=r^{\lambda_{0m}}\ ,\ \lambda_{01}=-\lambda_{02}=\sqrt{\frac{A_{\theta\theta}}{A_{rr}}}\ ,\\ &\varphi_{01}(r)=r\ ,\ \varphi_{02}(r)=r^{-1}\ .\end{aligned} \tag{40}$$

To solve the third and fourth equations of (38), the exponential trial solutions

$$u_n^s(r)=ar^{\lambda}\ ,\ v_n^c(r)=\tilde{a}r^{\lambda}\ , \tag{41}$$

are introduced. Substitution into (38) leads to the following linear system for the coefficients a and $\tilde{a}$:

$$\begin{bmatrix} A_{rr}\lambda^2-A_{\theta\theta}-n^2G_{r\theta} & -(A_{r\theta}+G_{r\theta})n\lambda+(A_{\theta\theta}+G_{r\theta})n \\ (A_{r\theta}+G_{r\theta})n\lambda+(A_{\theta\theta}+G_{r\theta})n & G_{r\theta}\lambda^2-G_{r\theta}-n^2A_{\theta\theta}\end{bmatrix}\begin{bmatrix}a\\ \tilde{a}\end{bmatrix}=\begin{bmatrix}0\\0\end{bmatrix}\ . \tag{42}$$

To obtain non-vanishing solutions the determinant of the coefficient matrix of Eq. (42) must be zero:

$$A_{rr}G_{r\theta}\lambda^4-[A_{rr}(G_{r\theta}+n^2A_{\theta\theta})-A_{r\theta}(A_{r\theta}+2G_{r\theta})n^2+A_{\theta\theta}G_{r\theta}]\lambda^2+A_{\theta\theta}G_{r\theta}(n^2-1)^2=0 \tag{43}$$

The roots of the characteristic Eq. (43) are (n = 2, 3, 4, ...)

$$\lambda_{11} = -\lambda_{12} = \sqrt{\frac{\mu_1}{A_{rr}G_{r\theta}}}\,, \qquad \lambda_{13} = \lambda_{14} = 0 \quad ,$$
$$\lambda_{n1} = -\lambda_{n2} = \sqrt{\frac{\mu_n + \sqrt{\mu_n^2 - \kappa_n}}{2A_{rr}G_{r\theta}}} \quad , \quad \lambda_{n3} = -\lambda_{n4} = \sqrt{\frac{\mu_n - \sqrt{\mu_n^2 - \kappa_n}}{2A_{rr}G_{r\theta}}} \ , \tag{44}$$

where the real constants μ_n and κ_n are defined by

$$\mu_n = A_{\theta\theta}G_{r\theta} - A_{r\theta}(A_{r\theta} + 2G_{r\theta})n^2 + A_{rr}(G_{r\theta} + A_{\theta\theta}n^2)\,,$$
$$\kappa_n = 4A_{rr}A_{\theta\theta}G_{r\theta}^2(n^2-1)^2\ . \tag{45}$$

As in the previous section, Lekhnitskii's statement [27] can be applied and, hence, the roots λ_{nm} (n = 2, 3, 4, ..., m =1, 2, 3, 4) cannot have vanishing real parts. It can be shown that that leads to the constraint $A_{r\theta} < \sqrt{A_{rr}A_{\theta\theta}}$ for the admissible values of the elastic constants. For each λ_{nm} the ratio of the coefficients a and $\tilde{a}$ is determined from Equation (42). Hence, the coefficient functions of the Fourier series are

$$u_0(r) = \sum_{m=1}^{2} b_{0m}\phi_{0m}(r)\,, \quad v_0(r) = \sum_{m=1}^{2} a_{0m}\varphi_{0m}(r)\,,$$
$$u_n^s(r) = \sum_{m=1}^{4} a_{nm}\phi_{nm}(r)\,, \quad v_n^c(r) = \sum_{m=1}^{4} a_{nm}\varphi_{nm}(r)\,, \tag{46}$$
$$u_n^c(r) = \sum_{m=1}^{4} b_{nm}\phi_{nm}(r)\,, \quad v_n^s(r) = \sum_{m=1}^{4} -b_{nm}\varphi_{nm}(r)\,.$$

The coefficients a_{nm} and b_{nm} are determined from the boundary conditions and the functions ϕ_{nm} and φ_{nm} are given by

$$\phi_{13}(r) = \ln r\ , \quad \phi_{14}(r) = 1\,,$$
$$\varphi_{01}(r) = r\ , \quad \varphi_{02}(r) = r^{-1}\ , \quad \varphi_{13}(r) = \ln r + \frac{A_{r\theta} + G_{r\theta}}{A_{\theta\theta} + G_{r\theta}}\ , \quad \varphi_{14}(r) = 1\,, \tag{47}$$
$$\phi_{nm}(r) = r^{\lambda_{nm}}\ , \quad \varphi_{nm}(r) = \eta_{nm}r^{\lambda_{nm}}\ ,$$

where the coefficients η_{nm} are defined by

$$\eta_{nm} = \frac{A_{rr}\lambda_{nm}^2 - A_{\theta\theta} - n^2G_{r\theta}}{(A_{r\theta} + G_{r\theta})n\lambda_{nm} - (A_{\theta\theta} + G_{r\theta})n}, \ (n = 2,3,4,\ldots, m = 1,2,3,4)\ . \tag{48}$$

The boundary conditions of the problem consist of prescribed tractions at the periphery and an undeformable core:

$$\begin{aligned} &\sigma_r(R,\theta) = -p(\theta)\,, \quad \tau_{r\theta}(R,\theta) = q(\theta)\,, \\ &u_r(R_0,\theta) = 0\,, \qquad\quad u_\theta(R_0,\theta) = 0\,. \end{aligned} \tag{49}$$

It is assumed that $p(\theta)$ and $q(\theta)$ are well-behaving functions, and thus admit the Fourier series presentations

$$\begin{aligned} p(\theta) &= c_0 + \sum_{n=1}^{\infty}\left(d_n \sin n\theta + c_n \cos n\theta\right), \\ q(\theta) &= e_0 + \sum_{n=1}^{\infty}\left(f_n \sin n\theta + e_n \cos n\theta\right), \end{aligned} \tag{50}$$

where the Fourier coefficients are calculated by the following integrals

$$\begin{aligned} &c_0 = \frac{1}{2\pi}\int_0^{2\pi} p(\theta)d\theta,\ c_n = \frac{1}{\pi}\int_0^{2\pi} p(\theta)\cos n\theta d\theta\,,\ d_n = \frac{1}{\pi}\int_0^{2\pi} p(\theta)\sin n\theta d\theta\,, \\ &e_0 = \frac{1}{2\pi}\int_0^{2\pi} q(\theta)d\theta,\ e_n = \frac{1}{\pi}\int_0^{2\pi} q(\theta)\cos n\theta d\theta\,,\ f_n = \frac{1}{\pi}\int_0^{2\pi} q(\theta)\sin n\theta d\theta\,. \end{aligned} \tag{51}$$

The Fourier series presentations of radial and shear stress are obtained from the constitutive equations (34) with the aid of the Fourier series of displacements (37) and Eq. (46)

$$\begin{aligned} &\sigma_r(r,\theta) = \sum_{m=1}^{2} b_{0m}\left[A_{rr}\phi'_{0m}(r) + \frac{A_{r\theta}}{r}\phi_{0m}(r)\right] + \\ &\sum_{n=1}^{\infty}\sum_{m=1}^{4} a_{nm}\left\{A_{rr}\phi'_{nm}(r) + \frac{A_{r\theta}}{r}\left[\phi_{nm}(r) - n\varphi_{nm}(r)\right]\right\}\sin n\theta + \\ &\sum_{n=1}^{\infty}\sum_{m=1}^{4} b_{nm}\left\{A_{rr}\phi'_{nm}(r) + \frac{A_{r\theta}}{r}\left[\phi_{nm}(r) - n\varphi_{nm}(r)\right]\right\}\cos n\theta\,, \\ &\tau_{r\theta}(r,\theta) = G_{r\theta}\sum_{m=1}^{2} a_{0m}\left[\varphi'_{0m}(r) - \frac{1}{r}\varphi_{0m}(r)\right] + \\ &\sum_{n=1}^{\infty}\sum_{m=1}^{4} b_{nm}\left[\frac{1}{r}\varphi_{nm}(r) - \frac{n}{r}\phi_{nm}(r) - \varphi'_{nm}(r)\right]\sin n\theta - \\ &\sum_{n=1}^{\infty}\sum_{m=1}^{4} a_{nm}\left[\frac{1}{r}\varphi_{nm}(r) - \frac{n}{r}\phi_{nm}(r) - \varphi'_{nm}(r)\right]\cos n\theta\,. \end{aligned} \tag{52}$$

Now the boundary conditions (49) can be applied, and the following equations for the coefficients a_{nm} and b_{nm} are obtained

$$\begin{bmatrix} 0 & -2G_{r\theta}R^{-2} \\ R_0 & R_0^{-1} \end{bmatrix}\begin{bmatrix} a_{01} \\ a_{02} \end{bmatrix} = \begin{bmatrix} e_0 \\ 0 \end{bmatrix},$$
$$\begin{bmatrix} (A_{r\theta}+A_{rr}\lambda_{01})R^{\lambda_{01}-1} & (A_{r\theta}+A_{rr}\lambda_{02})R^{\lambda_{02}-1} \\ R_0^{\lambda_{01}} & R_0^{\lambda_{02}} \end{bmatrix}\begin{bmatrix} b_{01} \\ b_{02} \end{bmatrix} = \begin{bmatrix} -c_0 \\ 0 \end{bmatrix}, \tag{53}$$

$$\begin{bmatrix} [A_{r\theta}(1-\eta_{11})+A_{rr}\lambda_{11}]R^{\lambda_{11}-1} & [A_{r\theta}(1-\eta_{12})+A_{rr}\lambda_{12}]R^{\lambda_{12}-1} & \left(A_{rr}-A_{r\theta}\frac{A_{r\theta}+G_{r\theta}}{A_{\theta\theta}+G_{r\theta}}\right)R^{-1} & 0 \\ G_{r\theta}[\eta_{11}(\lambda_{11}-1)+1]R^{\lambda_{11}-1} & G_{r\theta}[\eta_{12}(\lambda_{12}-1)+1]R^{\lambda_{12}-1} & G_{r\theta}\frac{A_{\theta\theta}-A_{r\theta}}{A_{\theta\theta}+G_{r\theta}}R^{-1} & 0 \\ R_0^{\lambda_{11}} & R_0^{\lambda_{12}} & \ln R_0 & 1 \\ \eta_{11}R_0^{\lambda_{11}} & \eta_{12}R_0^{\lambda_{12}} & \ln R_0+\frac{A_{r\theta}+G_{r\theta}}{A_{\theta\theta}+G_{r\theta}} & 1 \end{bmatrix}\begin{bmatrix} a_{11} \\ a_{12} \\ a_{13} \\ a_{14} \end{bmatrix} = \begin{bmatrix} -d_1 \\ e_1 \\ 0 \\ 0 \end{bmatrix},$$
$$\begin{bmatrix} [A_{r\theta}(1-\eta_{11})+A_{rr}\lambda_{11}]R^{\lambda_{11}-1} & [A_{r\theta}(1-\eta_{12})+A_{rr}\lambda_{12}]R^{\lambda_{12}-1} & \left(A_{rr}-A_{r\theta}\frac{A_{r\theta}+G_{r\theta}}{A_{\theta\theta}+G_{r\theta}}\right)R^{-1} & 0 \\ G_{r\theta}[\eta_{1,1}(\lambda_{1,1}-1)+1]R^{\lambda_{1,1}-1} & G_{r\theta}[\eta_{1,2}(\lambda_{1,2}-1)+1]R^{\lambda_{1,2}-1} & G_{r\theta}\frac{A_{\theta\theta}-A_{r\theta}}{A_{\theta\theta}+G_{r\theta}}R^{-1} & 0 \\ R_0^{\lambda_{11}} & R_0^{\lambda_{12}} & \ln R_0 & 1 \\ \eta_{11}R_0^{\lambda_{11}} & \eta_{12}R_0^{\lambda_{12}} & \ln R_0+\frac{A_{r\theta}+G_{r\theta}}{A_{\theta\theta}+G_{\theta\theta}} & 1 \end{bmatrix}\begin{bmatrix} b_{11} \\ b_{12} \\ b_{13} \\ b_{14} \end{bmatrix} = -\begin{bmatrix} c_1 \\ f_1 \\ 0 \\ 0 \end{bmatrix}, \tag{54}$$

$$\sum_{m=1}^{4}\left(A_{r\theta}(1-n\eta_{nm})+A_{rr}\lambda_{nm}\right)R^{\lambda_{nm}-1}a_{nm} = -d_n\ ,\ \sum_{m=1}^{4}\left(G_{r\theta}\left[\eta_{nm}(\lambda_{nm}-1)+n\right]\right)R^{\lambda_{nm}-1}a_{nm} = e_n,$$
$$\sum_{m=1}^{4}R_0^{\lambda_{nm}}a_{nm} = 0\ ,\ \sum_{i=1}^{4}\eta_{nm}R_0^{\lambda_{nm}}a_{nm} = 0\ ,\ (n=2,3,4,\ldots)\ ,$$
$$\sum_{m=1}^{4}\left(A_{r\theta}(1-n\eta_{nm})+A_{rr}\lambda_{nm}\right)R^{\lambda_{nm}-1}b_{nm} = -c_n\ ,\ \sum_{m=1}^{4}\left(G_{r\theta}\left[\eta_{nm}(\lambda_{nm}-1)+n\right]\right)R^{\lambda_{nm}-1}b_{nm} = -f_n,$$
$$\sum_{m=1}^{4}R_0^{\lambda_{nm}}b_{nm} = 0\ ,\ \sum_{m=1}^{4}\eta_{nm}R_0^{\lambda_{nm}}b_{nm} = 0\ ,\ (n=2,3,4,\ldots). \tag{55}$$

In the following, the terms of the first and second coefficient matrices of (53) are denoted by $\hat{C}_{ij}$ and $\tilde{C}_{ij}$, $(i,j=1,2)$, respectively. The terms of the coefficient matrices of (54) and (55) will be denoted by $C_{ij,n}$, (i,j = 1,2,3,4 , n = 1,2,3,...). With these notations, the solution to Eqs. (53)-(55) can be written as

$$a_{0m} = \hat{C}_{m1}^{-1}e_0 \quad , \quad b_{0m} = -\tilde{C}_{m1}^{-1}c_0 \quad ,$$
$$a_{nm} = -C_{m1,n}^{-1}d_n + C_{m2,n}^{-1}e_n\ , \quad b_{nm} = -C_{m1,n}^{-1}c_n - C_{m2,n}^{-1}f_n\ . \tag{56}$$

The characteristic sequences of the cylinder surface are defined as

$$\gamma_0 = \sum_{m=1}^{2} \tilde{C}_{m1}^{-1}\phi_{0m}(R)\ , \quad \chi_0 = \sum_{m=1}^{2} \hat{C}_{m1}^{-1}\varphi_{0m}(R)\ ,$$
$$\gamma_{n,1} = \sum_{m=1}^{4} C_{m1}^{-1}\phi_{nm}(R)\ , \chi_{n,1} = \sum_{m=1}^{4} C_{m1}^{-1}\varphi_{nm}(R)\ , \tag{57}$$
$$\gamma_{n,2} = \sum_{m=1}^{4} C_{m2}^{-1}\phi_{nm}(R)\ , \chi_{n,2} = \sum_{m=1}^{4} C_{m2}^{-1}\varphi_{nm}(R)\ .$$

Utilizing Eqs. (56) and (57) the Fourier coefficients of the displacements (46) evaluated at $r = R$ become

$$u_0(R) = -\gamma_0 c_0 \quad , \quad v_0(R) = \chi_0 e_0 \quad ,$$
$$u_n^s(R) = -\gamma_{n,1} d_n + \gamma_{n,2} e_n\ , v_n^c(R) = -\chi_{n,1} d_n + \chi_{n,2} e_n\ , \tag{58}$$
$$u_n^c(R) = -\gamma_{n,1} c_n - \gamma_{n,2} f_n\ ,\ v_n^s(R) = \chi_{n,1} c_n + \chi_{n,2} f_n\ .$$

Hence, the following Fourier series presentations are obtained for the cylinder surface displacements

$$\bar{u}_r(\theta) = u_r(R,\theta) = -\gamma_0 c_0 + \sum_{n=1}^{\infty}\left[\left(-\gamma_{n,1} d_n + \gamma_{n,2} e_n\right)\sin n\theta - \left(\gamma_{n,1} c_n + \gamma_{n,2} f_n\right)\cos n\theta\right],$$
$$\bar{u}_\theta(\theta) = u_\theta(R,\theta) = \chi_0 e_0 + \sum_{n=1}^{\infty}\left[\left(\chi_{n,1} c_n + \chi_{n,2} f_n\right)\sin n\theta + \left(-\chi_{n,1} d_n + \chi_{n,2} e_n\right)\cos n\theta\right]. \tag{59}$$

2.3 Linear, elastic, orthotropic thin strip

An elastic, orthotropic thin sheet of thickness $2h$ is loaded by the distributed pressures $p^+(x)$, $p^-(x)$, tangential tractions $q^+(x)$, $q^-(x)$ and web tensions T_{in} and T_{out} as shown in Figure 8. The coordinate system is in the center of the rectangular strip, so that the edges are at $x = \pm a$. It is assumed that at the ends of the strip the x-direction stress is uniform and shear stress vanishes. The components u_x^+, u_y^+ and u_x^-, u_y^- of the elastic surface displacements of the top and bottom faces, respectively, must be found

The Taylor series expansion of the shear stress with respect to y is

$$\tau_{xy}(x,y) = \frac{1}{2}\left[q^-(x) - q^+(x)\right] - \frac{y}{2h}\left[q^+(x) + q^-(x)\right] + \frac{1}{2}g(x)\left(y^2 - h^2\right) + 0(y^3)\ , \tag{60}$$

where $g(x)$ is an unknown function. The positive direction of the tangential tractions q^+ and q^- is towards the negative x-axis.

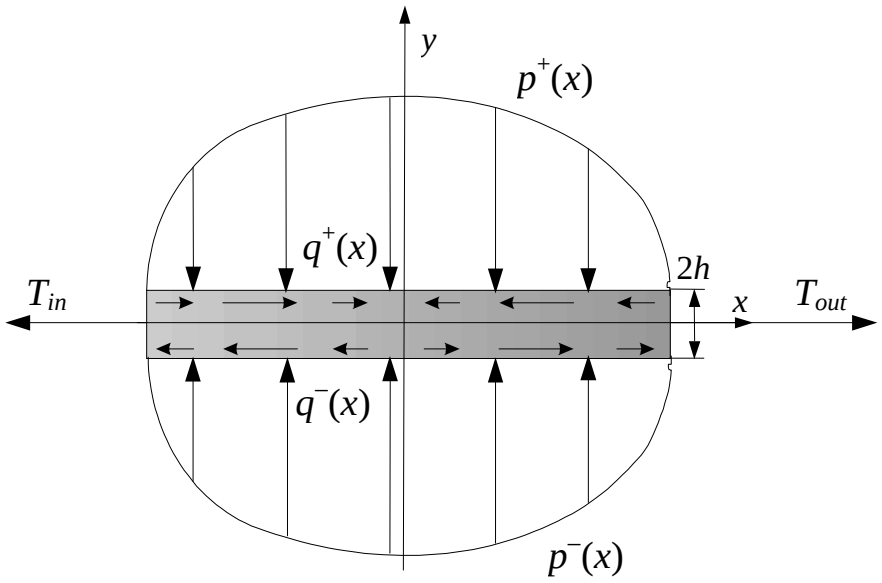

Figure 8. Orthotropic thin strip, loaded by tractions $p^+(x)$, $p^-(x)$, $q^+(x)$ and $q^-(x)$ and web tensions T_{in} and T_{out}.

Integration of $\sigma_x(x,y)$ from the horizontal equilibrium equation of (11) yields

$$\sigma_x(x,y)=\frac{1}{2h}\left\{T_{in}+\int_{-a}^{x}\left[q^+(\zeta)+q^-(\zeta)\right]d\zeta\right\}-y\int_{-a}^{x}g(\zeta)d\zeta+0(y^2)\,. \tag{61}$$

The vertical equilibrium equation of (11) is integrated first from h to y and then from $-h$ to y; the resulting equations are then added to get the expression for $\sigma_y(x,y)$ and subtracted to obtain the relationship between the tangential and normal tractions. The final expression for $\sigma_y(x,y)$ is

$$\sigma_y(x,y)=-\frac{1}{2}\left[p^+(x)+p^-(x)\right]-\frac{y}{2h}\left[p^+(x)-p^-(x)\right]+\frac{y^2-h^2}{4h}\left[q'^+(x)+q'^-(x)\right]-\frac{y}{6}\left(y^2-h^2\right)g'(x)+0(y^4)\,. \tag{62}$$

Now the stresses (60), (61) and (62) satisfy the equations of equilibrium (11) and the boundary conditions of the problem. What remains is to find expressions for the displacements $u_x(x,y)$ and $u_y(x,y)$ which satisfy the linear constitutive equations of the orthotropic material

$$\begin{aligned}
\frac{\partial u_x}{\partial x} &= c_{11}\sigma_x + c_{12}\sigma_y \ , \\
\frac{\partial u_y}{\partial y} &= c_{12}\sigma_x + c_{22}\sigma_y \ , \\
\frac{\partial u_x}{\partial y} &+ \frac{\partial u_y}{\partial x} = c_{66}\tau_{xy} \ ,
\end{aligned} \tag{63}$$

where c_{11}, c_{12}, c_{22} and c_{66} are the *orthotropic compliances* of the solid. Integration of the first and second equations above yields the expressions

$$\begin{aligned}
&u_x(x,y) = \frac{c_{11}}{2h}\left\{T_{out}\left(x+a\right) + \int_{-a}^{x}(x-\zeta)\left[q^+(\zeta)+q^-(\zeta)\right]d\zeta\right\} - c_{11}y\int_{-a}^{x}(x-\zeta)g(\zeta)d\zeta - \\
&\frac{c_{12}}{2}\int_{-a}^{x}\left[p^+(\zeta)+p^-(\zeta)\right]d\zeta - c_{12}\frac{y}{2h}\int_{-a}^{x}\left[p^+(\zeta)-p^-(\zeta)\right]d\zeta + c_{12}\frac{y^2-h^2}{4h}\left[q^+(x)+q^-(x)\right] - \\
&c_{12}\frac{y^2-h^2}{4h}\left[q^+(-a)+q^-(-a)\right] - c_{12}\frac{y}{6}\left(y^2-h^2\right)\left[g(x)-g(-a)\right] + u_x(-a,y) + 0(y^2) \ , \\
&u_y(x,y) = c_{12}\frac{y}{2h}\left\{T_{out} + \int_{-a}^{x}\left[q^+(\zeta)+q^-(\zeta)\right]d\zeta\right\} - c_{12}\frac{y^2}{2}\int_{-a}^{x}g(\zeta)d\zeta - \\
&c_{22}\frac{y}{2}\left[p^+(x)+p^-(x)\right] - c_{22}\frac{y^2}{4h}\left[p^+(x)-p^-(x)\right] + c_{22}\frac{y^3/3-h^2y}{4h}\left[q'^+(x)+q'^-(x)\right] - \\
&c_{22}\frac{y^2}{24}\left(y^2-2h^2\right)g'(x) + u_y(x,0) + 0(y^3) \ .
\end{aligned} \tag{64}$$

It is required that $u_x(x,y)$ remains bounded as $h\to 0$. Inspection of the expression of $u_x(x,y)$ above leads to the following constraint for the external loading

$$\begin{aligned}
&T_{in}(x+a) + \int_{-a}^{x}(x-\zeta)\left[q^+(\zeta)+q^-(\zeta)\right]d\zeta = 0(h) \ , \\
&\Rightarrow \ T_{in} + \int_{-a}^{x}\left[q^+(\zeta)+q^-(\zeta)\right]d\zeta = 0(h) \ , \\
&\Rightarrow \ q^{+(n)}(\zeta) + q^{-(n)}(\zeta) = 0(h) \ , \ n = 0,1,2,...
\end{aligned} \tag{65}$$

The vertical displacement $u_y(x,y)$ must approach zero as $h\to 0$. When the result (65) is utilized, inspection of the expression of $u_y(x,y)$ in (64) leads to the following estimate for the order of magnitude

$$
\begin{aligned}
&u_y(x,0) = 0(h)\ , \\
&\Rightarrow \\
&u_y^{(n)}(x,0) = 0(h).
\end{aligned}
\tag{66}
$$

Utilizing the third equation of (63), the expressions above and the expression (60) for shear stress, the following equation is obtained when the coefficients of the order 0(1) are equated

$$
\begin{aligned}
&C_1 - c_{11}\int_{-a}^{x}(x-\zeta)g(\zeta)d\zeta - \frac{c_{12}}{2h}\int_{-a}^{x}\left[p^+(\zeta)-p^-(\zeta)\right]d\zeta + \frac{c_{12}h^2}{6}\left[g(x)-g(-a)\right] + \\
&u_y'(x,0) = \frac{c_{66}}{2}\left[q^-(x)-q^+(x)\right]\ ,
\end{aligned}
\tag{67}
$$

where the constant C_1 originates from the Taylor expansion

$$
u_x(-a,y) = C_0 + C_1 y + 0(y^2). \tag{68}
$$

Inserting the result (67) into (64) yields

$$
\begin{aligned}
&u_x(x,y) = \frac{c_{11}}{2h}\left\{T_{out}\left(x+a\right) + \int_{-a}^{x}(x-\zeta)\left[q^+(\zeta)+q^-(\zeta)\right]d\zeta\right\} - \frac{c_{12}}{2}\int_{-a}^{x}\left[p^+(\zeta)+p^-(\zeta)\right]d\zeta \\
&+ y\frac{c_{66}}{2}\left[q^-(x)-q^+(x)\right] + c_{12}\frac{y^2-h^2}{4h}\left[q^+(x)+q^-(x)\right] - c_{12}\frac{y^2-h^2}{4h}\left[q^+(-a)+q^-(-a)\right] \\
&- c_{12}\frac{y^3}{6}\left[g(x)-g(-a)\right] - yu_y'(x,0) + C_0 + C_2 y^2 + 0(y^2)\ , \\
&u_y(x,y) = c_{12}\frac{y}{2h}\left\{T_{out} + \int_{-a}^{x}\left[q^+(\zeta)+q^-(\zeta)\right]d\zeta\right\} - c_{22}\frac{y}{2}\left[p^+(x)+p^-(x)\right] + \\
&\frac{c_{11}c_{22}-c_{12}^2}{4c_{11}h}y^2\left[p^+(x)-p^-(x)\right] + c_{22}\frac{y^3/3-h^2y}{4h}\left[q'^+(x)+q'^-(x)\right] - \frac{c_{12}}{2c_{11}}y^2u_y''(x,0) + \\
&\frac{c_{12}c_{66}}{4c_{11}}y^2\left[q'^-(x)-q'^+(x)\right] - c_{22}\frac{y^4}{24}g'(x) + \frac{c_{11}c_{22}-c_{12}^2}{12c_{11}}y^2h^2g'(x) + u_y(x,0) + 0(y^3)\ .
\end{aligned}
\tag{69}
$$

The final results for the stresses, correct up to the order of 0(h) for shear stress and 0(1) for the vertical and horizontal stresses are now

$$\tau_{xy}(x,y)=\frac{1}{2}\left[q^{-}(x)-q^{+}(x)\right]-\frac{y}{2h}\left[q^{+}(x)+q^{-}(x)\right]+0(y^{2})\ ,$$
$$\sigma_{x}(x,y)=\frac{1}{2h}\left\{T_{in}+\int_{-a}^{x}\left[q^{+}(\zeta)+q^{-}(\zeta)\right]d\zeta\right\}+0(y)\ , \tag{70}$$
$$\sigma_{y}(x,y)=-p(x)+0(y)\ ,$$

where up to the order of 0(h)

$$p(x)=p^{+}(x)=p^{-}(x)\ . \tag{71}$$

The horizontal displacement correct up to the order of 0(1) and vertical displacement up to the order of 0(h) become

$$u_{x}(x,y)=\frac{c_{11}}{2h}(x+a)T_{in}+\frac{c_{11}}{2h}\int_{-a}^{x}(x-\zeta)\left[q^{+}(\zeta)+q^{-}(\zeta)\right]d\zeta-c_{12}\int_{-a}^{x}p(\zeta)d\zeta+C_{0}+0(y),$$
$$u_{y}(x,y)=\frac{c_{12}}{2h}\left\{T_{in}+\int_{-a}^{x}\left[q^{+}(\zeta)+q^{-}(\zeta)\right]d\zeta\right\}y-c_{22}p(x)y+u_{y}(x,0)+0(y^{2})\ . \tag{72}$$

3 WINDING CONTACT PROBLEM

3.1 Contact equations

Consider the basic winding configuration of Figure 1. Despite the growth of the wound roll diameter, steady state motion is assumed. Figure 9 depicts the wound roll and sheet (not in scale) in their undeformed states, comprising the momentary initial configurations of the deformed states during the winding. The center of the undeformed wound roll is at O_1 and the center of the undeformed sheet in the vertical direction is at O. The coordinate system $O_1X_1Y_1$ is attached to the wound roll and OXY to the sheet. After the deformation, point A_1 of the wound roll and point A^+ of the sheet are displaced to the same contact point A. The position vector of point A_1 of the wound roll in the $O_1X_1Y_1$ coordinate system is $\boldsymbol{r}_1$, the deformation $\boldsymbol{x}_1(\boldsymbol{r}_1)$ and the displacement $\boldsymbol{u}_1(\boldsymbol{r}_1)$. Correspondingly, the position vector of point A^+ of the sheet in the OXY coordinate system is $\boldsymbol{r}^+$, the deformation $\boldsymbol{x}^+(\boldsymbol{r}^+)$ and the displacement $\boldsymbol{u}^+(\boldsymbol{r}^+)$. The base unit vectors in the OXY coordinate system are denoted by $\boldsymbol{i}$ and $\boldsymbol{j}$. Hence, the vector presentations of the related quantities are

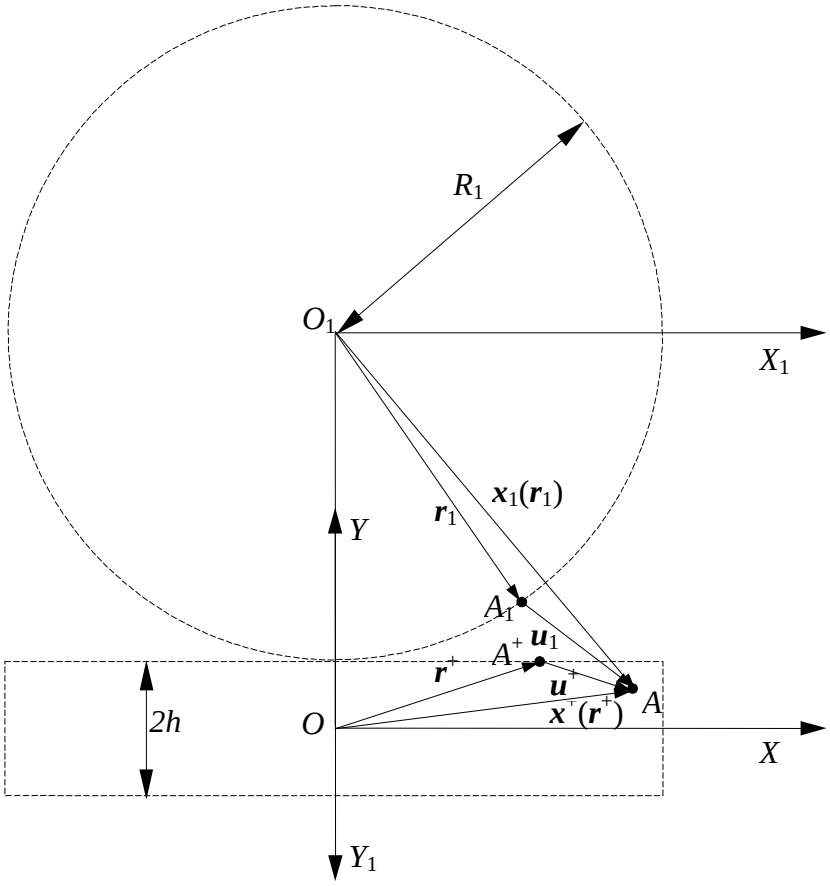

Figure 9. Undeformed wound roll and sheet

$$
\begin{aligned}
\boldsymbol{r}_1 &= X_1\boldsymbol{i} - Y_1\boldsymbol{j}\ , \qquad \boldsymbol{r}^+ = X^+\boldsymbol{i} + Y^+\boldsymbol{j}\ , \\
\boldsymbol{x}_1 &= x_1\boldsymbol{i} - y_1\boldsymbol{j}\ , \qquad \boldsymbol{x}^+ = x^+\boldsymbol{i} + y^+\boldsymbol{j}\ , \\
\boldsymbol{u}_1 &= u_{x1}\boldsymbol{i} + u_{y1}\boldsymbol{j} = (x_1 - X_1)\boldsymbol{i} - (y_1 - Y_1)\boldsymbol{j}\ , \\
\boldsymbol{u}^+ &= u_x^+\boldsymbol{i} + u_y^+\boldsymbol{j} = (x^+ - X^+)\boldsymbol{i} + (y^+ - Y^+)\boldsymbol{j}\ .
\end{aligned}
\tag{73}
$$

Since points A_1 and A^+ map to the same point A in space, the following vector equation can be written:

$$\vec{O_1O} + \boldsymbol{r}^+ + \boldsymbol{u}^+ - \boldsymbol{u}_1 - \boldsymbol{r}_1 = \boldsymbol{0}. \tag{74}$$

The x- and y-components of the equations (74) are

$$\begin{aligned} x^+ &= x_1 \ , \\ y^+ + y_1 &= R_1 + h \ . \end{aligned} \tag{75}$$

From the general theory of small displacements, it is known that the displacement field can be written as the sum of a rigid translation, infinitesimal rotation and pure stretch [29]. Hence, the displacements can be written as

$$\begin{aligned} u_x^+ = \hat{u}_x^+ - \theta^+ Y^+ - \delta_x^+ \ , \ u_y^+ = \hat{u}_y^+ + \theta^+ X^+ - \delta_y^+ \ , \\ u_{x1} = \hat{u}_{x1} - \theta_1 Y_1 - \delta_{x1} \ , \ u_{y1} = \hat{u}_{y1} + \theta_1 X_1 - \delta_{y1} \ , \end{aligned} \tag{76}$$

where $\hat{u}_x^+$, $\hat{u}_y^+$, $\hat{u}_{x1}$ and $\hat{u}_{y1}$ are the pure stretch displacements, θ^+ and θ_1 the infinitesimal rotation angles, δ_x^+ and δ_{x1} the horizontal and δ_y^+, and δ_{y1} the vertical translations of the sheet and cylinder, respectively. The following orders of magnitude with respect to the semi-contact width a can be assumed:

$$\begin{aligned} &u_y^+ \sim \hat{u}_y^+ \sim u_{y1} \sim \hat{u}_{y1} \sim \theta^+ X^+ \sim \theta_1 X_1 \sim \delta_y^+ \sim \delta_{y1} \sim u_x^+ \sim u_{x1} \sim a^2/R_1 \ , \\ &x^+ \sim x_1 \sim X^+ \sim X_1 \sim a \ . \end{aligned} \tag{77}$$

Combining the second equation of (75) and the expressions of the vertical displacements in (76) the indentation equation for the wound roll and sheet contact is obtained:

$$\hat{u}_{y1} + \hat{u}_y^+ = \delta^+ + R_1 - \sqrt{R_1^2 - (x^+ - u_{x1})^2} - \frac{\Delta^+}{R_1} x^+ \ , \tag{78}$$

where $\Delta^+ = R_1(\theta^+ + \theta_1) \sim a$ and $\delta^+ = \delta_y^+ + \delta_{y1} \sim a^2 / R_1$. By expanding the square root and retaining the lowest order terms (~ a^2), the following equation is obtained:

$$\hat{u}_{y1} + \hat{u}_y^+ = \delta^+ + \frac{1}{2R_1}\left(x^{+2} - 2\Delta^+ x^+\right) + 0(a^3)\,. \tag{79}$$

The corresponding equation for the winding drum and sheet contact is derived analogously, the result being

$$\hat{u}_{y2} - \hat{u}_y^- = \delta^- + \frac{1}{2R_2}\left(x^{-2} - 2\Delta^- x^-\right) + 0(a^3)\,. \tag{80}$$

Since the sheet is thin, the pressures are practically equal on both sides of the sheet and the coordinates x^+ and x^- differ by the order of the displacements. It then suffices to use either of the indentation equations, (79) or (80). However, due to reasons of symmetry, the usual practice is to sum the indentation equations for the upper and lower contacts. Thus, adding Eqs. (79) and (80), the following symmetric form of the indentation equation is obtained:

$$\hat{u}_{y1} + \hat{u}_{y2} + \hat{u}_y^+ - \hat{u}_y^- = \delta + \frac{1}{2}\left(\frac{1}{R_1} + \frac{1}{R_2}\right)\left(x^2 - 2\Delta x\right) + 0(a^3)\,, \tag{81}$$

where $\delta = \delta^+ + \delta^-$, $\Delta = \left(\Delta^+ / R_1 + \Delta^- / R_2\right)\left(1/R_1 + 1/R_2\right)^{-1}$ and x differs from the coordinates x^+ and x^- at most by the order of the displacements. Physically δ is the mutual approach of the cylinders and Δ the translation of the contact center in the x-direction. It can be easily shown that without loss of generality the origin of the coordinate system Oxy can be chosen so that it is at the center of the contact in the horizontal direction and Eq. (81) still holds. Furthermore, since displacement in the radial direction fulfills the relation $u_r = u_y + 0(a^3)$ in the vicinity of the nip, Eq. (81) can be written in terms of the radial displacements of the wound roll and winding drum:

$$\hat{u}_{r1} + \hat{u}_{r2} + \hat{u}_y^+ - \hat{u}_y^- = \delta + \frac{1}{2}\left(\frac{1}{R_1} + \frac{1}{R_2}\right)\left(x^2 - 2\varepsilon x\right) + 0(a^3)\,. \tag{82}$$

As mentioned in Chapter 1, some portions of the contact slip relative to each other and some stick together. Obviously, the tangential velocities of the contacting bodies must be equal in the areas that stick. In order to formulate this statement in mathematically useful form, the surface velocity of the material has to be expressed in terms of the strains. Hence, consider the stream tube

of Figure 10 in a steady, planar flow. According to Ref. [34] the density field ρ in the deformed state can be written as

$$\rho = \frac{\rho_0}{\sqrt{(1+2\varepsilon_1)(1+2\varepsilon_2)(1+2\varepsilon_3)}}, \tag{83}$$

where ρ_0 is the reference density prior to the deformation and ε_1, ε_2 and ε_3 are the principal strains. In the plane strain conditions $\varepsilon_z = 0$ and without loss of generality it may be assumed that $\varepsilon_z = \varepsilon_3 = 0$. Eq. (83), written in terms of the normal strain ε_n, tangential strain ε_t and shear strain γ_{nt} reads as

$$\rho = \frac{\rho_0}{\sqrt{(1+2\varepsilon_n)(1+2\varepsilon_t)-\gamma_{nt}^2}} \approx \frac{\rho_0}{\sqrt{(1+2\varepsilon_n)(1+2\varepsilon_t)}}. \tag{84}$$

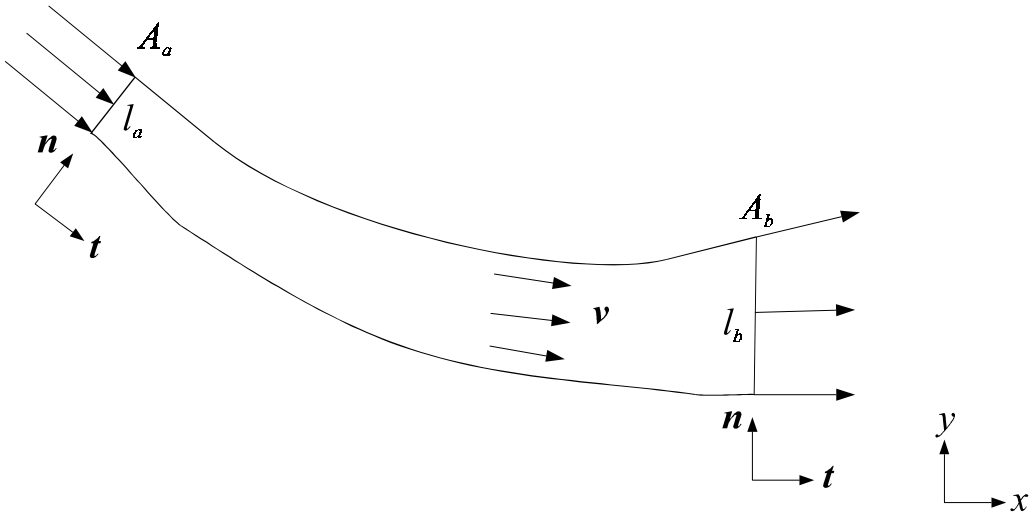

Figure 10. Stream tube in steady rolling conditions

Now it is assumed that the stream tube of Figure 10 is infinitesimally thin and is confined to the surface of the material. Application of the continuity equation [29]

$$\int_{A_a} \rho_a \boldsymbol{v}_a \cdot d\boldsymbol{A}_a = \int_{A_b} \rho_b \boldsymbol{v}_b \cdot d\boldsymbol{A}_b \tag{85}$$

yields

$$\frac{\rho_0}{\sqrt{(1+2\varepsilon_{na})(1+2\varepsilon_{ta})}} v_a A_a = \frac{\rho_0}{\sqrt{(1+2\varepsilon_{nb})(1+2\varepsilon_{tb})}} v_b A_b \ , \tag{86}$$

where v_a, A_a and v_b, A_b are the speed and cross-sectional area at the tube ends, respectively. Because there is no flow in the z-direction, the following relation holds [34]

$$\frac{l_b}{l_a} = \frac{l_0\sqrt{1+2\varepsilon_{nb}}}{l_0\sqrt{1+2\varepsilon_{na}}} = \frac{A_b}{A_a} \ . \tag{87}$$

Combining equations (86) and (5) then yields

$$\frac{v_a}{\sqrt{1+2\varepsilon_{ta}}} = \frac{v_b}{\sqrt{1+2\varepsilon_{tb}}} \ . \tag{88}$$

This result can be further simplified when it is assumed that the strains are small and only first order (and higher) terms are retained:

$$v_b = (1+\varepsilon_{tb}-\varepsilon_{ta})v_a \ . \tag{89}$$

Consider an arbitrary sticking contact point either on the upper or lower contact surface. The tangential speeds of the wound roll and winding drum are $V_{\theta 1}$ and $V_{\theta 2}$, respectively, and the tangential speeds of the upper and lower sheet surfaces are V^+ and V^-, respectively. According to Eq. (89) the equality of the tangential speeds of the contacting bodies can be written in the following form

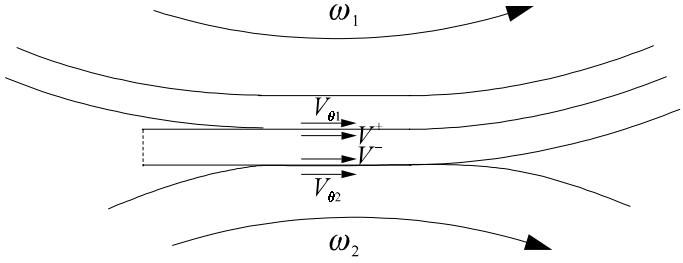

Figure 11. Tangential speeds of the media in contact

$$V_{\theta i} = (1+\varepsilon_{\theta i}-\varepsilon_{\theta_0 i})V_{01} = (1+\varepsilon^{\pm}-\varepsilon_0^{\pm})V_0^{\pm} = \ V^{\pm}, \tag{90}$$

where the + (−) superscript is used for i = 1 (2), and $\varepsilon_{\theta_0 i}$ and V_{0i} (i = 1,2) are the tangential strain and speed of the cylinder in some well defined reference state. Similarly, $\varepsilon_0^{\pm}$ and $V_0^{\pm}$ are the tangential strain and speed of the sheet in some reference state. Unstrained reference states are usually used whenever possible, but here for the sake of generality an arbitrary reference state is assumed. With some algebraic manipulation, Eq. (90) can be written in the form

$$\varepsilon^{\pm} - \varepsilon_{\theta i} - \left(\varepsilon_0^{\pm} - \varepsilon_{\theta_0 i}\right) + \xi^{\pm} + \xi^{\pm} / 2\left[\varepsilon^{\pm} + \varepsilon_{\theta i} - \left(\varepsilon_0^{\pm} + \varepsilon_{\theta_0 i}\right)\right] = 0 \ , \tag{91}$$

where the *creep ratio* $\xi^{\pm}$ is defined by

$$\xi^{\pm} = \frac{V_0^{\pm} - V_{0i}}{\left(V_0^{\pm} + V_{0i}\right)/2} \ . \tag{92}$$

Assuming that the strains are small, it is reasonable to assume that the creep ratio is also small compared to unity. Hence, the last term from the stick equation (91) can be neglected as a second order term and the following stick equation is obtained:

$$\varepsilon^{\pm} - \varepsilon_{\theta i} - \left(\varepsilon_0^{\pm} - \varepsilon_{\theta_0 i}\right) + \xi^{\pm} = 0 \ . \tag{93}$$

For contact regions, which are slipping, Amonton's friction law is assumed. The direction of the tangential traction must be opposite to the direction of slippage, hence the slip equations at contact point *x* are

$$\begin{aligned} q^{+}(x) &= \operatorname{sgn}\left(V^{+} - V_{\theta 1}\right)\mu^{+} p(x) \ , \\ q^{-}(x) &= \operatorname{sgn}\left(V^{-} - V_{\theta 2}\right)\mu^{-} p(x) \ , \end{aligned} \tag{94}$$

where $p(x)$ is the contact pressure, μ^{+} the layer-to-layer friction coefficient of the paper and μ^{-} the friction coefficient between the paper and the winding drum.

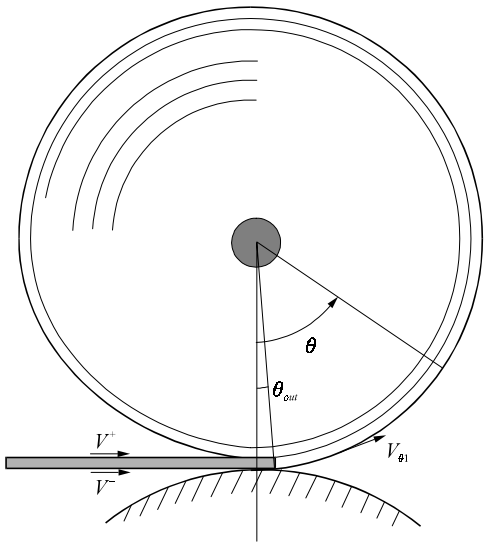

Figure 12. Elastic components: sheet and wound roll.

3.2 Wound-on-condition

Wound-On-Condition (WOC*)* states in mathematical terms that the sheet becomes part of the roll after the nip. This aspect has to be explicitly stated because the wound roll and sheet in the nip are modeled as individual objects. Also, because the wound roll is modeled as a cylinder instead of a spiral, the continuity

of the web tension at the trailing edge of the contact cannot be ensured or even stated. To derive WOC, consider the winding of the outermost lap (Figure 12). At the opposite side of the nip (θ = 180°) the internal stress field of the roll consists predominantly of the hoop stresses. It will be shown in Chapter 4.9 that if there exists a speed difference between the web and the roll, then this difference will monotonously increase along the undeformed (or slightly deformed) part of wound roll rim. However, experimental observations and J-line measurements [32,43] show that all significant layer-to-layer slippage occurs in the vicinity of the nip. Hence, it is presumable that the topmost paper layer does not slip at θ = 180°. The stick equation (93) written at this location reads as

$$\varepsilon^+(\pi) - \varepsilon_{\theta 1}(\pi) - \left(\varepsilon_0^+ - \varepsilon_{\theta_0 1}\right) + \xi^+ = 0 \ . \tag{95}$$

Solving for ξ^+ and substituting it back into Eq. (93) yields

$$\varepsilon^+ - \varepsilon_{\theta 1} - \left[\varepsilon^+(\pi) - \varepsilon_{\theta 1}(\pi)\right] = 0 \ . \tag{96}$$

The problem with this WOC is that in order to utilize it the sheet solution should be extended 180° further from the nip. This could be done but the governing equations would become nonlinear, as will be shown in Chapter 3.5. In this work, in order to confine the treatment to the nip area and to keep the problem within the linear theory, the sheet and the wound roll are assumed to stick immediately after the nip. This is equivalent to replacing the continuity of the web tension by a rigid "thumb pin" attachment of the web to the cylinder at the trailing edge of the nip. Hence, the *WOC* used in this work is

$$\varepsilon^+(x) - \varepsilon_{\theta 1}(x) - \left[\varepsilon^+(a) - \varepsilon_{\theta 1}(a)\right] = 0 \ , \tag{97}$$

where a is the contact half-width. An evaluation of the error caused by the approximation (97) is given in Chapter 4.9.

3.3 Hertz half-width equation for linear and orthotropic half-space

The influence of the tangential traction upon the normal pressure and contact area is generally small [24]. Hence, a good approximation of the pressure is obtained from the

corresponding frictionless problem. Because the approach δ of the wound roll and winding drum is not known, a differentiated form of the indentation equation (81) will be used:

$$\frac{\partial \bar{u}_{y1}}{\partial x} + \frac{\partial \bar{u}_{y2}}{\partial x} = \left(\frac{1}{R_1} + \frac{1}{R_2} \right) x \, . \tag{98}$$

In the previous equation, the compression of the sheet was neglected as a small quantity and the shift of the origin ε was set to zero due to the symmetry. The expressions of the displacements were derived in Section 2.1 in Eq. (32). Setting the tangential traction to zero and differentiating the latter equation yields

$$\frac{\partial \bar{u}_{yi}}{\partial x} = \frac{C_i}{\pi} \int_{-a}^{a} \frac{p(s)}{x-s} ds \, , \; i = 1,2 \, , \tag{99}$$

where, contrary to section 2.1, the positive direction of the displacements is directed out from the half-plane. The following integral equation for $p(x)$ is obtained when expression (99) is substituted into (98):

$$\int_{-a}^{a} \frac{p(s)}{x-s} ds = \frac{\pi E^*}{2R} x \, , \tag{100}$$

where the relative modulus E^* and radius R^* are defined as

$$\frac{1}{E^*} = \frac{1}{E_1} + \frac{1}{E_2} \; , \; \frac{1}{R^*} = \frac{1}{R_1} + \frac{1}{R_2} \; , \tag{101}$$

and the wound roll and winding drum *generalized moduli* E_i by

$$E_i = \frac{2\sqrt{G_i}\left(A_{yy,i} A_{xx,i} - A_{xy,i}^2 \right)}{\sqrt{A_{xx,i}\left(\sqrt{A_{yy,i} A_{xx,i}} + A_{xy,i} + 2G_i \right)\left(\sqrt{A_{yy,i} A_{xx,i}} - A_{xy,i} \right)}} \, . \tag{102}$$

With these notations, Eq. (100) becomes equivalent to the one studied in various textbooks (e.g. [24]) for isotropic materials. Hence, the solution also becomes notationally equivalent, i.e., the semi-half-width

$$a = 2\sqrt{\frac{PR^*}{\pi E^*}}\,, \tag{103}$$

and the pressure distribution

$$p(x) = \frac{2P}{\pi E^*}\sqrt{a^2 - x^2}\,,\ |x| \le a\,, \tag{104}$$

where P is the total load, i.e.,

$$P = \int_{-a}^{a} p(s)ds\,. \tag{105}$$

3.4 Discretized contact equations

As shown in Chapters 3.1 and 3.2, some of the contact equations are expressed in terms of kinematical quantities (Eqs. (82), (93) and (97)) and some in terms of the surface tractions (Eq. (94)). This leaves a freedom of choice as the unknown quantities. Here the most general convention is followed and the surface tractions are taken for the primary unknowns. Since the location and number of slip zones is not known in advance, it is obvious that no closed form analytical solution for the problems exists. Hence, to facilitate the numerical solution process the continuous distributions of the traction are replaced by a discrete set of "traction elements" and the contact equations are then satisfied at a discrete number of points. Thus, the following representations of the tractions are introduced

$$\begin{gathered} p(x) = \sum_{m=1}^{M} p_m \psi_m(x)\,, \\ q^+(x) = \sum_{m=1}^{M} q_m^+ \psi_m(x)\,,\ \ q^-(x) = \sum_{m=1}^{M} q_m^- \psi_m(x)\,, \end{gathered} \tag{106}$$

where the piecewise linear base functions are

$$\psi_m(x) = \begin{cases} (x - x_m + \Delta x)/\Delta x\,, & x_m - \Delta x \le x < x_m\,, \\ (x_m + \Delta x - x)/\Delta x\,, & x_m < x \le x_m + \Delta x\,, \\ 0 \qquad\qquad\ , & \text{elsewhere} \end{cases} \tag{107}$$

and the evenly spaced grid points

$$x_m = -a + (m-1)\Delta x\ ,\ m = 1,2,\ldots,M\ ,\ \Delta x = 2a/(M-1). \tag{108}$$

Note that with these definitions, $p_m = p(x_m)$ and $q_m^{\pm} = q^{\pm}(x_m)$ (m = 1,2,...,M). In what follows, the expressions for the normal (radial) surface displacement and tangential strain of either the half-space or cylinder and the sheet will be derived in terms of the unknowns p_m, $q_m^{\pm}$ and T_{out}. At the leading edge of the contact, the normal and tangential tractions must vanish due to the continuity requirements. Hence, $p_1 = q_1^{\pm} = 0$. At the trailing edge, the normal and tangential tractions vanish obviously on the winding drum side but can be non-zero on the wound roll side. However, the pressure between the topmost paper layer and the wound roll at the trailing edge is due to the hoop stress and is thus much less than the contact pressures. Hence, the tangential traction must also be relatively small. Thus, it will be assumed that $p_M = q_M^{\pm} = 0$.

The normal displacement can readily be calculated from the expressions (32) or (59) and the tangential strains are obtained in principle by differentiating the expressions for the tangential displacement. However, this brings about a uniqueness problem relating to the rolling direction of the material. Careful study of the elastic contact equations presented in this chapter reveal that the sense of the rolling direction is ambivalent, i.e., the problem has two solutions (at least). This manifests itself by noninvertible system matrixes. The sense of rolling is introduced properly by using either forward or backward difference approximation for the tangential strain [49]. In this work, the rolling direction was defined by Figure 1. Here the coordinate systems are chosen so that the coordinate tangential to the sheet always points in the direction of the mass flow and, hence, a backward difference approximation of the tangential strains provides the correct rotation sense.

For the half-space approximation, the expressions (106) of the surface tractions are inserted into the solutions (32) to get

$$\begin{aligned}
v_i(x) &= -\bar{u}_{yi}(x) = \frac{C_i}{\pi}\sum_{m=2}^{M-1} p_m \int_{-a}^{a} \psi_m(s)\ln|x-s|ds - \frac{A_i}{2}\sum_{m=2}^{M-1} q_m^{\pm}\left[\int_{-a}^{x}\psi_m(s)ds - \int_{x}^{a}\psi_m(s)ds\right],\\
u_i(x) &= \bar{u}_{xi} = -\frac{A_i}{2}\sum_{m=2}^{M-1} p_m\left[\int_{-a}^{x}\psi_m(s)ds - \int_{x}^{a}\psi_m(s)ds\right] - \frac{B_i}{\pi}\sum_{m=2}^{M-1} q_m^{\pm}\int_{-a}^{a}\psi_m(s)\ln|x-s|ds\ ,\\
\varepsilon_i(x) &\approx \frac{\bar{u}_{xi}(x) - \bar{u}_{xi}(x-\Delta x)}{\Delta x}\ ,\ (i = 1,2)\ ,
\end{aligned} \tag{109}$$

where q_m^+ corresponds to $i = 1$ (wound roll) and q_m^- to $i = 2$ (winding drum). The integrals in (109) can easily be evaluated to obtain the normal displacements and tangential strains at the grid points x_l:

$$
\begin{aligned}
v_{l,i} &= v_i(x_l) = \sum_{m=2}^{M-1} A_{lm,i}\, p_m + \sum_{m=2}^{M-1} B_{lm,i} q_m^{\pm} \ , \\
u_{l,i} &= u_i(x_l) = \sum_{m=2}^{M-1} \bar{C}_{lm,i}\, p_m + \sum_{m=2}^{M-1} \bar{D}_{lm,i} q_m^{\pm} \ , \\
\varepsilon_{l,i} &= \varepsilon_i(x_l) = \sum_{m=2}^{M-1} C_{lm,i}\, p_m + \sum_{m=2}^{M-1} D_{lm,i} q_m^{\pm} \ , \ (i = 1,2) \ ,
\end{aligned}
\tag{110}
$$

where the influence coefficients are

$$
\begin{aligned}
&A_{lm,i} = \frac{C_i \Delta x}{2\pi}\Big[-3 + (l-m-1)^2 \ln\left|(l-m-1)\Delta x\right| - 2(l-m)^2 \ln\left|(l-m)\Delta x\right| + \\
&(l-m+1)^2 \ln\left|(l-m+1)\Delta x\right|\Big] \ , \\
&B_{lm,i} = \begin{cases} A_i \Delta x/2 \ , & l < m \ , \\ -A_i \Delta x/2 \ , & l > m \ , \\ 0 \ , & l = m \ , \end{cases} \\
&\tilde{C}_{lm,i} = B_{lm,i} \ , \ D_{lm,i} = -B_i / C_i A_{lm,i} \ , \\
&C_{lm,i} = \left(\bar{C}_{lm,i} - \bar{C}_{l-1m,i}\right)/\Delta x \ , \ D_{lm,i} = \left(\bar{D}_{lm,i} - \bar{D}_{l-1m,i}\right)/\Delta x \ .
\end{aligned}
\tag{111}
$$

The surface displacements of the cylinder are presented in Eq. (59) as a function of the Fourier coefficients of the surface tractions. Here, however, the expressions (106) were used to discretize the tractions and, hence, the displacements have to be expressed as a function of the coefficients in the expansions (106). This can be done by inserting the expressions (106) into the integrals (51), defining the discrete Fourier transform and performing the integrations. The result is

$$
\begin{aligned}
&c_{n,i} = \sum_{m=2}^{M-1} \alpha_{nm,i}\, p_m \ , \ (n = 0,1,2,...) \ , \ d_{n,i} = \sum_{m=2}^{M-1} \beta_{nm,i}\, p_m \ , \ (n = 1,2,3,...) \ , \\
&e_{n,i} = \sum_{m=2}^{M-1} \alpha_{nm,i} q_m^{\pm} \ , \ (n = 0,1,2,...) \ , \ f_{n,i} = \sum_{m=2}^{M-1} \beta_{nm,i} q_m^{\pm} \ , \ (n = 1,2,3,...) \ ,
\end{aligned}
\tag{112}
$$

where

$$\alpha_{0m,i} = \frac{1}{2\pi R_i}\int_{-a}^{a}\psi_m(x)dx\ ,\ m=1,2,3,\ldots,M,$$
$$\alpha_{nm,i} = \frac{1}{\pi R_i}\int_{-a}^{a}\psi_m(x)\cos nx dx\ ,\ m=1,2,3,\ldots,M,\ n=1,2,3,\ldots \tag{113}$$
$$\beta_{nm,i} = \frac{1}{\pi R_i}\int_{-a}^{a}\psi_m(x)\sin nx dx\ ,\ m=1,2,3,\ldots,M,\ n=1,2,3,\ldots$$

When the Fourier coefficients (112) are inserted into the expansions (59) of the surface displacements, the following expressions are obtained:

$$v_i(x) = \bar{u}_{ri}(\theta) = -\sum_{m=2}^{M-1}\left[\alpha_{0m,i}\gamma_{0,i} + \sum_{n=1}^{\infty}\tilde{\alpha}_{nm,i}(x)\gamma_{n,1i}\right]p_m + \sum_{m=2}^{M-1}\left[\sum_{n=1}^{\infty}\tilde{\beta}_{nm,i}(x)\gamma_{n,2i}\right]q_m^{\pm}\ ,$$
$$u_i(x) = \bar{u}_{\theta i}(\theta) = \sum_{m=2}^{M-1}\left[\sum_{n=1}^{\infty}\tilde{\beta}_{nm,i}(x)\chi_{n,1i}\right]p_m + \sum_{m=2}^{M-1}\left[\alpha_{0m,i}\chi_{0,i} + \sum_{n=1}^{\infty}\tilde{\alpha}_{nm,i}(x)\chi_{n,2i}\right]q_m^{\pm}\ , \tag{114}$$
$$\varepsilon_i(x) = \frac{1}{R_i}\left[v_i(x) + \frac{u_i(x) - u_i(x-\Delta x)}{\Delta x}\right],$$

where

$$\alpha_{0m,i} = \frac{\Delta x}{2\pi R_i}\ ,$$
$$\tilde{\alpha}_{nm,i}(x) = \frac{4R_i}{\pi n^2 \Delta x}\sin\frac{n\Delta x}{2R_i}\cos\frac{n}{R_i}(x - x_m)\ , \tag{115}$$
$$\tilde{\beta}_{nm,i}(x) = \frac{4R_i}{\pi n^2 \Delta x}\sin\frac{n\Delta x}{2R_i}\sin\frac{n}{R_i}(x - x_m)\ .$$

The displacements and tangential strains evaluated at the grid points x_l can still be calculated from Eqs. (110) where the influence coefficients are now

$$A_{lm,i} = -\alpha_{0m,i}\gamma_{0,i} - \sum_{n=1}^{\infty}\tilde{\alpha}_{nm,i}(x_l)\gamma_{n,1i}\ ,\ B_{lm,i} = \sum_{n=1}^{\infty}\tilde{\beta}_{nm,i}(x_l)\gamma_{n,2i}\ ,$$
$$\bar{C}_{lm,i} = \sum_{n=1}^{\infty}\tilde{\beta}_{nm,i}(x_l)\chi_{n,1i}\ ,\ \bar{D}_{lm,i} = \alpha_{0m,i}\chi_{0,i} + \sum_{n=1}^{\infty}\tilde{\alpha}_{nm,i}(x_l)\chi_{n,2i}\ , \tag{116}$$
$$C_{lm,i} = \frac{1}{R_i}\left[A_{lm,i} + \frac{\bar{C}_{lm,i} - \bar{C}_{l-1m,i}}{\Delta x}\right],\ D_{lm,i} = \frac{1}{R_i}\left[B_{lm,i} + \frac{\bar{D}_{lm,i} - \bar{D}_{l-1m,i}}{\Delta x}\right].$$

The infinite sums in Eq. (116) cannot be calculated analytically but must be truncated to some finite number of terms N which, according to the Nyquist sampling theorem, should be greater than $\pi \max(R_1, R_2)(M-1)/a$. The computational burden can be remarkably reduced by noting that the influence coefficients (111) or (116) have to be computed only for l = 1, since for other values of index l the following symmetry properties of the influence coefficients can be utilized:

$$\begin{aligned}
&A_{lm,i} = A_{ml,i}\ ,\ l,m = 1,2,3,...,M\ \ ,\ A_{lm,i} = A_{1,m-l+1,i}\ ,\ l = 2,3,4,...,M\ ,\ l \le m \le M\ ,\\
&B_{lm,i} = -B_{ml,i}\ ,\ l,m = 1,2,3,...,M\ ,\ B_{lm,i} = B_{1,m-l+1,i}\ ,\ l = 2,3,4,...,M\ ,\ l \le m \le M\ ,\\
&\bar{C}_{lm,i} = -\bar{C}_{ml,i}\ ,\ l,m = 1,2,3,...,M\ ,\ \bar{C}_{lm,i} = \bar{C}_{1,m-l+1,i}\ ,\ l = 2,3,4,...,M\ ,\ l \le m \le M\ ,\\
&\bar{D}_{lm,i} = \bar{D}_{ml,i}\ ,\ l,m = 1,2,3,...,M\ \ ,\ \bar{D}_{lm,n} = \bar{D}_{1,m-l+1,i}\ ,\ l = 2,3,4,...,M\ ,\ l \le m \le M\ .
\end{aligned} \tag{117}$$

When the expressions (106) of the surface tractions are inserted into the sheet displacement solutions (72), the following equations are obtained:

$$\begin{aligned}
&v^+(x) - v^-(x) = u_y(x,h) - u_y(x,-h) = c_{12}\left\{T_{in} + \sum_{m=2}^{M-1}\left(q_m^+ + q_m^-\right)\int_{-a}^{x}\psi_m(\zeta)d\zeta\right\} -\\
&2c_{22}h\sum_{m=2}^{M-1} p_m\psi_m(x)\ ,\\
&\varepsilon^+(x) = \varepsilon^-(x) \approx \frac{u_x(x,\pm h) - u_x(x-\Delta x,\pm h)}{\Delta x} = \frac{c_{11}}{2h}T_{in} + \frac{c_{11}}{2h}\sum_{m=2}^{M-1}\left(q_m^+ + q_m^-\right)\int_{-a}^{x}\psi_m(\zeta)d\zeta\\
&+\frac{c_{11}}{2h\Delta x}\sum_{m=2}^{M-1}\left(q_m^+ + q_m^-\right)\int_{x-\Delta x}^{x}(x-\Delta x-\zeta)\psi_m(\xi)d\zeta - \frac{c_{12}}{\Delta x}\sum_{m=2}^{M-1}p_m\int_{x-\Delta x}^{x}\psi_m(\zeta)d\zeta\ ,
\end{aligned} \tag{118}$$

These expressions for $v^+ - v^-$ and $\varepsilon^\pm$ evaluated at the grid points x_l are needed in the indentation and stick equations:

$$\begin{aligned}
&v_l^+ - v_l^- = Ap_l + \sum_{m=2}^{M-1}B_{lm}^{\pm}\left(q_m^+ + q_m^-\right) + BT_{in}\ ,\\
&\varepsilon_l^{\pm} = \sum_{m=2}^{M-1}C_{lm}^{\pm}p_m + \sum_{m=2}^{M-1}D_{lm}^{\pm}(q_m^+ + q_m^-) + DT_{in}\ ,
\end{aligned} \tag{119}$$

where

$$A=-2c_{22}h,\ B=c_{12}\ ,\ B_{lm}^{\pm}=\begin{cases}0 & ,\ l<m\ ,\\ \dfrac{c_{12}}{2}\Delta x & ,\ l=m\ ,\\ c_{12}\Delta x & ,\ l>m\ ,\end{cases} \tag{120}$$

and

$$C_{lm}^{\pm}=\begin{cases}0 & ,\quad l<m\vee l>m+1\ ,\\ -\dfrac{c_{12}}{2}, & l=m\ ,\\ -\dfrac{c_{12}}{2}, & l=m+1\ ,\end{cases}\qquad D_{lm}^{\pm}=\begin{cases}0 & ,\ l<m\ ,\\ \dfrac{c_{11}\Delta x}{12h} & ,\ l=m\ ,\\ \dfrac{5c_{11}\Delta x}{12h} & ,\ l=m+1\ ,\\ \dfrac{c_{11}\Delta x}{2h} & ,\ l>m+1\ ,\end{cases}\quad D=\frac{c_{11}}{2h}\ . \tag{121}$$

Full dimensional analysis will not be carried out, but the unknowns and incoming web tension T_{in} will be nondimensionalized as follows:

$$\tilde{p}_m=\frac{p_m}{A_t}\ ,\ \tilde{q}_m^{\pm}=\frac{q_i^{\pm}}{A_t}\ ,\ \tilde{T}_{in}=\frac{T_{in}}{hA_t}\ , \tag{122}$$

where A_t is the tangential elastic modulus of the wound roll, i.e., either $A_{\theta\theta,1}$ or $A_{xx,1}$ depending on the chosen wound roll model. The normal displacement and tangential strain in the expressions (110) and (119) become

$$\begin{aligned}
&v_{l,i}=v_i(x_l)=\sum_{m=2}^{M-1}\tilde{A}_{lm,i}\tilde{p}_m+\sum_{m=2}^{M-1}\tilde{B}_{lm,i}\tilde{q}_m^{\pm}\ ,\\
&\varepsilon_{l,i}=\varepsilon_i(x_l)=\sum_{m=2}^{M-1}\tilde{C}_{lm,i}\tilde{p}_m+\sum_{m=2}^{M-1}\tilde{D}_{lm,i}\tilde{q}_m^{\pm}\ ,\ (i=1,2)\ ,\\
&v_l^{+}-v_l^{-}=\tilde{A}\tilde{p}_l+\sum_{m=2}^{M-1}\tilde{B}_{lm}^{\pm}\left(\tilde{q}_m^{+}+\tilde{q}_m^{-}\right)+\tilde{B}\tilde{T}_{in}\ ,\\
&\varepsilon_l^{\pm}=\sum_{m=2}^{M-1}\tilde{C}_{lm}^{\pm}\tilde{p}_m+\sum_{m=2}^{M-1}\tilde{D}_{lm}^{\pm}(\tilde{q}_m^{+}+\tilde{q}_m^{-})+\tilde{D}\tilde{T}_{in}\ ,
\end{aligned} \tag{123}$$

where

$$\begin{aligned}&\tilde{A}_{lm,i} = A_{lm,i}A_t\ ,\ \tilde{B}_{lm,i} = B_{lm,i}A_t\ ,\ \tilde{C}_{lm,i} = C_{lm,i}A_t\ ,\ \tilde{D}_{lm,i} = D_{lm,i}A_t\ ,\\ &\tilde{A} = AA_t\ ,\ \tilde{B}_{ij}^{\pm} = B_{ij}^{\pm}A_t\ ,\ \tilde{B} = BA_th\ ,\ \tilde{C}_{ij}^{\pm} = C_{ij}^{\pm}A_t\ ,\ \tilde{D}_{ij}^{\pm} = D_{ij}^{\pm}A_t\ ,\ \tilde{D} = DA_th\ .\end{aligned} \tag{124}$$

The indentation equation (82) written at grid point x_l is

$$v_{l,1} + v_{l,2} + v_l^+ - v_l^- - \delta + \Delta\left(\frac{1}{R_1} + \frac{1}{R_2}\right)x_l = \frac{1}{2}\left(\frac{1}{R_1} + \frac{1}{R_2}\right)x_l^{\,2}\ ,\ l = 1, 2, ..., M\ . \tag{125}$$

Utilizing equation (123), this can be written as

$$\begin{aligned}&\sum_{m=2}^{M-1}\left(\tilde{A}_{lm,1} + \tilde{A}_{lm,2} + \delta_{lm}\tilde{A}\right)\tilde{p}_m - \delta + \Delta\left(\frac{1}{R_1} + \frac{1}{R_2}\right)x_l = \frac{1}{2}\left(\frac{1}{R_1} + \frac{1}{R_2}\right)x_l^2 -\\ &\sum_{m=2}^{M-1}\left(\tilde{B}_{lm}^{\pm} + \tilde{B}_{lm,1}\right)\tilde{q}_m^+ - \sum_{m=2}^{M-1}\left(\tilde{B}_{lm}^{\pm} + \tilde{B}_{lm,2}\right)\tilde{q}_m^- - \tilde{B}\tilde{T}_{in}\ .\end{aligned} \tag{126}$$

This constitutes the *Normal Problem* [25] of the winding nip. The pressures $\tilde{p}_m$, the indentation depth δ and the tangential shift of the origin ε are left on the left-hand side because they are considered as unknowns of the normal problem. The tangential tractions $\tilde{q}_m^+$ and $\tilde{q}_m^-$ are moved to the right hand side of the equation because they are considered as known quantities.

It was earlier discussed that the radial pressure is small at the trailing edge of the contact and, hence, the tangential strain there can be estimated to be

$$\varepsilon^+(a) = \frac{c_{11}}{2h}T_{out}\ . \tag{127}$$

Thus, the stick equation (97) for the sheet-roll contact becomes

$$\varepsilon^+ - \varepsilon_{\theta_1} + \varepsilon_{\theta_1}(a) - \frac{c_{11}}{2h}T_{out} = 0\ . \tag{128}$$

The reference strains in the stick equation (93) can be freely chosen. For the sheet-drum contact the reference strains are chosen to vanish and, hence, the stick equation is written as

$$\varepsilon^- - \varepsilon_{\theta_2} + \xi^- = 0\ . \tag{129}$$

As a recapitulation, the stick equations written at the grid points x_l are

$$\begin{aligned} &\varepsilon_l^+ - \varepsilon_{l,1} + \varepsilon_{M,1} - \frac{c_{11}}{2h} T_{out} = 0 \ , \\ &\varepsilon_l^- - \varepsilon_{l,2} + \xi^- = 0 \ . \end{aligned} \tag{130}$$

When Eq. (123) is inserted to Eqs. (130) the stick equations become

$$\begin{aligned} &\sum_{m=2}^{M-1} \left(\tilde{D}_{lm}^{\pm} + \tilde{D}_{Mm,1} - \tilde{D}_{lm,1} \right) \tilde{q}_m^+ + \sum_{m=2}^{M-1} \tilde{D}_{lm}^{\pm} \tilde{q}_m^- - \tilde{D} \tilde{T}_{out} = \sum_{m=2}^{M-1} (\tilde{C}_{lm,1} - \tilde{C}_{Mm,1} - \tilde{C}_{lm}^{\pm}) \tilde{p}_m - \tilde{D} \tilde{T}_{in} \ , \\ &\sum_{m=2}^{M-1} \tilde{D}_{lm}^{\pm} \tilde{q}_m^+ + \sum_{m=2}^{M-1} \left(\tilde{D}_{lm}^{\pm} - \tilde{D}_{lm,2} \right) \tilde{q}_m^- + \xi^- = \sum_{m=2}^{M-1} (\tilde{C}_{lm,2} - \tilde{C}_{lm}^{\pm}) \tilde{p}_m - \tilde{D} \tilde{T}_{in} \ . \end{aligned} \tag{131}$$

At the contact points which are slipping, the slip equations (94) are applied:

$$\begin{aligned} q_l^+ &= \mu^+ \operatorname{sgn} \upsilon^+ p_l \ , \\ q_l^- &= \mu^- \operatorname{sgn} \upsilon^- p_l \ , \end{aligned} \tag{132}$$

where the relative (non-dimensional) speed differences $\upsilon^{\pm}$ are calculated as

$$\begin{aligned} \upsilon^+ &= \varepsilon_l^+ - \varepsilon_{l,1} + \varepsilon_{M,1} - \frac{c_{11}}{2h} T_{out} \ , \\ \upsilon^- &= \varepsilon_l^- - \varepsilon_{l,2} + \xi^- \ . \end{aligned} \tag{133}$$

The equations (131) and (132) constitute the *Tangential Problem* of the winding nip. In contrast to the normal problem, the tangential tractions $\tilde{q}_m^+$ and $\tilde{q}_m^-$, wound-on tension T_{out} and the sheet-drum creep ratio ξ^- are considered as unknowns and the pressures $\tilde{p}_m$ are given. The significance of the division between normal and tangential problems will become obvious in the next section, 3.5, where the full description of the solution procedure will be given.

The net tangential loads Q^+ and Q^- and the compressive load P expressed in terms of the tractions at the grids points can be easily calculated from the expansions (106)

$$\begin{aligned} P &= \int_{-a}^{a} p(x) dx = \int_{-a}^{a} \sum_{m=2}^{M-1} p_m \psi_m(x) dx = \Delta x \sum_{m=2}^{M-1} p_m \ , \\ Q^{\pm} &= \Delta x \sum_{m=2}^{M-1} q_m^{\pm} \ . \end{aligned} \tag{134}$$

Utilizing the equation above, the torque balance of cylinder 2 (winding drum) and the horizontal balance of the sheet (1) can be written as

$$\begin{aligned} &\Delta x\sum_{m=2}^{M-1} q_m^- = -\frac{M_2}{R_2}\ , \\ &T_{out} - \Delta x\sum_{m=2}^{M-1}\left(q_m^+ + q_m^-\right) = T_{in}\ . \end{aligned} \tag{135}$$

Finally, Eqs. (135) written in terms of the nondimensional unknowns becomes

$$\begin{aligned} &\sum_{m=2}^{M-1} \tilde{q}_m^- = -\frac{M_2}{\Delta x R_2 A_t} = -\tilde{M}_2\ , \\ &\frac{h}{\Delta x}\tilde{T}_{out} - \sum_{m=2}^{M-1}\left(\tilde{q}_m^+ + \tilde{q}_m^-\right) = \frac{h}{\Delta x}\tilde{T}_{in}\ . \end{aligned} \tag{136}$$

3.5 Extended model accounting for the wound roll wrap

The Wound-On-Condition was defined in Chapter 3.2 as a mathematical statement describing that the incoming web becomes part of the wound roll after the nip. The contact equations of the previous chapter were derived under the WOC assuming the incoming sheet would stick to the wound roll surface immediately after the nip. The reason for using this arguably strong assumption was dictated more by the practical considerations than the physical. If the stick had been assumed to occur on the opposite side of the nip in the wound roll, the contact problem would have to have been solved for about 180º on the roll periphery instead of the typical 1-10º nip angle. The planar web theory derived in Chapter 2.3 could not have been used on the roll periphery, where the pressure between the topmost sheet and paper roll is due to the hoop tension. In addition, the hoop pressure depends on the curvature of the roll periphery. Although the strains and displacements are assumed infinitesimal, the deviation of the radius of curvature from the radius of the undeformed cylinders can be finite and hence should be accounted for. This makes the contact equations inherently nonlinear.

In this chapter the theory for the winding contact problem extended to the wound roll wrap is presented. Instead of assuming that the incoming sheet sticks to the wound roll immediately after the nip, sticking is assumed to occur at the opposite side of the nip, i.e., the WOC of Eq (96) will be used. The theory of the elastic solution of the cylinders can be directly applied to this extended

loading area but a new theory for the elastic solution of the web of arbitrary curvature is needed. Following the "Simplicity argument" stated in Chapter 1, the web model at this stage is chosen to be as simple as is practically reasonable.

Accounting for the wound roll wrap mostly affects the compilation of the influence coefficients of the wound roll. The additional contribution of the hoop pressure results in additional, rather complex terms in the expressions of the influence coefficients of the radial displacement and tangential strain. On the other hand, the calculation of the corresponding influence coefficient presentations for the web and winding drum are straightforward without much change to the previous chapter.

Consider the torque balance of the wound roll and winding drum and tangential force balance of the paper web in the nip and wrap (Figure 13). It should be noted that now the web tensions, T_{out} after the nip and *WOT* on the opposite side of the nip, are unequal. Since *WOT* is the primary unknown for this problem, T_{out} will be eliminated to obtain

$$\begin{aligned} &WOT = T_{in} + Q^- + Q^+ + Q_w^+ \ , \\ &WOT - Q^+ - Q_w^+ = \frac{M_1}{R_1} \ , \\ &Q^- = -\frac{M_2}{R_2} = F \ , \end{aligned} \qquad (137)$$

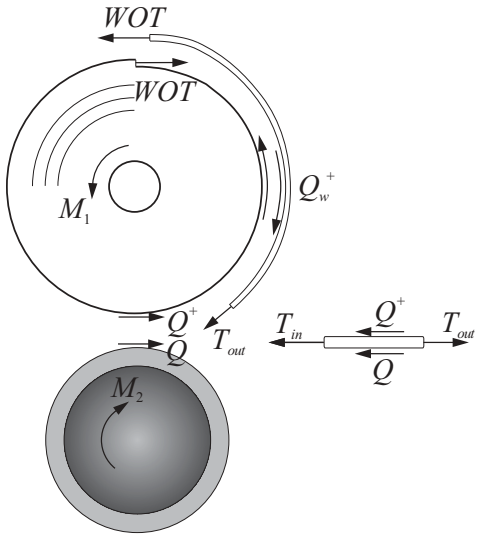

Figure 13. Tangential total contact loads and torques of the system.

where the net total tangential tractions are

$$Q^{\pm} = \int_{-a}^{a} q^{\pm}(\zeta) d\zeta \ , \ Q_w^+ = \int_{a}^{\pi R_1} q^+(\zeta) d\zeta \qquad (138)$$

A small slice of a perfectly flexible thin sheet wrapped around a deformed paper roll with a local radius of curvature ρ^+ is shown in Figure 14. As in Chapter 2.3, the tangential traction between the web and the roll (drum) is denoted by q^+ (q^-). Because of the hoop pressure acting on the convex side of the web, the pressures on the roll side p^+ and on the drum side p^- are unequal. The nominal web tension is *T*. After taking the limit $\Delta\varphi \to 0$ the force balance equations for the web in the radial and tangential directions become

$$p^+ = p^- + \frac{T}{\rho^+} \ , \qquad \frac{dT}{ds} = q^+ + q^- \ , \tag{139}$$

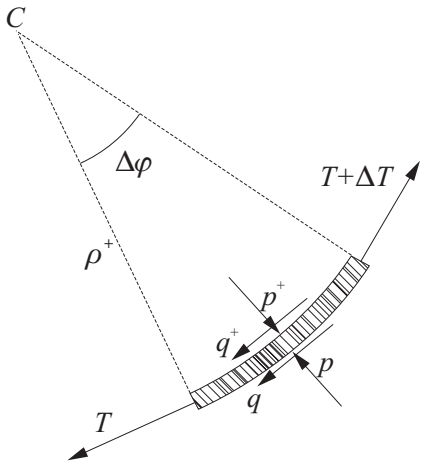

Figure 14. Loads on a web slice of arbitrary curvature.

where the infinitesimal arc length increment satisfies under small displacement theory

$$ds = \rho^+ d\varphi = R_1 d\theta_1 \ . \tag{140}$$

The expression for the web tension can be integrated directly from the last equation of (139):

$$T(s) = T_{in} + \int_{-a}^{s} \left[q^+(\zeta) + q^-(\zeta) \right] d\zeta \ , \tag{141}$$

and thus the wound roll pressure p^+ becomes

$$p^+(s) = p^-(s) + \frac{1}{\rho^+(s)} \left\{ T_{in} + \int_{-a}^{s} \left[q^+(\zeta) + q^-(\zeta) \right] d\zeta \right\} . \tag{142}$$

Since the web is assumed to be very thin, the changes in the web thickness are small compared to the deformations of the wound roll. Hence, the thickness of the web can be considered as constant without much error in the indentation equation (125) and thus in the pressure distribution. In addition, Poisson's ratio of paper is known to be very small and hence, the term linking the normal pressure to the tangential strain will be disregarded. Accordingly, the expression for the tangential strain of the web becomes ($\varepsilon^+ = \varepsilon^- \equiv \varepsilon^{\pm}$)

$$\varepsilon^{\pm}(s) = \frac{T(s)}{2hA_{\theta\theta}} = \frac{1}{2hA_{\theta\theta}} \left\{ T_{in} + \int_{-a}^{s} \left[q^-(\zeta) + q^+(\zeta) \right] d\zeta \right\} . \tag{143}$$

The tangential displacement of web u_t can be integrated from Eq. (143):

$$u_t(s) = \int_{-a}^{s} \varepsilon^{\pm}(\zeta) d\zeta = \frac{1}{2hA_{\theta\theta}} \int_{-a}^{s} T(\zeta) d\zeta = \frac{1}{2hA_{\theta\theta}} \left\{ T_{in} (s+a) + \int_{-a}^{s} \int_{-a}^{\zeta} \left[q^-(\eta) + q^+(\eta) \right] d\eta d\zeta \right\} . \tag{144}$$

The pressure $p^-(s)$ and tangential tractions $q^+(s)$ and $q^-(s)$ are chosen as the unknown loads of the problem. Following the outline of the previous chapter, the continuous distribution of these unknown tractions are discretized and the contact equations are then satisfied at a discrete number of points. The following expressions for the tractions are introduced

$$\begin{gathered} p^-(s) = \sum_{m=2}^{M-1} p_m \psi_m(s) \ , \\ q^+(s) = \sum_{m=2}^{M+\tilde{M}} q_m^+ \psi_m(s) \ , \ q^-(s) = \sum_{m=2}^{M-1} q_m^- \psi_m(s) \ , \end{gathered} \tag{145}$$

where the piecewise linear base functions are

$$\psi_m(s) = \begin{cases} \dfrac{s - s_{m-1}}{s_m - s_{m-1}} \ , \ s_{m-1} \le s < s_m \ , \\ \dfrac{s_{m+1} - s}{s_{m+1} - s_m} \ , \ s_m < s \le s_{m+1} \ , \ m = 1, 2, ..., M + \tilde{M} \ , \\ 0 \qquad , \text{elsewhere} \end{cases} \tag{146}$$

and the grid points $-a = s_1 < s_2 < s_3 \ \ldots \ < s_M = a < s_{M+1} < s_{M+2} < \ \ldots \ < s_{M+\tilde{M}} = \pi R_1$ will in general be unevenly distributed. One possible discretization scheme is

$$s_m = \begin{cases} -a + (m-1)\Delta s \ , & m = 1, 2, ..., M \ , \quad \Delta s = 2a/(M-1) \ , \\ a + (m-M)\Delta \tilde{s} \ , & m = M+1, M+2, ..., M+\tilde{M} \ , \quad \Delta \tilde{s} = (\pi R_1 - a)/\tilde{M} \ , \end{cases} \tag{147}$$

i.e., the discretization is uniform within the nip area and the wrap but the spacing is different. In practice, the spacing in the wound roll wrap can be much sparser since the pressure and hence the tangential traction is much smaller there than within the nip.

The proper sense of rolling is introduced by taking the backward difference approximation for the tangential strain:

$$\varepsilon^{\pm}(s) \approx \frac{u_t(s) - u_t(s - \Delta s)}{\Delta s} = \frac{1}{2hA_{\theta\theta}} T_{in} + \frac{1}{2h\Delta s A_{\theta\theta}} \int_{s-\Delta s}^{s} \int_{-a}^{\zeta} \left[q^-(\eta) + q^+(\eta) \right] d\eta d\zeta \ . \tag{148}$$

Using the notations (122) the expression for the tangential web strain at the grid points s_l becomes:

$$\varepsilon_l^{\pm} = \frac{1}{2}\tilde{T}_{in} + \sum_{m=2}^{M+\tilde{M}} \mathcal{D}_{lm}^{+}\tilde{q}_m^{+} + \sum_{m=2}^{M-1} \mathcal{D}_{lm}^{-}\tilde{q}_m^{-} \ , \tag{149}$$

where

$$\begin{aligned} \mathcal{D}_{lm}^{+} &= \frac{1}{2(s_l - s_{l-1})h} \int_{s_l-\Delta s}^{s_l} \int_{-a}^{\zeta} \psi_m(\eta) d\eta d\zeta \ , \ l, m = 2,3,...,M+\tilde{M} \ , \\ \mathcal{D}_{lm}^{-} &= \frac{1}{2(s_l - s_{l-1})h} \int_{s_l-\Delta s}^{s_l} \int_{-a}^{\zeta} \psi_m(\eta) d\eta d\zeta \ , \ l = 2,3,...,M+\tilde{M} \ , \ m = 2,3,...,M-1 \ . \end{aligned} \tag{150}$$

Although the cylinder solutions (59) are directly applicable to the wrap, the dependence of the wound roll pressure on the tangential tractions and the incoming web tension introduces additional terms in the expressions of the displacements of the wound roll.

The Fourier presentations of the surface tractions were

$$\begin{aligned} p^{\pm}(s) &= c_{0,i} + \sum_{n=1}^{\infty} \left(d_{n,i} \sin n\frac{s}{R_i} + c_{n,i} \cos n\frac{s}{R_i} \right), \\ q^{\pm}(s) &= e_{0,i} + \sum_{n=1}^{\infty} \left(f_{n,i} \sin n\frac{s}{R_i} + e_{n,i} \cos n\frac{s}{R_i} \right), \end{aligned} \tag{151}$$

where the Fourier coefficients are calculated by the following integrals

$$\begin{aligned} c_{0,i} &= \frac{1}{2\pi R_i} \int_0^{2\pi R_i} p^{\pm}(s) ds, \ c_{n,i} = \frac{1}{\pi R_i} \int_0^{2\pi R_i} p^{\pm}(s) \cos n\frac{s}{R_i} ds \ , \ d_{n,i} = \frac{1}{\pi R_i} \int_0^{2\pi R_i} p^{\pm}(s) \sin n\frac{s}{R_i} ds \ , \\ e_{0,i} &= \frac{1}{2\pi R_i} \int_0^{2\pi R_i} q^{\pm}(s) ds, \ e_{n,i} = \frac{1}{\pi R_i} \int_0^{2\pi R_i} q^{\pm}(s) \cos n\frac{s}{R_i} ds \ , \ f_{n,i} = \frac{1}{\pi R_i} \int_0^{2\pi R_i} q^{\pm}(s) \sin n\frac{s}{R_i} ds \ . \end{aligned} \tag{152}$$

The expressions of the Fourier coefficients on the winding drum side remain unaltered. However, in the wound roll side there will be an additional term in $c_{0,1}$, $c_{n,1}$ and $d_{n,1}$ due to the hoop stress. Inserting the expression (142) into Eq. (152) yields for *i*= 1:

$$
\begin{aligned}
c_{0,1} &= \frac{1}{2\pi R_1}\int_0^{2\pi R_1} p^-(s)ds + \frac{1}{2\pi R_1}\int_0^{2\pi R_i}\frac{1}{\rho^+(s)}\left\{T_{in}+\int_{-a}^{s}\left[q^+(\xi)+q^-(\xi)\right]d\xi\right\}ds\,,\\
c_{n,1} &= \frac{1}{\pi R_1}\int_0^{2\pi R_1} p^-(s)\cos n\frac{s}{R_1}ds + \frac{1}{\pi R_1}\int_0^{2\pi R_i}\frac{1}{\rho^+(s)}\left\{T_{in}+\int_{-a}^{s}\left[q^+(\xi)+q^-(\xi)\right]d\xi\right\}\cos n\frac{s}{R_1}ds\,,\\
d_{n,1} &= \frac{1}{\pi R_1}\int_0^{2\pi R_1} p^-(s)\sin n\frac{s}{R_1}ds + \frac{1}{\pi R_1}\int_0^{2\pi R_i}\frac{1}{\rho^+(s)}\left\{T_{in}+\int_{-a}^{s}\left[q^+(\xi)+q^-(\xi)\right]d\xi\right\}\sin n\frac{s}{R_1}ds\,.
\end{aligned}
\qquad (153)
$$

An expression for the radius of curvature is needed for the calculation of (153). When the radial displacement u_{r1} is known, the expression of the curvature $1/\rho^+$ becomes [35]:

$$
\frac{1}{\rho^+(s)} = \frac{1}{R_1}\left\{1 - R_1\left[u_{r1}''(s) - 2\frac{u_{r1}}{R_1^2}\right]\right\}\,. \qquad (154)
$$

The radius of curvature depends on the solution and, hence, introduces a nonlinearity in the problem. Here an iterative approach is proposed: the iteration of the radius of curvature is added as the outmost loop of the solution algorithm. In other words, the curvature (154) is calculated using the radial displacement of the previous iteration loop. It should be noted that small displacements were assumed when deriving Eq. (154) and that positive (negative) sign of ρ^+ implies that the center of curvature lies on the same (opposite) side of the wound roll periphery as the roll center. In order to facilitate the calculation of the integrals (153), the square bracketed term of (154) is expressed as

$$
u_{r1}''(s) - 2\frac{u_{r1}}{R_1^2} = \sum_{m=1}^{M+\tilde{M}} \vartheta_m \psi_m(s)\,. \qquad (155)
$$

By inserting Eqs. (154) and (155) into Eq. (153) the expressions for the Fourier coefficients become

$$
\begin{aligned}
c_{n,1} &= \sum_{m=2}^{M-1}\alpha_{nm,1}p_m + \sum_{m=2}^{M+\tilde{M}}\Gamma_{nm}^+ q_m^+ + \sum_{m=2}^{M-1}\Gamma_{nm}^- q_m^- + \hat{\Gamma}_n T_{in}\,,\ n = 0,1,2,\ldots\,,\\
d_{n,1} &= \sum_{m=2}^{M-1}\beta_{nm,1}p_m + \sum_{m=2}^{M+\tilde{M}}\Lambda_{nm}^+ q_m^+ + \sum_{m=2}^{M-1}\Lambda_{nm}^- q_m^- + \hat{\Lambda}_n T_{in}\,,\ n = 1,2,3,\ldots\,,
\end{aligned}
\qquad (156)
$$

where the coefficients of the winding drum pressures are

$$\alpha_{0m,1} = \frac{1}{2\pi R_1}\int_{-a}^{a}\psi_m(s)ds\ ,\ m=1,2,3,...,M\ ,$$
$$\alpha_{nm,1} = \frac{1}{\pi R_1}\int_{-a}^{a}\psi_m(s)\cos n\frac{s}{R_1}ds\ ,\ m=1,2,3,...,M\ ,\ n=1,2,3,...\ , \qquad (157)$$
$$\beta_{nm,1} = \frac{1}{\pi R_1}\int_{-a}^{a}\psi_m(s)\sin n\frac{s}{R_1}ds\ ,\ m=1,2,3,...,M\ ,\ n=1,2,3,...\ ,$$

the coefficients of the wound roll tangential tractions are

$$\Gamma_{0m}^{+} = \frac{1}{2\pi R_1}\int_{0}^{2\pi R_1}\frac{1}{\rho^{+}(s)}\int_{-a}^{s}\psi_m(\zeta)d\zeta ds\ ,\ m=2,3,...,M+\tilde{M}\ ,$$
$$\Gamma_{nm}^{+} = \frac{1}{\pi R_1}\int_{0}^{2\pi R_1}\frac{\cos(ns/R_1)}{\rho^{+}(s)}\int_{-a}^{s}\psi_m(\zeta)d\zeta ds\ ,\ m=2,3,...,M+\tilde{M},\ n=1,2,3,...\ , \qquad (158)$$
$$\Lambda_{nm}^{+} = \frac{1}{\pi R_1}\int_{0}^{2\pi R_1}\frac{\sin(ns/R_1)}{\rho^{+}(s)}\int_{-a}^{s}\psi_m(\zeta)d\zeta ds\ ,\ m=2,3,...,M+\tilde{M},\ n=1,2,3,...\ ,$$

the coefficients of the winding drum tangential tractions are

$$\Gamma_{0m}^{-} = \frac{1}{2\pi R_1}\int_{0}^{2\pi R_1}\frac{1}{\rho^{+}(s)}\int_{-a}^{s}\psi_m(\zeta)d\zeta ds\ ,\ m=2,3,...,M\ ,$$
$$\Gamma_{nm}^{-} = \frac{1}{\pi R_1}\int_{0}^{2\pi R_1}\frac{\cos(ns/R_1)}{\rho^{+}(s)}\int_{-a}^{s}\psi_m(\zeta)d\zeta ds\ ,\ m=2,3,...,M\ ,\ n=1,2,3,...\ , \qquad (159)$$
$$\Lambda_{nm}^{-} = \frac{1}{\pi R_1}\int_{0}^{2\pi R_1}\frac{\sin(ns/R_1)}{\rho^{+}(s)}\int_{-a}^{s}\psi_m(\zeta)d\zeta ds\ ,\ m=2,3,...,M\ ,\ n=1,2,3,...\ ,$$

and the coefficients of the incoming web tension are

$$\hat{\Gamma}_0 = \frac{1}{2\pi R_1}\int_{0}^{2\pi R_1}\frac{1}{\rho^{+}(s)}ds\ ,$$
$$\hat{\Gamma}_n = \frac{1}{\pi R_1}\int_{0}^{2\pi R_1}\frac{\cos(ns/R_1)}{\rho^{+}(s)}ds,\ n=1,2,3,...\ , \qquad (160)$$
$$\hat{\Lambda}_n = \frac{1}{\pi R_1}\int_{0}^{2\pi R_1}\frac{\sin(ns/R_1)}{\rho^{+}(s)}ds,\ n=1,2,3,...\ .$$

When the expressions (156) are inserted into the elastic solution of the cylinder (59), the influence coefficient presentations for the wound roll radial displacement and tangential strain are obtained as

$$
\begin{aligned}
v_{l,1} &= v_1(x_l) = \sum_{m=2}^{M-1} \tilde{A}_{lm,i}\,\tilde{p}_m + \sum_{m=2}^{M+\tilde{M}} \tilde{B}^{+}_{lm,1}\tilde{q}^{+}_m + \sum_{m=2}^{M-1} \tilde{B}^{-}_{lm,1}\tilde{q}^{-}_m + \tilde{B}_{l,1}T_{in}\ , \\
\varepsilon_{l,1} &= \varepsilon_1(x_l) = \sum_{m=2}^{M-1} \tilde{C}_{lm,i}\,\tilde{p}_m + \sum_{m=2}^{M+\tilde{M}} \tilde{D}^{+}_{lm,1}\tilde{q}^{+}_m + \sum_{m=2}^{M-1} \tilde{D}^{-}_{lm,1}\tilde{q}^{-}_m + \tilde{D}_{l,1}T_{in}\ .
\end{aligned}
\tag{161}
$$

Now the equations at disposal are the indentation equation

$$
v_{l,1} + v_{l,2} - \delta + \Delta\left(\frac{1}{R_1} + \frac{1}{R_2}\right)x_l = \frac{1}{2}\left(\frac{1}{R_1} + \frac{1}{R_2}\right)x_l^{\,2}\ ,\ l = 1,2,...,M\ ,
\tag{162}
$$

and the stick equations

$$
\begin{aligned}
&\varepsilon^{+}_l - \varepsilon_{l,1} + \varepsilon_{M+\tilde{M},1} - \frac{1}{2hA_{\theta\theta}}WOT = 0\ ,\ l = 2,3,...,M+\tilde{M}-1 \\
&\varepsilon^{-}_l - \varepsilon_{l,2} + \xi^{-} = 0\ ,\ \ l = 2,3,...,M-1\ ,
\end{aligned}
\tag{163}
$$

or the slip equations

$$
\begin{aligned}
q^{+}_l &= \mu^{+}\,\mathrm{sgn}\,\upsilon^{+}\,p^{+}_l\ ,\ l = 2,3,...,M+\tilde{M}\ , \\
q^{-}_l &= \mu^{-}\,\mathrm{sgn}\,\upsilon^{-}\,p_l\ ,\ l = 2,3,...,M\ .
\end{aligned}
\tag{164}
$$

3.6 Modified Panagiotopoulos Process

The numerical solution scheme is described here for the contact equations confined to the nip area as presented in Chapter 3.4. The generalization to the extended theory of Chapter 3.5 is straightforward.

The unknowns of the problem are $p_2,\ldots,p_{M-1}$, $q_1^{\pm},\ldots,q_M^{\pm}$, $\delta, a, \Delta, \xi^{-}$ and T_{out}. The equations at disposal are the indentation equation (126) and the stick/slip equations (131) and (132) written at discrete points within the contact area and the equilibrium equations (136). The appropriate solution process is a variation of the *Panagiotopoulos Process* [36]. For the sake of simplicity the contact half-width *a* is taken as a given quantity as explained before and, hence, the iteration of the contact area is excluded from the Panagiotopoulos process. The problem is now solved by the following algorithm:

Step 0. Initiate with $q_l^+ = q_l^- = 0$, $(l = 2,3,...,M-1)$.

Step 1. Calculate p_l $(l = 2,3,...,M-1)$, Δ and δ from the normal problem.

Step 2. Assume stick at all points x_l. With p_l obtained from Step 1, calculate q_l^+, q_l^-, ξ^- and T_{out} from the tangential problem and total equilibrium.

Step 3. If $\left|q_l^\pm\right| > \mu^\pm p_l$, then index *l* is placed in $S^\pm$ (index set: area of slip in upper or lower contact).

If $\left|q_l^\pm\right| \le \mu^\pm p_l$, then *l* is placed in $A^\pm$ (index set: area of adhesion in upper or lower contact).

Step 4. If *l* is in $S^\pm$, then $q_l^\pm = \mu^\pm \operatorname{sgn}(v_l^\pm) p_l$. If *l* is in $A^\pm$, then the corresponding stick equation is used. In conjunction with the global equilibrium equations (135), these are linear equations. Solve them.

Step 5. If *l* is in $A^\pm$, as well as the just-found $\left|q_l^\pm\right| > \mu^\pm p_l$, then *l* is placed in the area of slip $S^\pm$.

Step 6. If $A^\pm$ is changed in Step 5, then go to Step 4.

Step 7. If *l* is in $S^\pm$, and $q_l^\pm$ and the relative speed between the surfaces have the wrong sign with respect to each other ($q^\pm v^\pm \le 0$), then *l* is placed in $A^\pm$.

Step 8. If $S^\pm$ is changed in Step 7, then go to Step 4.

Step 9. If the difference between the just calculated and the previous shear stresses is larger than the required tolerance, go to Step 1. Otherwise, stop.

When the iteration of the contact width is required, then it must be done at a loop one level higher than the Panagiotopoulos process. In present work this loop, which calls the Panagiotopoulos process successively, is implemented as a simple secant method. In order to obtain ±1 N/m accuracy for the normal load *P*, typically three iteration loops are needed.

4 NUMERICAL RESULTS

Although the theory accounting for the possible variation in the web tension of the topmost paper layer wrapping the wound roll behind the nip was derived in Chapter 3.5, in the following the numerical results will be based on the theory confined to the nip area as presented in Chapter 3.4. This is justified since it will be shown in Chapter 4.9 that the slip behavior behind the nip has a minor effect on the wound-on tension.

4.1 Independent winding parameters

For the winding configuration of Figure 1 the winding parameters are the compressive total load *P*, the winding force *F* and the incoming web tension T_{in}. However, the nip-induced tension is not dependent on all of them, as the next theorem proves.

Winding theorem:

Let $\mathcal{F}$ *denote the relation between the nip-induced tension NIT, the other dependent variables* p_m, q_m^+, q_m^-, ξ^-, δ *and* Δ *and the independent variables F,* T_{in} *and P of the contact problem for given material parameters, i.e.,*

$$\mathcal{F}(\mathrm{NIT}, p_m, q_m^+, q_m^-, \xi^-, \delta, \Delta; F, T_{in}, P) = 0 \ . \tag{165}$$

Then for a given solution (165) and arbitrary T_{in}^* *there exists* ξ^{-*} and δ^* *so that*

$$\mathcal{F}(\mathrm{NIT}, p_m, q_m^+, q_m^-, \xi^-, \delta, \Delta; F, T_{in}, P) = \mathcal{F}(\mathrm{NIT}, p_m, q_m^+, q_m^-, \xi^{-*}, \delta^*, \Delta; F, T_{in}^*, P) = 0 \ . \tag{166}$$

Proof.

It is assumed that the following equations hold

1) The indentation equation:

$$\begin{aligned}&\sum_{m=2}^{M-1}\left(A_{lm,1} + A_{lm,2} + \delta_{lm}A\right)p_m - \delta + \Delta\left(\frac{1}{R_1} + \frac{1}{R_2}\right)x_l = \frac{1}{2}\left(\frac{1}{R_1} + \frac{1}{R_2}\right)x_l^2 - \\ &\sum_{m=2}^{M-1}\left(B_{lm}^{\pm} + B_{lm,1}\right)q_m^+ - \sum_{m=2}^{M-1}\left(B_{lm}^{\pm} + B_{lm,2}\right)q_m^- - BT_{in} \ ,\end{aligned} \tag{167}$$

2) The stick equations (at the stick points):

$$\begin{aligned} \upsilon^{+} &= \sum_{m=2}^{M-1}\left(D_{lm}^{\pm}+D_{Mm,1}-D_{lm,1}\right)q_m^{+}+\sum_{m=2}^{M-1}D_{lm}^{\pm}q_m^{-}-\sum_{m=2}^{M-1}(C_{lm,1}-C_{Mm,1}-C_{lm}^{\pm})\,p_m-D\cdot\mathrm{NIT}=0\ , \\ \upsilon^{-} &= \sum_{m=2}^{M-1}D_{lm}^{\pm}q_m^{+}+\sum_{m=2}^{M-1}\left(D_{lm}^{\pm}-D_{lm,2}\right)q_m^{-}+\xi^{-}-\sum_{m=2}^{M-1}(C_{lm,2}-C_{lm}^{\pm})\,p_m+DT_{in}=0\ , \end{aligned} \tag{168}$$

3) The slip equations (at the slip points):

$$\begin{aligned} q_l^{+} &= \mu^{+}\operatorname{sgn}\upsilon^{+}p_l\ , \\ q_l^{-} &= \mu^{-}\operatorname{sgn}\upsilon^{-}p_l\ , \end{aligned} \tag{169}$$

4) Rotational balance of the winding drum and horizontal balance of the sheet:

$$\begin{aligned} \Delta x\sum_{m=2}^{M-1}q_m^{-} &= F\ , \\ \Delta x\sum_{m=2}^{M-1}\left(q_m^{+}+q_m^{-}\right) &= \mathrm{NIT} \end{aligned} \tag{170}$$

Let us define

$$\delta^{*}=\delta+B(T_{in}^{*}-T_{in})\ ,\ \xi^{-^{*}}=\xi^{-}-D(T_{in}^{*}-T_{in})\ . \tag{171}$$

With these definitions, Eqs. (167)-(170) hold, with δ^{*} in place of δ, $\xi^{-^{*}}$ in place of ξ^{-} and T_{in}^{*} in place of T_{in}. This proves the theorem. ■

Hence, it suffices to study the winding nip behavior as a function of P and F; the results will be applicable for arbitrary admissible ($0<T_{in}<$ web breaking tension) values of T_{in}. The interpretation of the Winding Theorem can be seen from Eqs. (123): Due to the Poisson's effect, an increase in tension reduces the thickness of the sheet. Hence, the mutual approach of the cylinders is decreased as shown by (171) ($B < 0$). The tangential strain of the web is increased as seen from the last Eq. of (123). However, the cylinder solutions are independent of T_{in} and, hence, the surface speeds of the cylinder must remain unaltered. Because the surface tractions are equal for all web tensions, the slip and stick zone distributions must be equal. The conclusion is that the web speed also remains independent of the web tension. In order to accommodate this, the web speed in the undeformed state must be reduced and hence the creep ratio is reduced as shown by (171) ($D > 0$).

4.2 Basic mechanism of nip-induced tension

With the indentation (126), stick (131) and slip (132) equations established in Chapter 3 and the Panagiotopoulos process of Section 3.6 in hand, the necessary apparatus for carrying out numerical simulations of the winding nip behavior is now available. Unfortunately the parameter space of the problem is huge. Thus, it is only possible to cover a very limited portion of that space in this study. In order to make the results more concrete, a decision was made to present the results in dimensional units. Before starting to explore the influence of the winding parameters, the layer-to-layer friction coefficient, wound roll and winding drum radius, winding drum cover and paper orthotropic elastic constants, the basic mechanism of the nip-induced tension will be described in this section. The basic material parameter values used in this section and most of the subsequent sections are shown in **Table 1.** Steel's elastic modulus and Poisson's ratio were used for the winding drum. The winding force F was 100 N/m (the winding drum is braking) and the compressive load P = 1900 N/m. According to the winding theorem of the previous section the results are applicable to all admissible values of T_{in}. In the following, the general stick and slip behavior of the winding nip is explained. It should be emphasized that the treatment of this section is restricted to the rigid winding drum!

Table 1.
Material parameter values used in the calculations

Parameter	Notation	Value
Paper to roll friction coefficient	μ^+	0.2
Paper to drum friction coefficient	μ^-	0.4
Wound roll radius	R_1	0.3 m
Winding drum radius	R_2	0.5 m
Radial elastic constant	A_{rr}	20 MPa
Tangential elastic constant	$A_{\theta\theta}$	3 GPa
Cross elastic constant	$A_{r\theta}$	5 MPa
Shear modulus	$G_{r\theta}$	10 MPa

The tangential tractions q^+ (solid line) and q^- (dashed line) together with the traction bounds μ^+p (lighter gray shading) and μ^-p (darker gray shading) are shown in Figure 15 (a) and the relative tangential speed differences v^+ (solid line), v^- (dashed line) and the web tension (dash-dotted line) within the nip in Figure 15 (b).

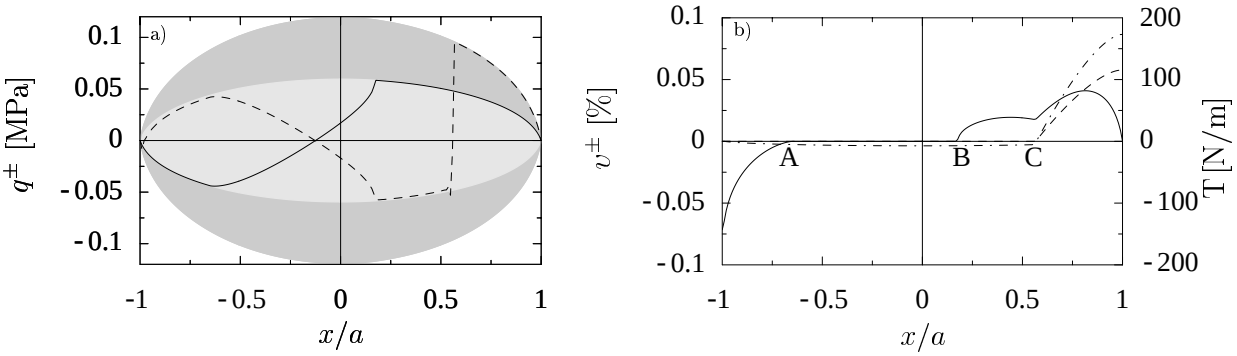

Figure 15. (a) Tangential tractions of the upper (solid line) and lower (dashed line) contacts and the friction limits $\mu^{-}p$ (darker gray shading) and $\mu^{+}p$ (lighter gray shading) and (b) the relative tangential speed differences v^{+} and v^{-} in the web-roll contact (solid line) and web-drum contact (dashed line) and web tension (dash-dotted line).

When the paper web enters the nip there is first a slip zone in the web-roll contact (non-zero relative speed) and a stick zone in the web-drum contact (this applies whenever $\mu^{-} > \mu^{+}$). Because v^{+} is negative, the web is moving slower than the wound roll in this region. At point A, the web-roll contact starts to stick and the web-drum contact remains sticking. After this region, at point B, the web-roll contact will slip till the end of the contact area so that the web moves faster than the roll. In some cases this slip zone can be split into two consecutive slip zones separated by a very short stick area located at the vicinity of point C. The web-drum contact remains in stick still for a while before it starts to slip from C to the trailing edge of the contact. Now both the upper and lower contacts are slipping so that the web is moving faster than the wound roll and winding drum. In this region, from C to the trailing edge of the contact, the increase in web tension develops. It should be noted that the tangential strain ε^{-} cannot change in the area from the leading edge to point C, as the sheet and the rigid winding drum are in contact. For a thin sheet it can be seen from Eq. (72) that $\varepsilon^{+} = \varepsilon^{-}$ and, hence, that ε^{+} cannot change either. The slight decrease in the web tension in the area from the leading edge to point C is due to Poisson's effect and the normal (radial) compression of the sheet.

The general mechanism of the winding nip behavior, applicable when the winding drum is rigid, was described above. Only the relative lengths of the slip zones and possibly the slip directions vary with the winding parameters. In order to facilitate the future analysis of the influence of various parameters and material parameters on the winding nip behavior, the following three "slip ratios" are defined:

$$s_{r1} = \frac{\text{length of the line from -1 to A}}{\text{nip width}} = \text{"leading edge roll slip ratio"}$$
$$s_{r2} = \frac{\text{length of the line from B to 1}}{\text{nip width}} = \text{"trailing edge roll slip ratio"} \qquad (172)$$
$$s_d = \frac{\text{length of the line from C to 1}}{\text{nip width}} = \text{"dual slip ratio"}$$

The sign of these slip ratios is chosen to be positive if the sheet advances the roll or drum and negative if the sheet falls behind.

4.3 Influence of the winding force

In this section the influence of the winding force on the NIT and contact width is studied as a function of the net compressive load *P*. The material parameter values used in the calculations correspond to **Table 1**. The winding force *F* takes values –500, -400, -200, 0 and 100 N/m. The case *F* = 0 N/m corresponds to center winding and the other values correspond generally to hybrid winding except when T_{in} = -*F*, which correspond to surface winding.

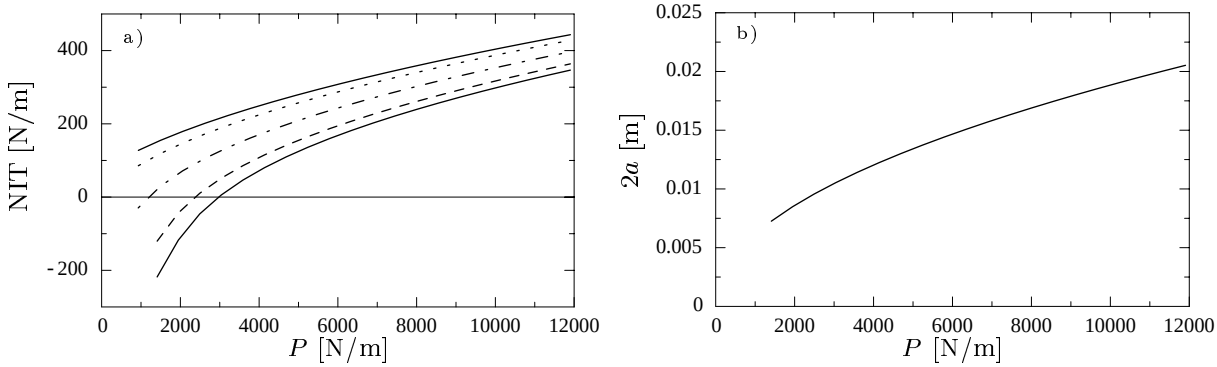

Figure 16. (a) Nip-Induced Tension and (b) the nip width as a function of the net compressive load *P* for the following winding forces: -500 N/m (lowest solid line), -400 N/m (dashed line), -200 N/m (dash-dotted line), 0 N/m (dotted line) and 100 N/m (highest solid line).

The Nip-Induced Tension and nip width are shown in Figures 14 (a) and (b), respectively. First, it can be concluded that NIT is to some extent influenced by the winding force while the nip width is practically independent of it. Secondly, for all *P*, the higher the winding force the higher the NIT. Furthermore, the influence of *F* seems to be more pronounced for a small *P*.

Calculation shows that, likewise with the nip width, the mutual approach of the paper roll and winding drum is also independent of the winding force. Hence, the theory presented by

Jalkanen [23] and Särkelä [48] cannot be valid, since NIT was only a function of the mutual approach of the winding drum and paper roll (Eq. (9)) in their model.

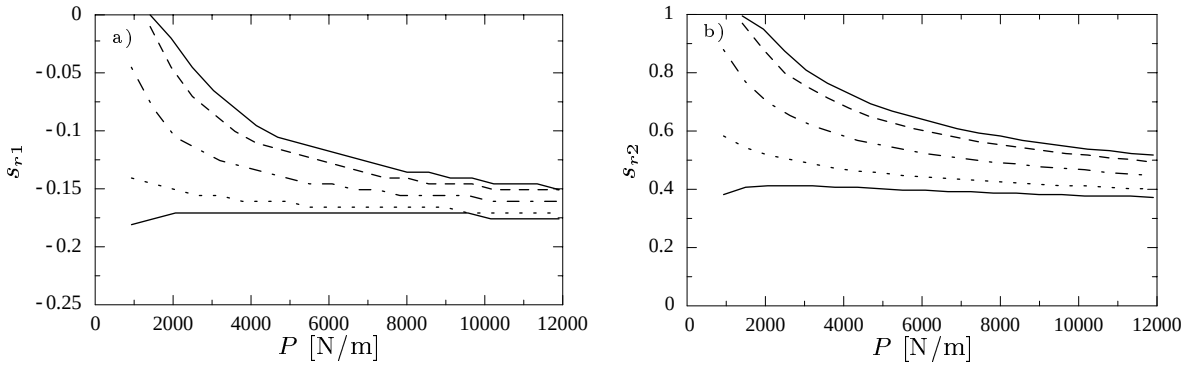

Figure 17. (a) Leading and (b) trailing edge roll slip ratios as a function of the net compressive load P for the following winding forces: -500 N/m (highest solid line), -400 N/m (dashed line), -200 N/m (dash-dotted line), 0 N/m (dotted line) and 100 N/m (lowest solid line).

The leading and trailing edge roll slip ratios are shown in Figures 15 (a) and (b), respectively. The non-smooth character of the slip ratio curves reflects the discretization of the contact, which in this example consists of 200 equidistant grid points. The influence of F is more pronounced for small P values on the roll slip ratios as well. When the winding force value is 100 N/m, the roll slip ratios are almost independent of P, while for lower winding force values the influence of the compressive load is much stronger. It is interesting to note that $s_{r1} = 0$ and $s_{r2} = 1$ for very low values of P and F, i.e., the sheet-roll contact is in total slippage so that the sheet advances the roll. From the signs of s_{r1} and s_{r2} it can be concluded that at the leading edge slip zone, the roll always advances the sheet and at the trailing edge slip zone the sheet always advances the roll.

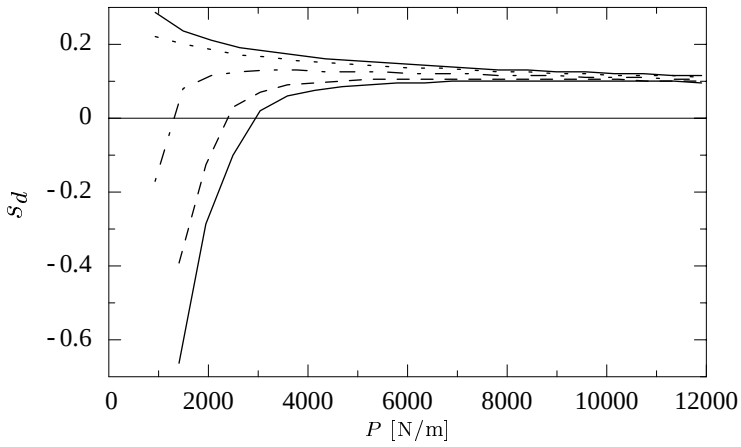

Figure 18. The dual slip ratio as a function of the net compressive load P for the following winding forces: -500 N/m (lowest solid line), -400 N/m (dashed line), -200 N/m (dash-dotted line), 0 N/m (dotted line) and 100 N/m (highest solid line).

The dual slip ratio is shown in Figure 18. The signs of the dual slip ratio and NIT correspond each other. For $F \geq 0$ N/m the dual slip ratio decreases with P and for $F \leq$ -200 N/m it increases. As P increases all curves seem to approach a common limit, which is about 0.1 in this example. Hence, for high nip loads the absolute length of the dual slip zone is proportional to the nip width and independent of F and P.

4.4 Influence of the layer-to-layer friction coefficient

The nip-induced tension as a function of the layer-to-layer friction coefficient is shown in Figure 19 for two nip load values a) 1910 and b) 4897 N/m. At first glance the expected behavior, the decrease of the nip-induced tension as the layer-to-layer friction coefficient increases, seems to occur. Surprisingly, however, for the lower nip load at the winding force values F = -500, -400 and –200 N/m the NIT curves exhibit a local maximum in the lower μ^+ range of the plot. For the higher nip load in Figure (b) the NIT curve corresponding to F = -500 N/m also attains a maximum. Another interesting feature is that the curves NIT(μ^+) seem to be steeper for higher compressive loads P.

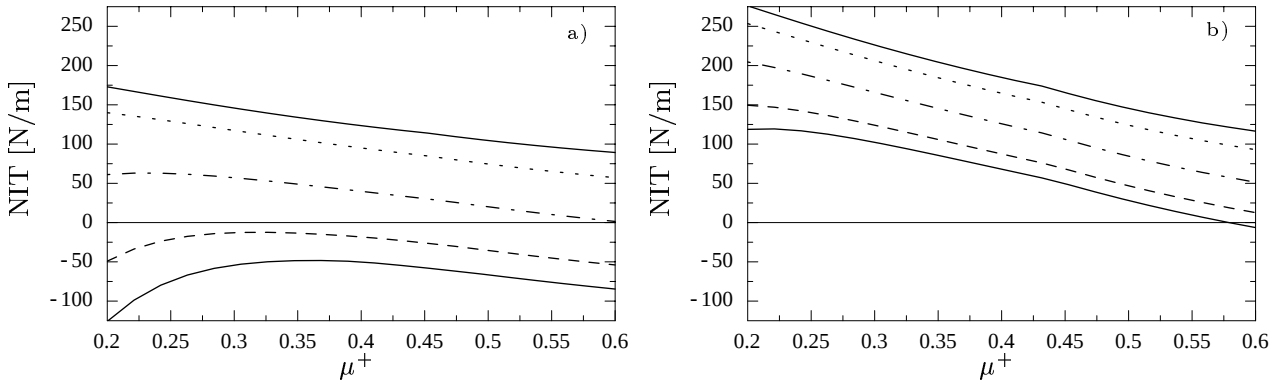

Figure 19. Nip-Induced Tension as a function of the layer-to-layer friction coefficient μ^+ for the following winding forces: -500 N/m (lowest solid line), -400 N/m (dashed line), -200 N/m (dash-dotted line), 0 N/m (dotted line) and 100 N/m (highest solid line). μ^- = 0.4, (a) P = 1910 and (b) P = 4897 N/m.

The general winding nip slip behavior, described in Section 4.2, applies only to $\mu^+ < \mu^-$. Figure 20 (b) shows how the case $\mu^+ > \mu^-$ deviates from the winding nip behavior described in Section 4.2, which is exemplified in panel (a). The coefficient of friction between the winding drum and the sheet is in both cases 0.4 and the layer-to-layer friction coefficient is 0.3 in panel (a) and 0.5 in panel (b). In panel (b), another dual slip zone emerges at the leading edge of the contact, where the sheet slightly advances the winding drum. Unlike the more common case, described in Chapter

4.2, the trailing edge slip zone starts to develop at the winding drum-sheet contact prior to the wound roll-sheet contact. First, the drum advances the sheet and the nip-induced tension decreases. Next, on the very last portion of the nip, the sign of the relative speed changes and finally some 125 N/m of total NIT is developed. In panel (a) the total NIT is 206 N/m.

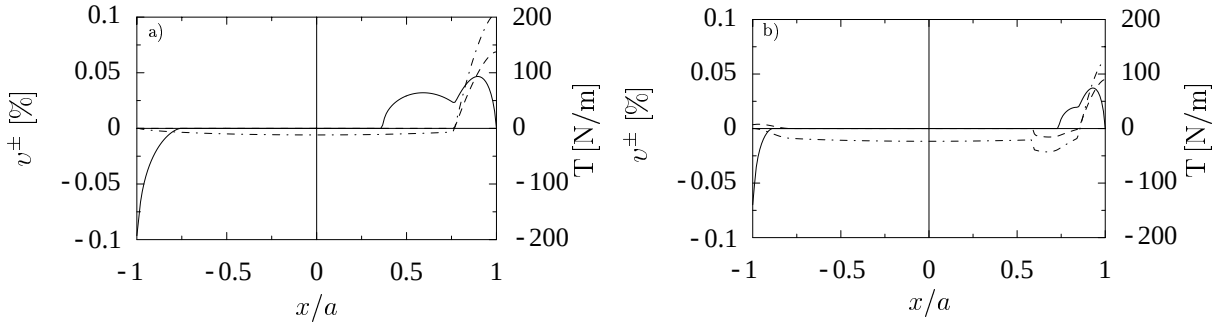

Figure 20. The relative tangential speed differences on the web-roll contact (solid line) and web-drum contact (dashed line) and nip-induced tension (dash-dotted line) for (a) $0.3 = \mu^{+} < \mu^{-} = 0.4$ and (b) $0.5 = \mu^{+} > \mu^{-} = 0.4$.

4.5 Influence of the wound roll and winding drum radius

The five curves of Figure 21 show the behavior of the nip-induced tension as a function of the wound roll radius R_1. The nip load is a constant P = 4850 N/m and the winding force attains the values –500, -400, -200, 0 and 100 N/m. In panels (a) and (b) the winding drum radii are 0.25 and 0.5 m, respectively. The other material parameter values correspond to **Table 1**. The following trends can be concluded

- the NIT decreases as the paper roll radius increases
- the change in NIT is more pronounced for small roll radii; for $R_1 > 0.5$ m the change in NIT is negligible.
- the influence of the roll radius on NIT decreases as the winding force decreases
- when the winding drum radius is larger, less NIT is produced but the curves are steeper

Inspection of the dual slip ratio shows what can be anticipated: s_d decreases as either the roll or drum radius increases. Hence, in order to deduce by simple reasoning that the NIT increases as the roll radius decreases it remains to be shown that the NIT is an increasing function of the dual slip ratio s_d. Indeed, approximating the actual pressure distribution to be Hertzian and applying the results of Section 4.2, the following dependence is obtained:

$$\mathrm{NIT}(s_d) = \int_y^a \left[q^+(x) + q^-(x) \right] dx = (\mu^+ + \mu^-) \int_y^a p(x) dx \approx \frac{2P}{\pi} (\mu^+ + \mu^-) \int_{1-2|s_d|}^1 \sqrt{1-\xi^2}\, d\xi$$
$$= \frac{P}{2\pi} (\mu^+ + \mu^-) \left[\pi - 4(1-2|s_d|)\sqrt{(1-|s_d|)|s_d|} - 2\arcsin(1-2|s_d|) \right] \quad (173)$$

It can be easily shown that the resulting function NIT(s_d) is an increasing function and, hence, the conclusion is that NIT increases as the radius decreases. It should be noted that (173) could be used for the experimental determination of NIT if the dual slip ratio could be measured by some means.

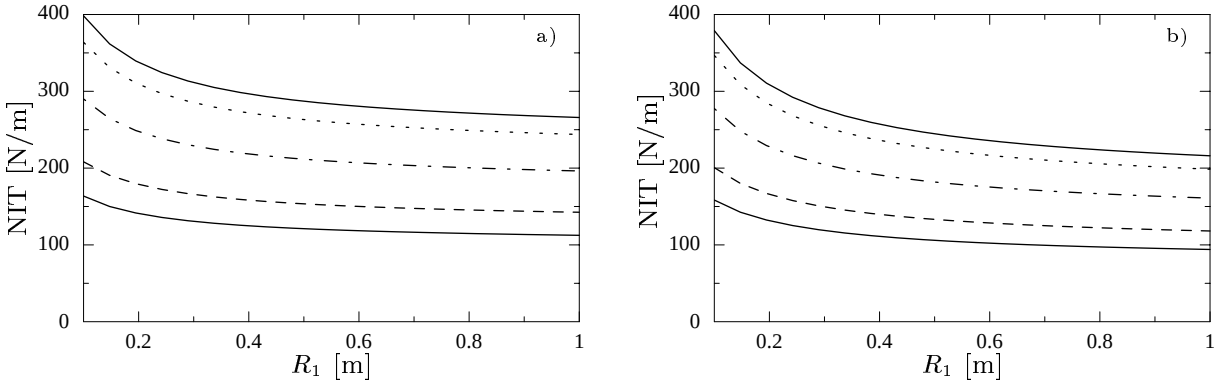

Figure 21. Nip-induced tension as a function of the paper roll radius R_1 for the following winding forces: -500 N/m (lowest solid line), -400 N/m (dashed line), -200 N/m (dash-dotted line), 0 N/m (dotted line) and 100 N/m (highest solid line). P = 4850 N/m, (a) R_2 = 0.25 and (b) R_2 = 0.5 m.

The five curves of Figure 22 show the behavior of the nip-induced tension as a function of the winding drum radius R_2. The nip load is a constant P = 4850 N/m and the winding force attains the values –500, -400, -200, 0 and 100 N/m. In panels (a) and (b) the wound roll radii are 0.25 and 0.5 m, respectively. The other material parameter values correspond to **Table 1**. All the conclusions drawn when inspecting the influence of the wound roll radius apply also to the winding drum.

J. D. Pfeiffer concluded from extensive winding simulation tests, done by rolling a drum on a flat horizontal bed with several paper layers clamped rigidly from the other end, that the NIT seems to be inversely proportional to the square root of the drum diameter [41]. When the simulated results are curve fitted, the conclusion is that nip-induced tension is actually inversely proportional to the square root of the relative radius $R = (1/R_1+1/R_2)^{-1}$, not to the drum radius. Pfeiffer's inaccuracy is understandable because his experimental set-up consisted of an infinite wound roll radius.

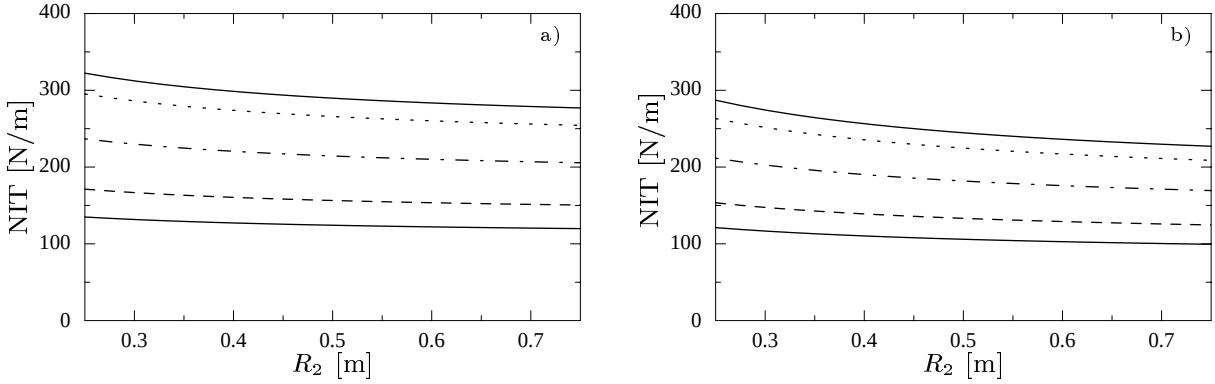

Figure 22. Nip-induced tension as a function of the winding drum radius R_2 for the following winding forces: -500 N/m (lowest solid line), -400 N/m (dashed line), -200 N/m (dash-dotted line), 0 N/m (dotted line) and 100 N/m (highest solid line). P = 4850 N/m, (a) R_1 = 0.25 and (b) R_1 = 0.5 m.

4.6 Winding drum cover design aspects

The nip-induced tension and nip width are shown in Figures 21 and 22 as a function of the winding drum modulus of elasticity E_2, respectively. The results are calculated for five distinct values of Poisson's ratio ν_2 – 0.1, 0.2, 0.3, 0.4 and 0.499. In panels (a) and (b) the compressive load P is 2000 and 5000 N/m, respectively. The cover thickness is 2cm and the other material parameter values corresponds to **Table 1**. It should be noted that the x-axis is plotted on a logarithmic scale.

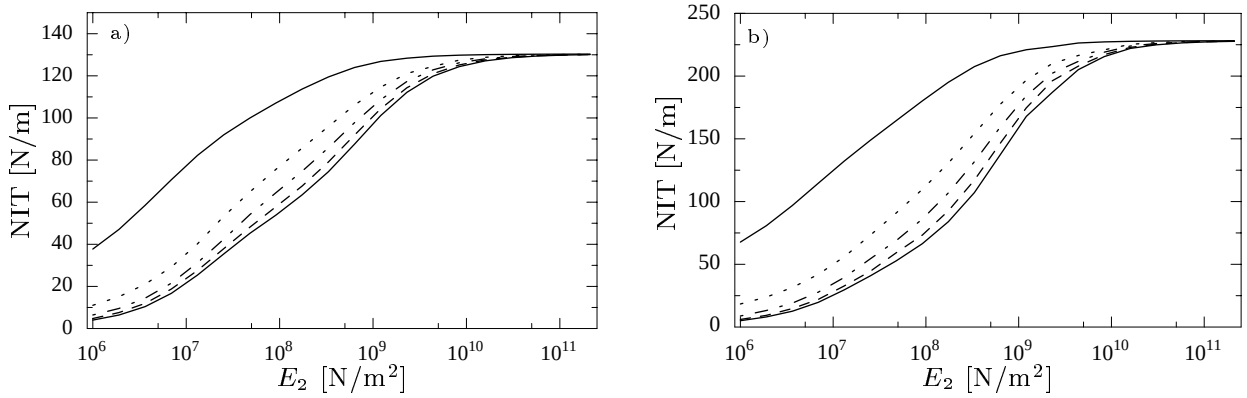

Figure 23. Nip-induced tension as a function of the winding drum modulus of elasticity E_2 for the following values of the Poisson's ratio: 0.1 (lowest solid line), 0.2 (dashed line), 0.3 (dash-dotted line), 0.4 (dotted line) and 0.499 (highest solid line), (a) P = 2000 N/m and (b) P = 5000 N/m.

The nip-induced tension increases approximately logarithmically in the range of $E_2 \in [10^6,10^{10}]$ N/m^2. When $E_2 > 10^{10}$ N/m^2 the NIT is independent of either the modulus of elasticity or Poisson's ratio. As E_2 is below 10^{10} N/m^2 the nip-induced tension increases as Poisson's ratio increases. At the lower values of Poisson's ratio the influence is negligible but when Poisson's ratio approaches 0.5, which is the value of an incompressible material, the influence of ν_2 becomes

significant. The qualitative picture does not seem to depend on the magnitude of the compressive loading P. Most of the conclusions above also apply to the nip width. Perhaps the influence of Poisson's ratio is even less. In addition, the nip width becomes independent of Poisson's ratio and the modulus of elasticity even for smaller values of $E_2 - 2a$ is practically constant when E_2 is above 10^9 N/m^2.

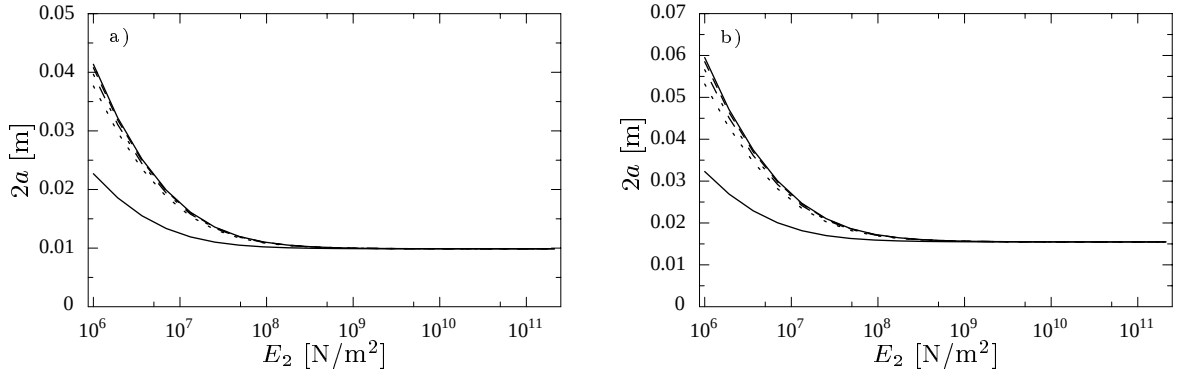

Figure 24. Nip width as a function of the winding drum modulus of elasticity E_2 for the following values of the Poisson's ratio: 0.1 (highest solid line), 0.2 (dashed line), 0.3 (dash-dotted line), 0.4 (dotted line) and 0.499 (lowest solid line), (a) P = 2000 N/m and (b) P = 5000 N/m.

It is interesting to compare the winding contact stresses when winding with soft covered and rigid winding drum. The tangential tractions and relative tangential speed differences for a winding drum with a 2cm thick cover, a cover modulus of elasticity $1 \cdot 10^7$ N/m^2 and Poisson's ratio 0.1, are shown in Figure 25. The other material parameters correspond to **Table 1** and the winding force is 100 N/m. When Figure 25 is compared to Figure 15 the most striking difference is perhaps that the tangential tractions are more than 50 % smaller. The slip behavior in the sheet paper roll contact is basically unchanged: at the leading edge of the contact there is a slip zone where the sheet lags the paper roll and at the trailing edge there is another slip zone where the sheet advances the paper roll. The slip pattern of the winding drum contact differs in two respects: there is also a slip zone in the leading edge of the contact (sheet lags the drum) and the slip direction changes from positive (sheet advances) to negative (sheet lags) very near the trailing edge. In addition, the magnitude of the relative tangential speed difference is larger on the winding drum contact, since the tangential strain is larger due to the compliance of the drum cover (at the edges the absolute value of the relative tangential speed $\bar{v}$ is about 0.35 %). Now the NIT development mechanism is more complex, since the tangential stress on the sheet can also vary noticeably when there is a stick zone in the winding drum contact. Indeed, most of the variation in the tangential stress occurs when both contacts stick. The web tension attains it lowest value at the nip center when it has dropped almost 150 N/m. The

consequence of this is that if the incoming web tension T_{in} is less than 150 N/m, then the web tension is negative in the vicinity of the nip center.

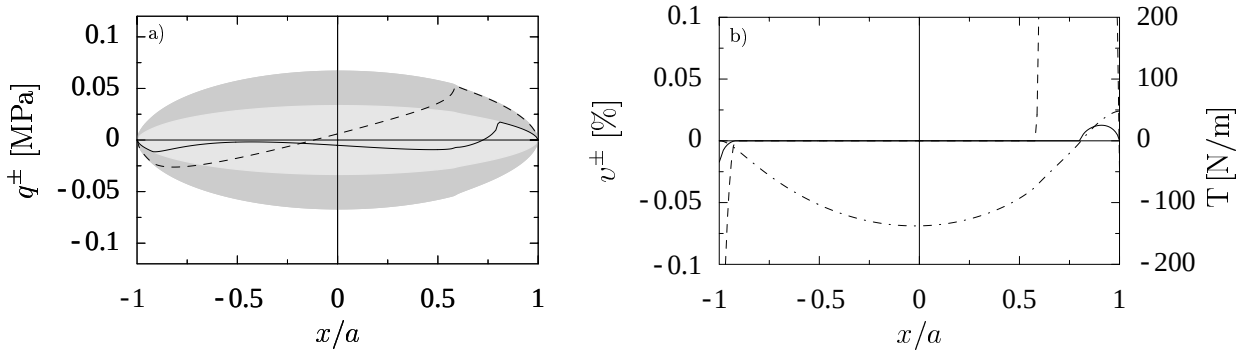

Figure 25. (a) Tangential tractions of the upper (solid line) and lower (dashed line) contacts and the friction limits $\mu^{-}p$ (darker gray shading) and $\mu^{+}p$ (lighter gray shading) and (b) the relative tangential speed differences in the web-roll contact (solid line) and web-drum contact (dashed line) and the web tension increase (dash-dotted line).

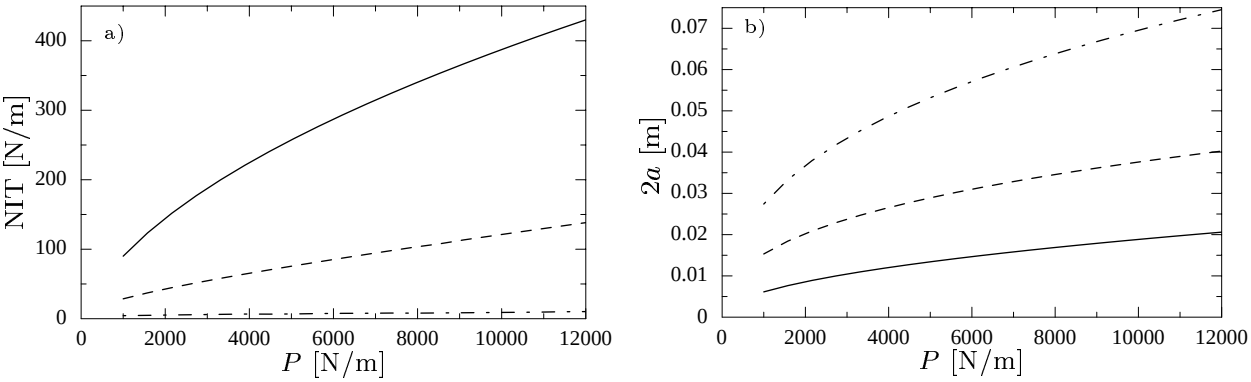

Figure 26. (a) Nip-induced tension and (b) the nip width as a function of the net compressive load P for the following winding drum covers: hard with $E_2 = 2.11 \cdot 10^{11}$ N/m^2 and $\nu_2 = 0.3$ (solid line), 2cm rubber layer with $E_2 = 1 \cdot 10^6$ N/m^2 and $\nu_2 = 0.499$ (dashed line) and 2cm cellular elastomer layer with $E_2 = 1 \cdot 10^6$ N/m^2 and $\nu_2 = 0.1$ (dash-dotted line).

The nip-induced tension and nip width for a winding drum with rigid, rubber and cellular elastomer covers are shown in Figure 26 as a function of the compressive load P. In order to simplify the treatment the elastic behavior of the rubber is approximated by the isotropic constitutive equations with Poisson's ratio of 0.499. The modulus of elasticity of the rubber and cellular elastomer are taken to be $1 \cdot 10^6$ N/m^2 while Poisson's ratio of the elastomer is 0.1. The thickness of the cover is taken to be 2cm. For the cellular elastomer, the NIT is very small and practically independent of P. This agrees with the result of Peters [38]. The NIT for the rubber cover is also noticeably smaller than what it is for the winding drum. However, it increases with P so that the derivative of the NIT curve decreases. This disagrees with Peters [38], who claims that the derivative of the NIT curve with respect to P increases.

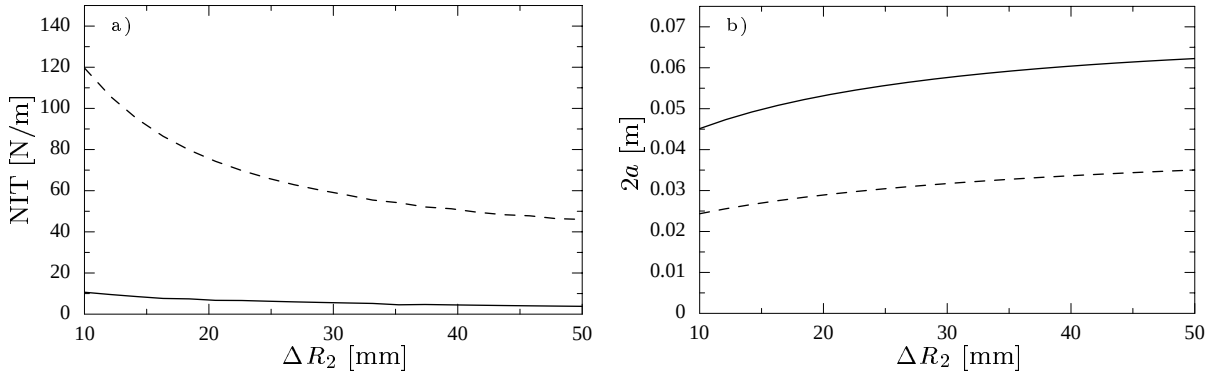

Figure 27. (a) Nip-induced tension and (b) the nip width as a function of the winding drum cover thickness ΔR_2 for the following winding drum covers: rubber with $E_2 = 1{\cdot}10^6$ N/m^2 and $\nu_2 = 0.499$ (dashed line) and cellular elastomer with $E_2 = 1{\cdot}10^6$ N/m^2 and $\nu_2 = 0.1$ (solid line).

The variation of the NIT and nip width with the winding drum cover thickness ΔR_2 for rubbery material (Poisson's ratio 0.499) and cellular elastomer (Poisson's ratio 0.1) are shown in Figures 25 (a) and (b), respectively. The modulus of elasticity of the winding drum is taken to be $1{\cdot}10^6$ N/m^2 and the compressive load P = 5000 N/m. The other material parameters correspond to **Table 1**. As the NIT is very small for the cellular elastomer, the influence of the cover thickness is insignificant in the absolute scale. On the other hand, for the rubbery material the cover thickness has a definite effect on NIT. Namely, the NIT decreases as the cover thickness increases. The dependence of the cover thickness upon NIT is more pronounced when the rubber winding drum cover is thin (~ 10mm).

4.7 Influence of the elastic constants of the paper

The influence of the orthotropic elastic constants on the nip-induced tension is studied in Figure 28. The tangential elastic constant $A_{\theta\theta}$ runs on the x-axis and the curve parameter in each panel is the radial elastic constant A_{rr}, taking the values 4 (solid line), 20 (dashed line) and 100 Mpa (dash-dotted line). The value of the cross elastic constant $A_{r\theta}$ is 0.1 MPa in the left column, 1 MPa at the center and 40 MPa in the right column. The value of the shear modulus $G_{r\theta}$ is 1MPa in the top row, 20 MPa in the midmost row and 100 MPa in the bottom row. The radial nip load is 5 kN/m and the winding force 100 N/m for every panel.

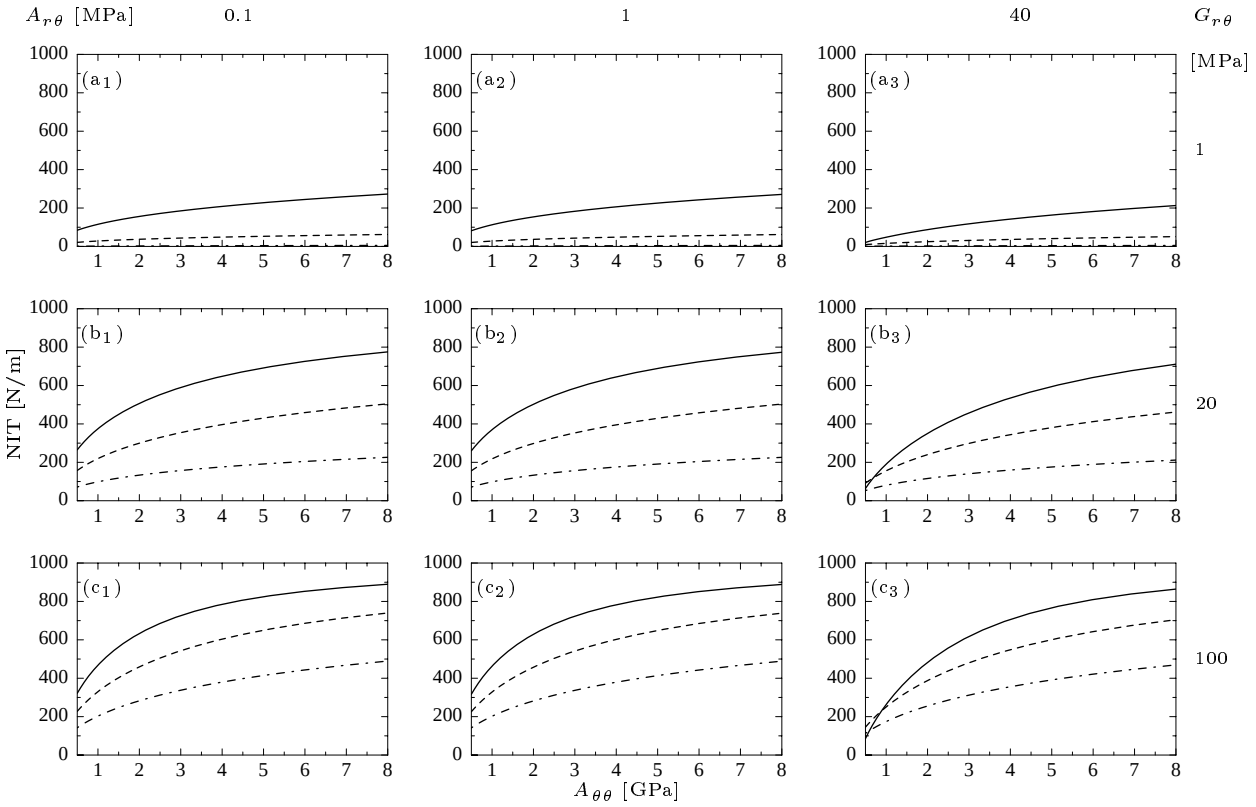

Figure 28. Nip-induced tension as a function of the tangential roll elastic constant $A_{\theta\theta}$ for the following radial roll elastic constants A_{rr}: $4 \cdot 10^6$ N/m² (solid line), $2 \cdot 10^7$ N/m² (dashed line) and 10^8 N/m² (dash-dotted line). Frames with letter label tags (a_i), (b_i) and (c_i) (i = 1,2,3) correspond to the shear modulus $G_{r\theta}$ values 1, 20 and 100 MPa, respectively. Index tags 1,2 and 3 correspond to the cross elastic modulus $A_{r\theta}$ values 0.1, 1 and 40 MPa, respectively.

The following conclusions can be drawn from the figure:

- NIT increases as the tangential elastic constant $A_{\theta\theta}$ increases.
- NIT increases usually as the radial elastic constant A_{rr} decreases. The only exception in the studied range of the elastic constants is seen when $A_{\theta\theta} \in$ [0.5,0.6] GPa, $A_{r\theta}$ = 40 MPa and $G_{r\theta}$ = 100 MPa.
- NIT increases as the shear modulus $G_{r\theta}$ increases
- For small values (≤ 1 MPa) of the cross elastic constant $A_{r\theta}$, NIT is independent of $A_{r\theta}$. For larger values of $A_{r\theta}$, NIT decreases as $A_{r\theta}$ increases

The influence of the orthotropic elastic constants on the dual slip ratio is studied in Figure 29. The *x*-axis, row, and column set up correspond to Figure 28. Again, the non-smooth character of the curves is due to the finite discretization of the contact width. As in the NIT curves, the dual slip ratio increases as the tangential and radial elastic constants and shear modulus increases. However, unlike the NIT, the dual slip ratio increases as the cross elastic constant increases. The reason for

this is that due to the radial stress and strong interaction between the tangential and radial directions the web tension is decreased in the stick zone of the winding drum. This phenomena is depicted in Figure 30 where the web tension of the sheet within the nip area is shown for $A_{\theta\theta}$ =7 GPa, A_{rr} = 20 MPa, $G_{r\theta}$ = 100 MPa and $A_{r\theta}$ = 40 MPa (solid line) and 1 MPa (dashed line). The radial nip load is 5 kN/m and the winding force is 100 N/m. The web tension decreases almost 100 N/m prior to the dual slip zone for $A_{r\theta}$ = 40 MPa, whereas it remains constant for $A_{r\theta}$ = 1 MPa. The tension increases in the dual slip zone more for the larger value of the cross elastic constant but the net increase over the whole nip range still remains smaller.

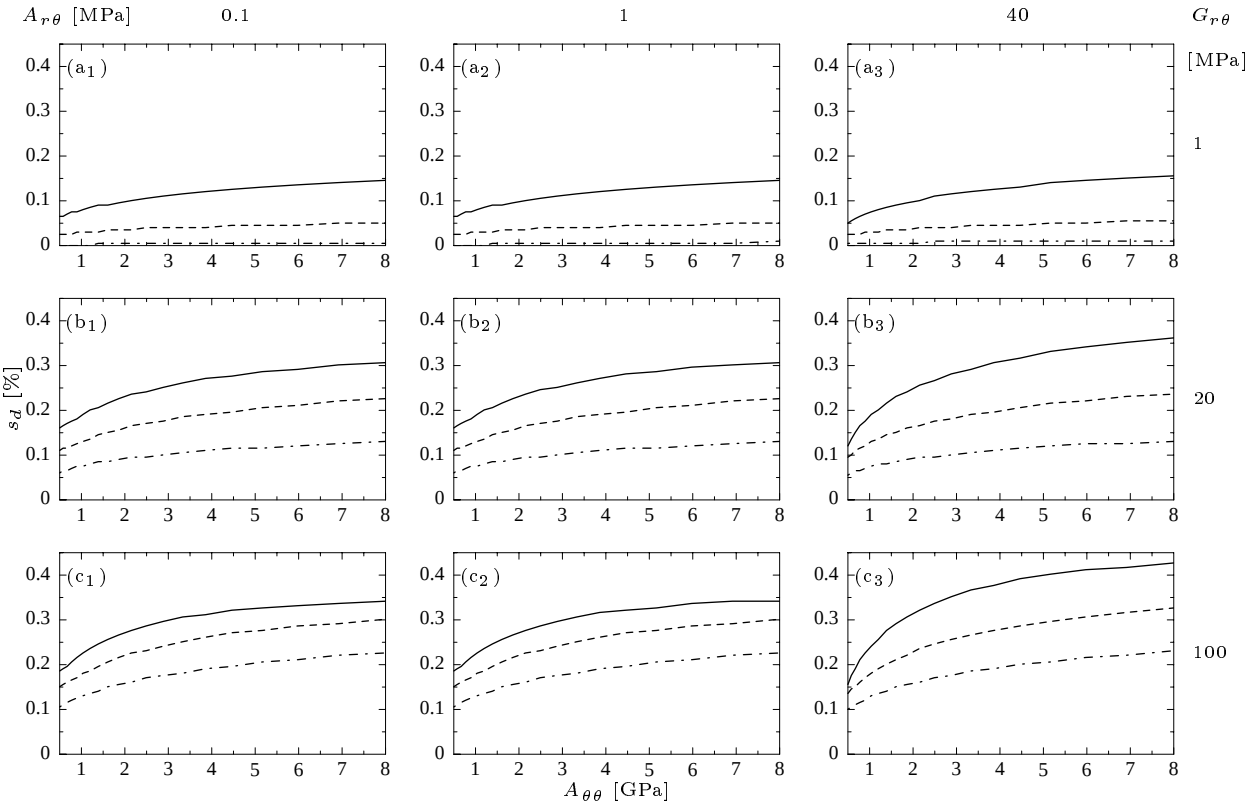

Figure 29. Dual slip ratio s_d as a function of the tangential roll elastic constant $A_{\theta\theta}$ for the following radial roll elastic constants A_{rr}: $4{\cdot}10^6$ N/m² (solid line), $2{\cdot}10^7$ N/m² (dashed line) and 10^8 N/m² (dash-dotted line). Frames with letter label tags (a_i), (b_i) and (c_i) (i = 1,2,3) correspond to the shear modulus $G_{r\theta}$ values 1, 20 and 100 MPa, respectively. Index tags 1,2 and 3 correspond to the cross elastic modulus $A_{r\theta}$ values 0.1, 1 and 40 MPa, respectively.

It should be noted that Eq. (173) was derived under the assumption that the web tension does not change in the stick zone of the winding drum. Therefore, it is not applicable to large cross elastic constants. However, for paper winding it seems to be a valid approximation since the cross elastic constant is know to be small (< 1 MPa)[26].

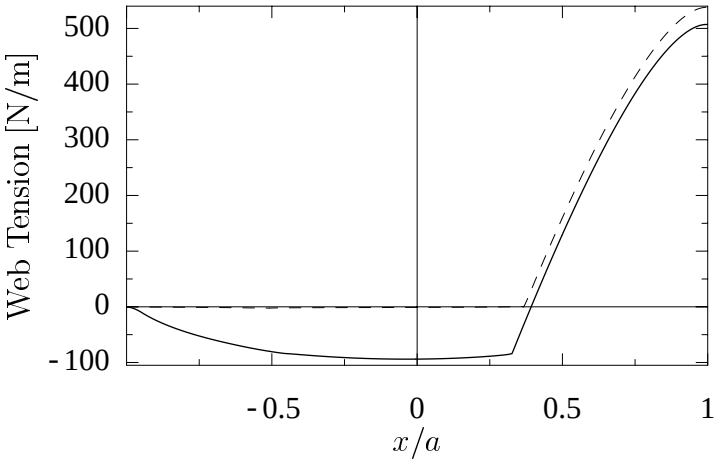

Figure 30. The web tension within the nip area for the cross elastic constant $A_{r\theta}$ = 40 MPa (solid line) and 1MPa (dashed line). The other elastic constants are $A_{\theta\theta}$ =7 GPa, A_{rr} = 20 MPa and $G_{r\theta}$ = 100 MPa. The radial nip load is 5 kN/m and the winding force is 100 N/m.

4.8 Computational aspects

The widely accepted and utilized constitutive law for a paper roll is a modification of the conventional 2D-plane strain, Hooke's law [19]:

$$\begin{aligned} \varepsilon_r &= c_{rr}(\sigma_r)\sigma_r + c_{r\theta}\sigma_\theta \,, \\ \varepsilon_\theta &= c_{r\theta}\sigma_r + c_{\theta\theta}\sigma_\theta \,, \\ \gamma_{r\theta} &= \tau_{r\theta} / G_{r\theta} \,, \end{aligned} \qquad (174)$$

where the orthotropic compliance c_{rr} is a function of the radial stress, whereas the other compliances and the shear modulus are constants. The functional form of the $c_{rr} = c_{rr}(\sigma_r)$ is usually determined from a stack modulus test [43,39] where a stack of paper is compressed between two rigid plates. The elastic modulus $E_r = E_r(\sigma_r) = 1/c_{rr}(\sigma_r)$ is then determined from the measured stress-strain curve. A sample of elastic modulus curves for newsprint, LWC and SC paper grades is shown in Figure 31. The measurements were carried out by Valmet Winders using the hydraulic press and instrumentation available at the KCL laboratory in Finland. It should be noted that these results are not general, rather than just arbitrary representatives of newsprint, SC and LWC paper grades. Figure 31 shows that the radial modulus varies noticeably in the pressure range of 0 to 1.5 MPa, which is roughly the range to be encountered in practice. This brings about a serious concern for the applicability of the linear theory presented in this work. However, as stated in the introduction, quantitatively the data obtained from the linear theory might be inaccurate but it is likely that the phenomenological behavior will still be correct. This hardening behavior in the out-of-plane

direction of the paper stack is partially explained by the escape of the air residing in between the paper layers and partially by the topological behavior of the fibers projecting from the sheet [43].

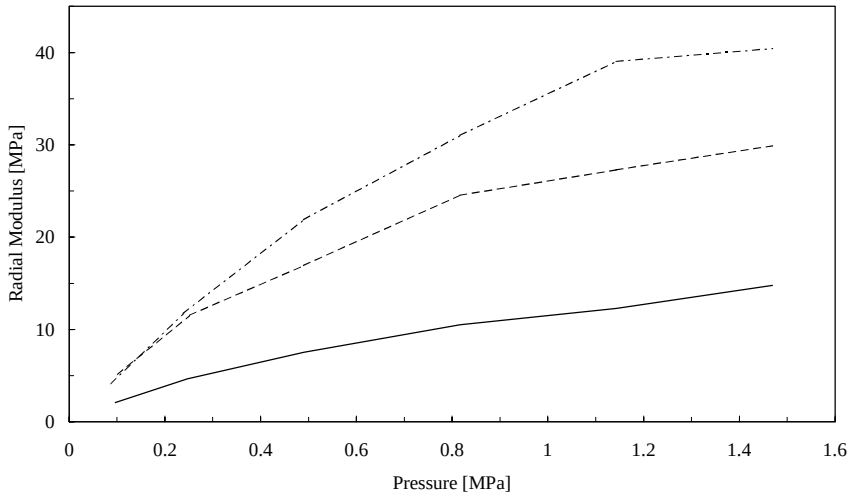

Figure 31. Radial (stack) modulus as a function of the normal pressure for the following paper grades: newsprint (solid line), SC (dashed line) and LWC (dash-dotted line).

The tangential (machine) direction elastic modulus as a function of the web tension for newsprint, SC and LWC grades is shown in Figure 32. In this direction, the modulus decreases when the tangential stress is increased. Although the variation of the modulus in the range 0 –1200 N/m is quite large, it might be relatively small in the range in which the web tension varies in the contact problem. Hence, with some caution, the tangential modulus, as a first approximation, can be considered a constant.

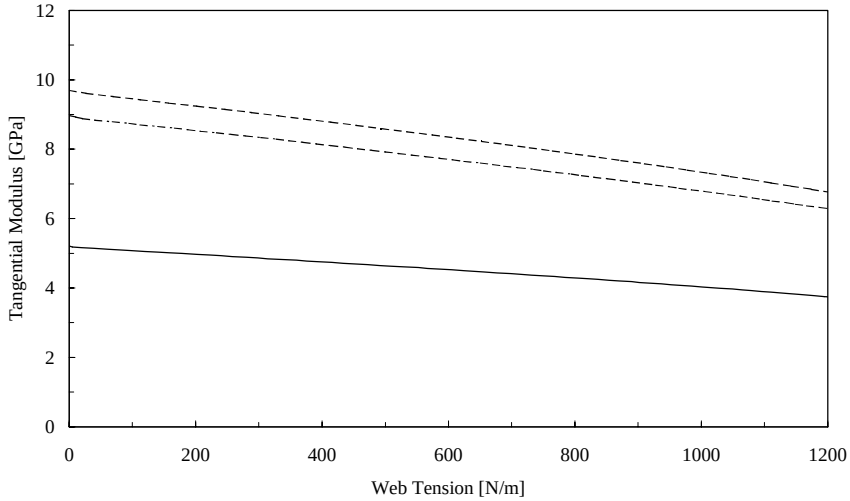

Figure 32. Tangential modulus as a function of the web tension for the following paper grades: newsprint (solid line), SC (dashed line) and LWC (dash-dotted line).

From the studies of the structural properties of paper, it is know that the cross compliance $c_{r\theta}$ or the cross elastic constant $A_{r\theta}$ are small quantities [30,37]. Furthermore, it was shown earlier in this chapter that for small $A_{r\theta}$ the contact mechanical solution is independent of the cross elastic constant. Hence, it obviously does not matter if $A_{r\theta}$ varies as a function of the stress state of the paper.

The most problematic elastic constant appeared to be the shear modulus, since firstly it is very hard to measure and secondly because it seems to affect greatly the contact mechanical solution of the winding nip. The only reference found where a numerical value for the shear modulus between the z- and machine direction was given is a recent study by Stenberg [47]. With special apparatus, he succeeded in measuring the shear modulus for thick board grades.

The application area of the half-space solution is of great interest, since the evaluation of the influence coefficients is much faster for the half-space solution than what it is for the cylinder solution. Numerical calculations show that the error (or deviation) in the NIT values is typically less than 3 % when the winding drum is rigid and the thickness of the paper layer wound around the core is more than 5 cm. For soft covered winding drums it is recommended to use the cylinder solution, since the error increases very fast as the thickness of the cover is reduced. Even with 5 cm cover thickness, the error in the NIT can be about 15 %.

The main reason why the half-space solution is faster to compute than the cylinder solution is the high number of terms needed in the Fourier series (116). Typically, 15000 - 35 000 terms have been used in the numerical calculations. The lower bound for the number of the needed Fourier terms N can be calculated from the Nyquist sampling theorem [2]. As soon as the Nyquist criterion is fulfilled, the number of terms in the Fourier series seems to be insignificant.

The number of equidistant grid points at the contact area M should be chosen large enough to enable the piecewise linear presentations of the contact tractions to approximate the solutions accurately enough. The approximation of the pressure does not present any problems, since its evolution is quite regular. However, the abrupt jump in the winding drum tangential traction (Figure 15), at the beginning of the trailing edge slip zone, requires a dense grid in order to obtain a feasible approximation of the tangential traction. The computation time and NIT as a function of the number of grid points are shown in Figure 33. The compressive radial load P is 2000 N/m, the winding force F = 0 N/m and the material parameters correspond to **Table 1**. The computation time increases exponentially and, hence, will set a bound to M. The NIT curve seems to converge, but quite slowly. For most of the calculated examples, a value of 200 was used for M as a compromise between the computation time and accuracy.

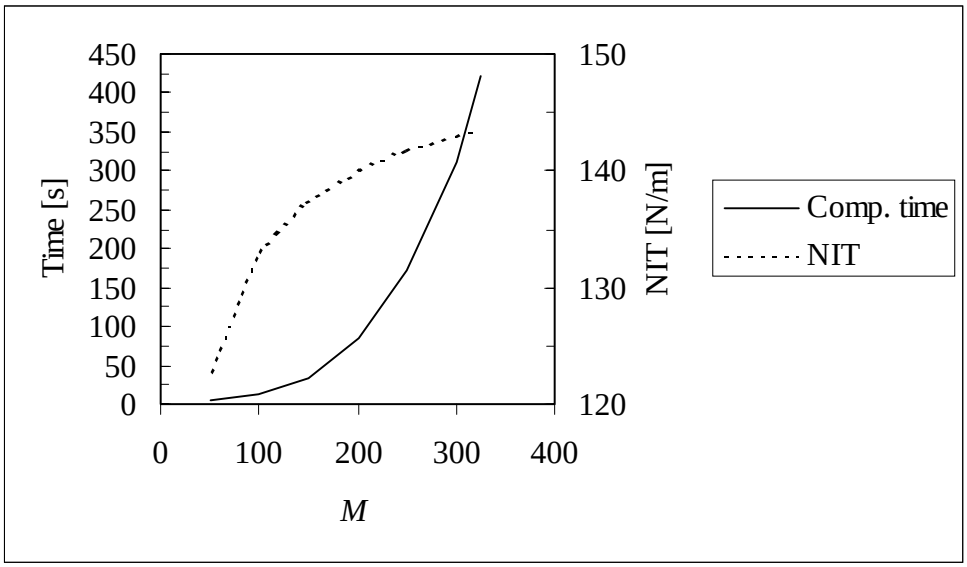

Figure 33. Computation time (solid line) and NIT (dashed line) as a function of the number of contact grid points.

Actually, the discretization error is dependent on the nip width $2a$ and the number of collocation points M. When either the nip load P or the size and elastic constants of the cylinders are changed, a is also changed. Hence, it should be noted that when the influence of the nip load and wound roll and winding drum radii and elastic constants on NIT were studied, the discretization length Δx was not constant. However, the variation in the accuracy related to this seems to be less than 5% when the nip width was within the range of 7mm–20mm (Figure 16). Hence, the trends in Chapters 4.3, 4.5, 4.6 and 4.7 should be unaffected by the non-uniformity of the error.

4.9 Evaluation of the Wound-On-Condition

Since all the numerical examples calculated so far show that the web-wound roll contact slips just before the trailing edge of the nip, it is presumable that the web will actually continue slipping behind the nip. How far will this slippage continue and what effect has it on the wound-on-tension? How great an error is created when the web is forced to stick to the wound roll at the trailing edge of the nip (WOC)? The purpose of the present chapter is to address these questions. In the following, it will be demonstrated that the slippage of the incoming web is restricted to a very small area immediately behind the nip. As shown in Chapter 4.7, the influence of the cross elastic constant $A_{r\theta}$ on the wound-on-tension is negligible. This justifies the use of the "wire" model of the web, presented in Chapter 3.5. According to Eq. (139) the force balance equations for the web behind the nip are

$$p^+ = \frac{T}{\rho^+}\ , \tag{175}$$

$$\frac{dT}{ds} = q^+. \tag{176}$$

It is assumed that the web slips so that

$$q^+ = \pm\mu^+ p^+. \tag{177}$$

By combining Eqs. (175)-(177) the following equation for web tension is obtained:

$$\frac{dT}{ds} = \pm\mu^+ \frac{T}{\rho^+(s)}. \tag{178}$$

Utilizing Eq. (154), the solution becomes

$$T(s) = T_{out} e^{\pm\mu^+ \int_a^s \frac{ds}{\rho^+}} \approx T_{out} e^{\pm\frac{\mu^+}{R_1}(s-a)} \left\{ 1 \pm \mu^+ \left[\frac{2}{R_1^2} \int_a^s u_{r1} d\zeta - u'_{r1}(s) + u'_{r1}(a) \right] \right\} \tag{179}$$

This shows that the leading term of the capstan formula is not affected by the deformation of the cylinder surface.

Consider next the wound roll surface far away from the nip area, where the deformations and strains due to the nip contact loads are small. The claim is that *the topmost layer cannot slip in that area of the wound roll!* To justify this, it is assumed that the topmost layer is slipping. For definiteness, assume that the web is faster than the roll, i.e., the + sign should be used in Eq. (177). To leading order the relative speed difference between the web and the roll (133) becomes

$$\upsilon^+ = \varepsilon^+ - \varepsilon_{\theta 1} + \xi^+ = \frac{T_0}{2hA_{\theta\theta,1}} e^{\mu^+\theta} - \varepsilon_{\theta 1} + \xi^+, \tag{180}$$

where θ is measured from a reference point within the slip area and T_0 is the web tension at that point. Since υ^+ is positive when the slip starts and by an intuitive argument (which will be justified later) the tangential traction q^+ increases more the tangential strain of the web than that of the roll surface, the speed difference keeps on growing. Consequently, the web cannot stick at any later stage and is forced to slip through the whole undeformed or slightly deformed area of the wound

roll, that is, almost a whole circumference back to the front of the nip. This does not, however, comply with experimental observation (the web tension of the topmost paper layer does not vary as much as Eq. (179) predicts and J-line measurements do not support as large a layer-to-layer movement). Thus, the web can slip only at locations where the growth rate of the tangential strain of the roll surface is comparable to that of the slipping web, i.e., very close to the nip area. The promised justification for the growth rates of the web and roll tangential strains is given in Figure 34. The loads used in the calculation are

$$p^+ = \begin{cases} \dfrac{T_0}{R_1} e^{\mu^+ \theta} & , 0 \le \theta < \pi \\ 0 & , \pi \le \theta < 2\pi \end{cases} , \quad q^+ = \mu^+ p \tag{181}$$

and the material parameters correspond to **Table 1** except that $\mu^+ = 0.5$. It should be remembered that the roll surface areas where the nip load deformations are small are considered. It can be seen that the growth rates differ by several decades in magnitude. Thus, it has been shown that the loads between the web and the wound roll have a much larger effect on the web than on the roll. Consequently, the argument seems to hold. The case when the web is moving slower than the roll can be treated analogously.

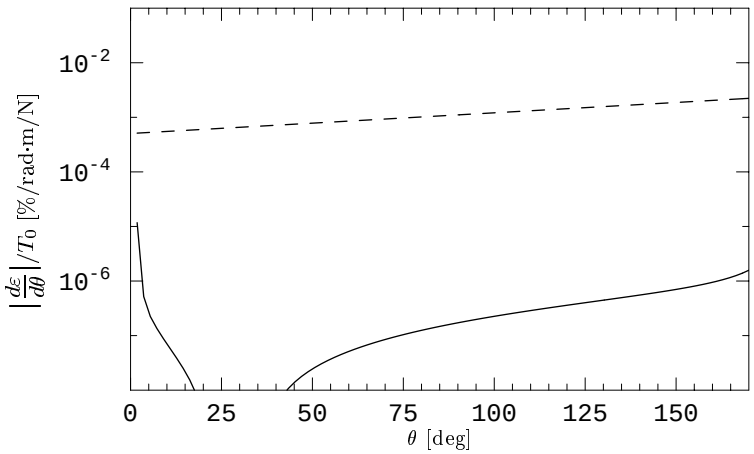

Figure 34. Magnitude of the growth rates of the tangential strains at the surface of the wound roll (solid line) and web (dashed line) under the surface tractions (181).

The next question is how far away from the nip area can the web still slip. This leads to the question: how far from the nip is the tangential strain of the roll due to the nip loads still of a substantial magnitude to significantly influence the relative speed difference v^+? Figure 35 (a) shows the tangential strain of the wound roll $\varepsilon_{\theta 1}$ in the vicinity of the nip for P = 10 kN/m and μ^+ =

0.7 and 0.2 (solid and dashed lines, respectively). It should be noted that $\varepsilon_{\theta 1}$ exhibits a rapid change only close to the nip area. Figure 35 (b) shows the rate of change of $\varepsilon_{\theta 1}$ and ε^+ behind the nip. It should be noted that the decay rate of $\varepsilon_{\theta 1}$ is higher than that of ε^+ only for $\theta < 0.5°$ and is much smaller for larger values of θ. If the web sticks at $\theta = \theta_s$, so that $v^+(\theta_s) = 0$, Eq. (180) implies

$$v^+(\theta_a) = \int_{\theta_a}^{\theta_s} \left(\frac{d\varepsilon_{\theta 1}}{d\theta} - \frac{d\varepsilon^+}{d\theta} \right) d\theta = \Delta\varepsilon_{\theta 1} - \Delta\varepsilon^+ \ . \tag{182}$$

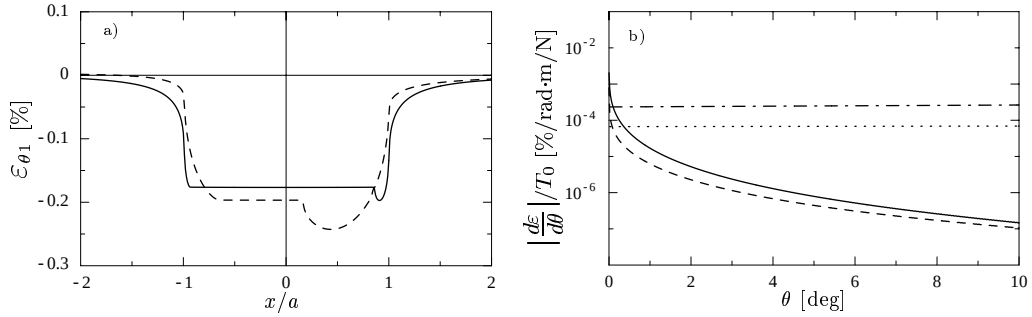

Figure 35. a) Roll surface tangential strain and b) magnitude of the growth rate of the roll surface and web tangential strains for P = 10 kN/m, μ^+ =0.7 (solid and dashed-dotted lines) and μ^+ =0.2 (dashed and dotted lines).

When typical values for the elastic constants of paper were used, a positive value of $\varepsilon_{\theta 1}$ was never observed within the nip zone. This was due to the dominance of the term u_r / r over the term $1/r\,\partial u_\theta / \partial\theta$ in the expression of the tangential strain (34). This term dominated, since the radial load P gives rise to large compressive (negative) radial displacements u_r within the nip zone. Behind the nip the radial displacements relaxed monotonically towards zero. Consequently, in all cases studied, strain $\varepsilon_{\theta 1}$ was an increasing function behind the nip. In principle, however, strain $\varepsilon_{\theta 1}$ could also be positive at the trailing edge of the nip under some extreme conditions (for small P, G and $M_1 \gg 0$, $M_2 \ll 0$, for example). It is also evident that in this case, $\varepsilon_{\theta 1}$ relaxes monotonically towards zero behind the nip. Now the following statements concerning the slip behavior behind the nip can be presented:

Case 1. $v^+(a) < 0$ and $\varepsilon_{\theta 1}(a) < 0$

Now $\varepsilon_{\theta 1}$ increases and ε^+ decreases behind the nip so that $\Delta\varepsilon_{\theta 1} > 0$ and $\Delta\varepsilon^+ < 0$. This means that the stick condition (182) cannot be fulfilled so that the topmost layer must slip all the way around the wound roll wrap, which contradicts experimental observation.

Accordingly, *the topmost paper layer cannot slip at all behind the nip* (i.e., it must be that $v^+(a) = 0$).

Case 2. $v^+(a) > 0$ and $\varepsilon_{\theta 1}(a) < 0$

Now both $\varepsilon_{\theta 1}$ and ε^+ increase behind the nip so that $\Delta\varepsilon_{\theta 1} > 0$ and $\Delta\varepsilon^+ > 0$. According to Eq. (182) $\Delta\varepsilon_{\theta 1}$ must be larger than $\Delta\varepsilon^+$ for the sheet to stick. As demonstrated in Figure 35 (b), this is possible only in the immediate vicinity of the nip edge. Accordingly, *the topmost paper layer can slip only within a small region behind the nip.*

Case 3. $v^+(a) < 0$ and $\varepsilon_{\theta 1}(a) > 0$

Now both $\varepsilon_{\theta 1}$ and ε^+ decrease after the nip so that $\Delta\varepsilon_{\theta 1} < 0$ and $\Delta\varepsilon^+ < 0$. A similar argumentation to Case 2 can be given. Accordingly, *the topmost paper layer can slip only within a small region behind the nip.*

Case 4. $v^+(a) > 0$ and $\varepsilon_{\theta 1}(a) > 0$

Now $\varepsilon_{\theta 1}$ decreases and ε^+ increases behind the nip so that $\Delta\varepsilon_{\theta 1} < 0$ and $\Delta\varepsilon^+ > 0$. A similar argumentation to Case 1 can be given. Accordingly, *the topmost paper layer cannot slip at all behind the nip* (i.e., it must be that $v^+(a) = 0$).

In general, the relative speed difference v^+ at the trailing edge is positive for center winding (Case 2) but can also be negative for surface winding with small nip loads (Case 1). Hence, in center winding the web slips for some distance behind the nip whereas in surface winding with small nip loads the web must stick immediately at the nip edge. The relative error introduced to WOT by assuming the stick state at the trailing edge of the nip (WOC) can be estimated from the capstan formula (179). A conservative estimate is $\theta_s = 5°$ and $\mu^+ = 0.5$ leading to a 4.5% relative error. Finally, it should be noted that in the previous considerations numerical results calculated using WOC have been utilized to justify the use of WOC. A comparison to experimental results for WOT in Chapter 5 shows, however, that the relative error in the calculated value of WOT (and T_{out}) is small. Since WOC could be substituted in the contact mechanical equations by a given value of T_{out}, it can be concluded that the solution using WOC must be a good approximation for the exact solution employing the contact mechanical equations behind the nip (Chapter 3.5). This completes the above considerations about WOC.

5 COMPARISON WITH EXPERIMENTAL DATA

Since at least the radial modulus of the wound roll is dependent on the local stress state, the application of the present linear theory in practice will bring about the difficulty of choosing the elastic constants of the linear theory to represent the nonlinear nature of the paper appropriately. The tangential elastic constant $A_{\theta\theta}$ can be easily measured and, within the web tension variation range during winding, could be considered as constant (Figure 32). The cross elastic constant $A_{r\theta}$ has been demonstrated to have a negligible effect on WOT predicted by the present theory. Hence, at least in principle, the arbitrary (within the linear theory) radial elastic constant A_{rr} and the unknown shear modulus $G_{r\theta}$ could be used as tuning parameters to obtain a close fit between experiment and theory.

In this chapter the validity of the winding theorem of Chapter 4.1 is evaluated using experimental data measured on WHRC's WIT-WOT winder (page 15). In addition, the WOT vs. nip load curves produced by the present theory are compared with the corresponding experimental curves for center winding. The radial elastic constant A_{rr} and shear modulus $G_{r\theta}$ will be fit to produce the measured WOT at one measurement point and then used when calculating all other data points. Experimentally measured values will be used for the other material parameters.

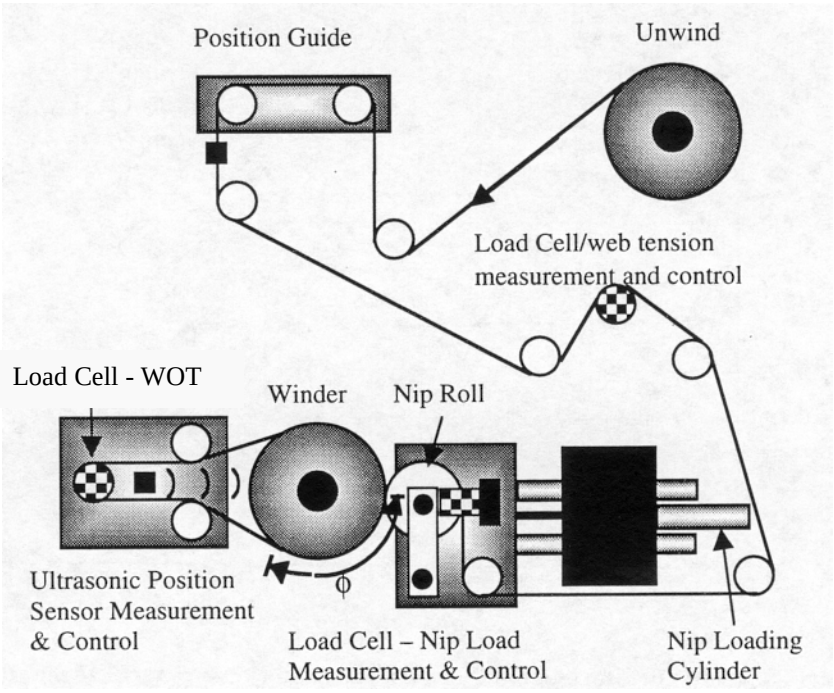

Figure 36. WHRC's WIT-WOT winder.

The WIT-WOT winder used to obtain the experimental data is shown in Figure 36. The unwind tension is measured by a load cell and a feedback signal is fed to the unwind drive to keep the tension at a set value. At the winding section the web is guided through a 180° wrap of the nip roll to the winding roll. After wrapping the winding roll for about 90°, the web is steered to another load cell and then finally back to the wound roll. The measurement of this load cell is inferred as WOT and the unwind tension as T_{in}. The radial nip load between the winding roll and the nip roller is measured with a third load cell and feedback-controlled by the nip loading cylinder. Whether this type of WOT measurement is an interfering test method has been studied by Good *et al.* [15]. When the internal pressures of the newsprint rolls wound with and without leading the web through the WOT load cell in otherwise identical conditions were compared, it was found that the internal pressures of the rolls wound without the WOT measurement were higher. Their conclusion was that the outer lap of the web must slip while wrapping the winding roll.

Here, however, the results of Chapter 4.9 will be utilized and the web tension will be evaluated exactly at that point where the web exits to the WOT load cell. Assuming that the web sticks to the wound roll at this exit point and utilizing Eq. (128) gives

$$WOT_{meas} = 2hA_{\theta\theta}\left[\varepsilon_{\theta 1}(\theta_1 \approx 90^\circ) - \varepsilon_{\theta 1}(a)\right] + T_{out} \ , \tag{183}$$

where WOT_{meas} is the value predicted by the theory for the load cell measurements. The tangential strain of the wound roll at $\theta_1 = 90^\circ$ can be evaluated from Eq. (114). The material parameters used in the calculations are shown in **Table 2** and the experimental and theoretical values in **Table 3**. The experimental and theoretical results are also shown in Figure 37.

Table 2.
Material parameter values used in the calculations

Parameter	Notation	Value
Paper to roll friction coefficient	μ^+	0.19
Paper to drum friction coefficient	μ^-	0.2
Wound roll radius	R_1	0.1 m
Winding drum radius	R_2	0.0762 m
Radial elastic constant	A_{rr}	27 MPa
Tangential elastic constant	$A_{\theta\theta}$	3.38 GPa
Cross elastic constant	$A_{r\theta}$	5 MPa
Shear modulus	$G_{r\theta}$	10 Mpa
Web thickness	$2h$	66 μm

The values of the radial elastic constant and shear modulus were chosen so that the results of the theory and experiments coincided when P = 3502 N/m and T_{in} = 350 N/m.

Table 3.
Experimental and theoretical wound-on-tensions in center winding

T_{in} N/m	**175**	**175**	**263**	**263**	**350**	**350**
Nip Load N/m	**Exp.**	**Theory**	**Exp.**	**Theory**	**Exp.**	**Theory**
350	**266**	257	**327**	345	**410**	432
876	**316**	324	**416**	412	**482**	499
1751	**416**	405	**496**	494	**566**	581
3502	**525**	524	**598**	612	**700**	699
5837	**637**	643	**715**	731	**815**	818

The theoretical values agree surprisingly well with the experimental ones as can be seen from **Table 3** and Figure 37. One possible explanation for the close fit can be that the shear modulus also increases with the radial pressure. When the nip load is increased, higher values for the radial elastic constant and the shear modulus should be used but, as was shown in Chapter 4.7, an increase of the radial elastic constant decreases NIT while an increase of the shear modulus increases NIT and, hence, opposing effects, possibly canceling each other, are generated.

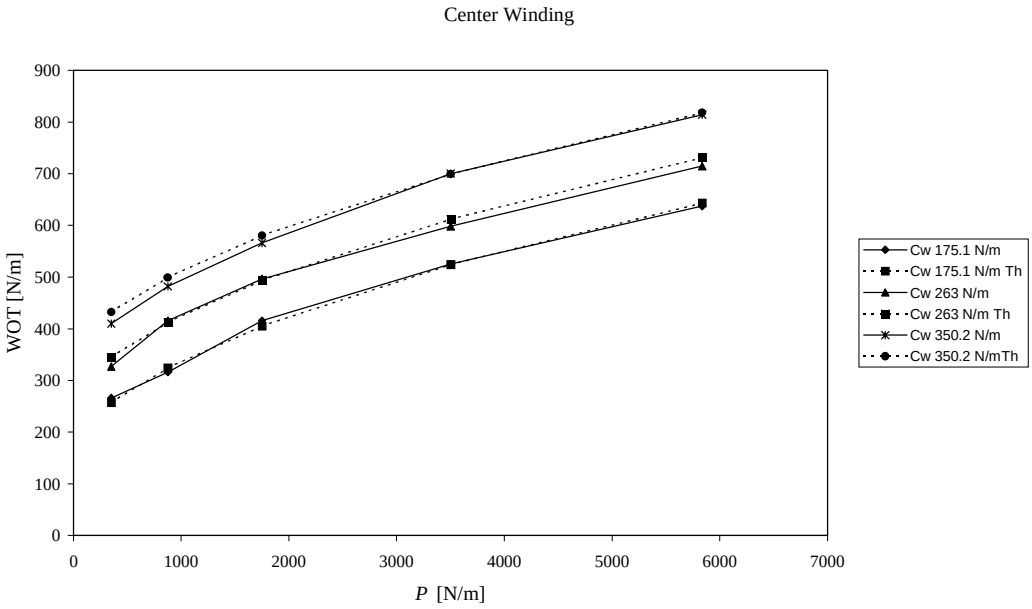

Figure 37. Experimental (solid lines) and theoretical (dashed lines) wound-on-tension curves for the incoming web tensions 175, 263 and 350 N/m.

For the center winding configuration the winding force is zero and, hence, for a constant nip load the prerequisites for the application of the winding theorem of Chapter 4.1 are fulfilled. Since the difference between T_{out} and the measured WOT is constant for a given nip load (winding

theorem), the experimental data could be used to determine NIT (plus an additive constant depending solely on *P*). The evaluated experimental NIT values and the correspondig averages and standard deviations are shown in **Table 4**. Apart from very low nip loads, the NIT seems to be independent of the incoming web tension to a good relative accuracy. The same conclusion was drawn by Good *et al.* [15] in their article on WIT-WOT measurements.

Table 4.
Experimental nip-induced-tension in center winding

T_{in} N/m **Nip Load N/m**	175	263	350	**Average**	**Standard deviation**
350	91	64	60	72	17
876	141	153	132	142	10
1751	240	233	216	230	13
3502	350	335	350	345	9
5837	462	452	464	459	7

6 CONCLUSIONS

The aim of this thesis was to develop a contact mechanical model for the winding nip. Being aware of the potential pitfalls, a linear elastic description was used for the paper roll and paper sheet. The liberty to avoid any unnecessary degree of difficulty was taken because of the novelty of the contact mechanical approach on the winding applications. The list of the most significant presumptions goes as follows:

1. The stress state was assumed a two-dimensional plane strain at the cross-sections.
2. All the contacting bodies were assumed to obey linear constitutive equations.
3. Steady state conditions were assumed.
4. The core of the wound roll was rigid.
5. The sheet was assumed to stick to the wound roll at the trailing edge of the contact.
6. Normal and tangential tractions were assumed to vanish at the trailing edge of the contact.
7. The nip-induced tension was assumed to develop at the topmost paper layer of the wound roll.

Because of these assumptions, the main outcome of the model should be regarded phenomenological and methodological with only a limited applicability to yield quantitatively accurate results.

With the mathematical apparatus, developed in Chapters 2 and 3, a wide numerical parameter study was carried out in Chapter 4. A specific stick and slip pattern was found to occur in the winding nip when the winding drum was hard. Hence, a general mechanism of the nip-induced tension was found to be due to the appearance of a simultaneous (double sided) slip zone in the vicinity of the trailing edge of the nip. In this slip zone the sheet moves faster than the wound roll and winding drum and, hence, the sheet tension increases.

When the influence of the winding parameters upon nip-induced tension was studied the following general trends were found:

- At very small nip load levels, NIT is approximately equal to the layer-to-layer friction coefficient times the nip load.
- Slope of the NIT-*P* curve decreases as the nip load increases
- Nip-induced tension increases with the winding force.

All these items comply with experimental results.

According to the numerical simulations, nip-induced tension decreases generally for increasing layer-to-layer friction coefficient. This complies with experimental results. The numerical simulations showed that if the sheet-drum friction coefficient is less than the layer-to-layer friction coefficient, then nip-induced tension will be much less than in the opposite case. No experimental data was available to verify this.

According to the numerical simulations, nip-induced tension decreases for increasing the winding drum and wound roll radii. This complies with the experimental results presented in the references [12] and [41]. The rate of decrease was found to be approximately inversely proportional to the square root of the relative radius.

According to the numerical simulations, the nip-induced tension is decreased when the modulus of elasticity of the winding drum cover is reduced. It was also calculated that with a soft cellular elastomer cover the nip-induced tension was almost independent of the nip load. This complies with the results presented in [38].

According to the numerical simulations, nip-induced tension is generally increased when the tangential elastic constant and the shear modulus of the wound roll are increased and is decreased when the radial and cross elastic constants of the wound roll are increased. It was also shown that the cross elastic constant does not have any influence on nip-induced tension if it is small. This contradicts the NIT model of reference [16], where nip-induced tension was explained to be due to the cross elastic constant (or Poisson's ratio).

The validity of the wound-on-condition, stating that the web sticks to the wound roll surface at the nip exit, was justified numerically.

As a conclusion it can be stated that all the numerical simulations are very intelligible and most of the predictions comply well with the experimental results found in the literature.
In order to improve the exploitability of the winding contact model the following adjustments will be made in the future:

1. The winding drum wrap will be included.
2. The non-linear compressive modulus of paper will be accounted for.

With the above-mentioned modifications, the substance of the winding nip model would be improved at a level where it could give quantitatively reliable results. A further obvious extension to a 3D winding nip model does not seem feasible in the near future because of the enormous demands on the computing capacity.

REFERENCES

1. Altmann, H. C., Formulas for Computing the Stresses in Center-Wound Rolls. *Tappi Journal* **51**(4), pp. 176-179 (1968).
2. Bendat, J. S. and Piersol, A. G., *Engineering Applications of Correlation and Spectral Analysis*. John Wiley & Sons, New York, 1980.
3. Bentall, R.H. and Johnson, K. L, An Elastic Strip in Plane Rolling Contact, *Journal of International Mechanical Sciences*, **10**, pp. 637-663 (1968).
4. Bentall, R.H. and Johnson, K. L, Slip in the Rolling Contact of Two Dissimilar Elastic Rollers, *Journal of International Mechanical Sciences*, **9**, pp. 389-404 (1967).
5. Bjarnehed, H. L., Rigid Punch on Stressed Orthotropic Half-Plane with Partial Slip, *ASME Journal of Applied Mechanics*, **58**, pp. 128-133 (1991).
6. Carter, F. W., On the Action of a Locomotive Driving Wheel. *Proceedings, Royal Society*, **A112**, p. 151 (1926).
7. Cattaneo, C., Sul contatto di due corpi elastici: distribuzione locale degli sforzi. *Rendiconti dell' Accademia nazionale dei Lincei*, **27**, Ser 6 (1938).
8. Donnell, L. H., Bending of Rectangular Beams. *ASME Journal of Applied Mechanics*, **19**, p. 152 (1952).
9. Donnell, L. H., *Beams, Plates and Shells*. McGraw-Hill, New York, 1976.
10. Duva, J. M. and Simmonds, J. G., Elementary Static Beam Theory is as Accurate as You Please. *ASME Journal of Applied Mechanics*, **57**, pp. 134-137 (1990).
11. Flamant, *Comptes Rendus*, **114**, 1465, Paris, 1892.
12. Frye, K. G., *Winding*. Tappi Press, Atlanta, 1990.
13. Gilbert, R. P. and Wei, L., Function Theoretic Solutions to Problems of Orthotropic Elasticity. *Journal of Elasticity* **15**, pp. 143-154 (1985).
14. Good, J. K. and Pfeiffer, J. D., Tension Losses During Centerwinding. *Proceedings of TAPPI Finishing and Converting Conference*, pp. 297-305 (1992).
15. Good, J. K., Hartwig, J. and Markum, R., A Comparison of Center and Surface Winding Using the Wound-In-Tension Method. *Proceedings of the Fifth International Conference on Web Handling*, Oklahoma, Stillwater (1999).
16. Good, J., K. and Wu, Z., The Mechanism of Nip-Induced Tension in Wound Rolls, *Journal of Applied Mechanics*, **60**, pp. 942-947 (1993).
17. Gueldenberg, B. and Welp, E. G., Quantitative Analysis of Nip-Induced Tension by Use of Digital Image Processing. *Proceedings of the Fifth International Conference on Web Handling*, Oklahoma, Stillwater (1999).
18. Hahn, H. T. and Levinson, M., Indentation of an Elastic Layer Bonded to a Rigid Cylinder–II. Unidirectional Slipping with Coulomb Friction. *Journal of International Mechanical Sciences*, **16**, pp. 503-514 (1974).
19. Hakiel, Z., Nonlinear Model for Wound Roll Stresses, *Tappi Journal* **70**(5), pp. 113-117 (1987).
20. Hertz, H., Über die Berührung fester elastischer Körper. *J. reine und angewandte Mathematik*, **92**, pp. 156-171 (1882).

21. Hertzen, R. von and Jorkama, M., On the Solution of the Generalized Biharmonic Equation, Unpublished manuscript, 1999, 29 p.

22. Hua, K. L., Lin, W. and Wu, C-Q., *Second-order Systems of Partial Differential Equations in the Plane*. Pitman Advanced Publishing Program, Boston, 1985.

23. Jalkanen, E., M., J., *Influence of Certain Winding Parameters on the Formation and Structure of Newsprint Paper Rolls* (In Finnish). Master's Thesis, Helsinki University of Technology, 1968.

24. Johnson, K. L., *Contact Mechanics*. Cambridge University Press, Cambridge, 1985.

25. Jorkama, M. and von Hertzen R., Contact Mechanical Approach to the Winding Nip. *Proceedings of the Fifth International Conference on Web Handling*, Oklahoma, Stillwater (1999).

26. Komulainen, P., *A Simulation Model for Paper Winding and its Reliability* (In Finnish). Master's Thesis, Helsinki University of Technology, 1970.

27. Lekhnitskii, S. G., *Theory of Elasticity of an Anisotropic Elastic Body*, Holden-Day, San Francisco, 1963.

28. Lurie, S.A. and Vasiliev, V.V., *The Biharmonic Problem in the Theory of Elasticity*, Gordon and Breach Publishers, Luxembourg, 1995.

29. Malvern, L. E., *Introduction to the Mechanics of a Continuous Medium*. Prentice-Hall, New Jersey, 1969.

30. Mann, R. W., Baum, G. A. and Habeger, C. C., Determination of all nine orthotropic elastic constants for machine-made paper. *Tappi Journal* **63**(5), pp. 163-166 (1980).

31. Mantič, V. and París, F., Explicit Formulae of the Integral Kernels and C-matrix in the 2D Somigliana Identity for Orthotropic Materials. *Engineering Analysis with Boundary Elements* **15**, pp. 283-288 (1995).

32. McDonald, J. D. and Ménard, A., Layer-to-Layer Slippage within Paper Rolls During Winding. *Journal of Pulp and Paper Science* **25**(4), pp. 148-153 (1999).

33. Nakamura, G. and Tanuma, K., A Formula for the Fundamental Solution of Anisotropic Elasticity. *Quarterly Journal of Mechanics and Applied Mathematics*, **50**(2), pp. 179-194 (1997).

34. Novozhilov, V. V., *Foundations of the Nonlinear Theory of Elasticity*. Dover Publications, Inc., Mineola, NewYork, 1999.

35. O'Neill, B., *Elementary Differential Geometry*. Academic Press, Inc., Orlando, 1966.

36. Panagiotopoulos, P. D., A Nonlinear Programming Approach to the Unilateral Contact and Friction-Boundary Value Problem in the Theory of Elasticity. *Ingenieur Archiv* **44**, pp. 421-432 (1975).

37. Persson, K., *Material Model for Paper, Experimental and Theoretical aspects.* Department of Solid Mechanics, Lund Institute of Technology, Lund, Sweden, 1991.

38. Peters, H. F., Stressless Winding. *Wochenblatt für Papierfabrikation* **7**, pp. 356-357 (1997).

39. Pfeiffer, J, D., Measurement of the K2 Factor for Paper. *Tappi Journal* **64**(4), pp. 105-106 (1981).

40. Pfeiffer, J, D., Surface Winding to Overcome Strain Deficiency. *Proceedings of TAPPI Finishing and Converting Conference*, 1990.

41. Pfeiffer, J, D., The Mechanics of a Rolling Nip on Paper Webs. *Tappi Journal* **51**(8), pp. 77A-85A (1968).

42. Pickett, G., Application of the Fourier Method to the Solution of Certain Boundary Problems in the Theory of Elasticity, *Journal of Applied Mechanics*, **66**, pp. A-176 - A-182 (1944).

43. Roisum, D. R., *The Mechanics of Winding*. Tappi Press, Atlanta, GA, 1994

44. Rudin, W., *Principles of Mathematical Analysis*, McGraw-Hill, New York, 1976

45. Soong, T.-C. and Li, C., The Rolling Contact of Two Elastic-Layer-Covered Cylinders Driving a Loaded Sheet in the Nip. *Journal of Applied Mechanics* **48**, pp. 889-894 (1981).

46. Soong, T.-C. and Li, C., The Steady Rolling Contact of Two Elastic-Layer Bonded Cylinders with a Sheet in the Nip, *International Journal of Mechanical Sciences* **23**, pp. 263-273 (1981).

47. Stenberg, N., *Mechanical Properties in the Thickness direction of Paper and Paperboard*. Licentiate's Thesis, Royal Institute of Technology, Stockholm,1999.

48. Särkelä, V., *A Simulation Model for Paper Winding* (In Finnish). Master's Thesis, Helsinki University of Technology, 1970.

49. Tervonen, M., *Numerical Models for Plane Viscoelastic Rolling Contact of Covered Cylinders and a Deforming Sheet*, Doctoral Thesis, Acta Univ. Oul. C 100, Finland, 1997, 123 p.

50. Ting, T. C. T., *Anisotropic Elasticity: Theory and Applications*. Oxford University Press, New York 1996.

51. Tomlin, G. R. and Butterfield, R., Elastic Analysis of Zoned Orthotropic Continua. *ASCE Journal of the Engineering Mechanics Division*, **100** (EM3), pp. 511-529 (1974).

52. Tullini, N. and Savoia, M., Elasticity Interior Solution for Orthotropic Strips and the Accuracy of Beam Theories. *ASME Journal of Applied Mechanics*, **66**, pp. 368-373 (1999).

53. Vijayarangan, T., *A Study on Nip Mechanics in Surface Winding*. Master's Thesis, Oklahoma State University, 1994.

54. Welp, E.G. and Gueldenburg, B., Analysis of the Kinematic and Dynamic Process During Winding Based on a Systematology of Models for Winding Mechanics, *Proceedings of the Fourth International Conference on Web Handling*, Oklahoma, Stillwater, pp. 71-89 (1997).